REPUBLIQUE ALGÉRIENNE DÉMOCRATIQUE ET POPULAIRE

Ministère de l'enseignement supérieur et de la recherche scientifique

UNIVERSITÉ AMAR TELIDJI LAGHOUAT

Faculté de technologie-Département d'Électronique

MEMOIRE DE MAGISTER

Présenté en vue de l'obtention du diplôme de magister en génie électrique

Option : Signaux et Télécommunication

Thème

Design of Metamaterial Agile Microwave Devices

Présenté par

Mr. LAAMARI Mohammed Elmamoun

Ingénieur en électronique

Devant le jury composé de:

Mr. Djilali MAHI	Professeur à l'Université de Laghouat	Président
Mr. Mouloud BOUZOUAD	Professeur à l'Université de Laghouat	Encadreur
Mr. Abdelkrim SEGHIER	M. Assistant à l'Université de Laghouat	Co-encadreur
Mr. Djamel BENATIA	Professeur à l'Université de Batna	Examinateur
Mr. Bachir BENTRIA	Professeur à l'Université de Laghouat	Examinateur

Année universitaire 2014-2015

1. ملخص

الهدف الأساسي من هذا العمل هو تصميم مكونات (devices) موجات صغرى (microwaves) مرنة (agile) باستعمال مافوق المواد "metamaterials". لهذا الغرض قمنا بتصميم سطح (طبقة) ثنائي الأبعاد (2D) مافوق مادي مرن. لإدخال المرونة في هذا الأخير، قمنا بتصميم خلية مافوق مادية مرنة نتحصل عليها بالطبع على عازل كهربائي ناقل على شكل صليب متصل أو منفصل يمكن التحكم فيه باستخدام نظام سيطرة خارجي (مفاتيح التحويل، قواطع، صمامات ثنائية، MEMS ...). لهذه الخلية المرنة سلوكين مختلفين (حسب وضعية القواطع لوصل أو فصل شكل الصليب الناقل): الأول يوافق سلوك وسط ذو معامل انكسار قريب من الصفر والثاني يوافق سلوك وسط ذو معامل انكسار اكبر من الواحدة. يستخدم هذا السطح مافوق المادي المرن كمادة قابلة لبرمجة استجابتها الكهرومغناطيسية بما أنه من الممكن برمجة سلوك كل خلية (بكسل) من الطبقة على حدة أي اختيار العواملها التكوينية (constitutive parameters). بهذا نتحصل على طبقة (2D) ما فوق مادية مرنة "منقطة"، استجابتها الكهرومغناطيسية يمكن برمجتها من خلال التحكم في كل خلية على حدة. برص عدد من هذه الطبقات المرنة فوق بعضها نتحصل على كتلة مافوق مادية مرنة ثلاثية الأبعاد 3D (2D و½) قابلة للبرمجة و ليس لها وظيفة محددة مسبقا. هذه الكتلة مافوق المادية المرنة يمكن برمجتها لأداء وظائف مختلفة.بحيث يمكننا برمجتها لمحاكاة مكونات موجات صغرى (microwave devices) خاملة مختلفة مثل الدلائل الموجية (waveguide) ذات الأحجام والأشكال المختلفة (دائرية، مستطيلة، ...). إن الكتلة مافوق المادية المرنة تتصرف باعتبارها عنصر موجات صغرى (microwave) "مرن الوظيفة".

2. Abstract

The main goal of this work is to design agile metamaterial microwave devices. For this purpose we conceive an agile metamaterial layer (2 D). To introduce agility in the latter metamaterial, we propose an agile unit cell, made of connected / disconnected cross like conductor, which can flip, using an external switching systems (switches, diodes, MEMs…), between two different behaviors. The first one corresponds to an effective medium with a refractive index close to zero and the second one corresponds to an effective medium having a refractive index greater than unity. The agile metamaterial layer is used as a programmable material in which it is possible to program the electromagnetic response (constitutive parameters) of each unit cell (pixel) of the layer. This leads to a "*pixilated*" (2 D) agile metamaterial layer whose electromagnetic response can be programmed by acting on each unit cell. By stacking several agile metamaterial layers we obtain an artificial 3 D (2 D and ½) agile metamaterial (programmable) bulk which has no predefined function. This 3 D agile metamaterial bulk can be programmed to fulfill various functions. It behaves as a programmable component. In other words, it can be programmed to emulate different passive microwave devices such as waveguides having different shapes (circular, rectangular, etc…) and different size. The 3D agile metamaterial bulk constitutes a "functioning agile" microwave device.

3. Résumé

L'objectif principal de ce travail est de concevoir des composants microonde agiles à base de métamatériaux. Pour cette raison, nous avons conçu une surface métamatériau agile (2 D). Pour introduire l'agilité dans cette dernière, nous avons proposé une cellule élémentaire agile, à base d'un conducteur en forme de croix connectée / déconnectée, qui peut basculer entre deux comportements différents, en utilisant un système de commutation externe (commutateurs, diodes, MEMS ...). Le premier correspond à un milieu effectif d'indice de réfraction proche de zéro et le deuxième correspond à un milieu effectif d'indice de réfraction supérieur à l'unité. Chaque surface métamatériau agile forme une couche dont il est possible de programmer la réponse électromagnétique (choix des paramètres constitutifs) de chaque cellule élémentaire (pixel) et est utilisée comme un matériau programmable. Cela conduit à une couche métamatériau (2 D) agile "pixélisée" dont la réponse électromagnétique peut être programmée en agissant sur chaque cellule élémentaire. En empilant plusieurs de ces couches métamatériaux agiles, on obtient un bloc 3 D (2 D et ½) artificiel de métamatériau agile (programmable) qui n'a pas de fonction prédéfinie. Ce bloc de métamatériau agile peut être programmé pour remplir diverses fonctions et se comporte comme un composant programmable. En d'autres termes, Il peut être programmé pour émuler différents dispositifs micro-ondes passifs tels que des guides d'ondes de différentes tailles et formes (circulaire, rectangulaire, etc ...). Le bloc métamatériau agile constitue un dispositif micro-onde « agile en fonction ».

Acknowledgements

First I would like to express my gratitude to my supervisor Prof. Mouloud BOUZOUAD for his support and continuous encouragement throughout my research. I really appreciate his guidance, insights and suggestions on this research, which will be a valuable experience for my career.

I gratefully acknowledge my thesis committee president and members Prof. Djilali MAHI, Prof. Djamel BENATIA and Prof. Bachir BENTRIA for their remarks and suggestions on my dissertation.

I also pass my sincere thanks to all my current technical colleagues and Metamaterials team at Telecommunications Signal and Systems Laboratory for their generous helps and constructive discussions.

The most and for most, my special appreciations go to my family for their extensive encouragements and continuous supports during these past years, which gave me all the strength needed to successfully finish my studies.

LAAMARI Mohammed Elmamoun

Table of contents

List of figures

Introduction

Metamaterials are applied in multiple domain of our daily life including communication and information technologies. They contribute effectively in the technology development due to their qualitative characteristics. One of the main characteristics is that a metamaterial can be designed and tailored to meet, in request, the desired electromagnetic properties.

We are interested in this work, by the design of a planar (2D) agile metamaterial (metamaterial layer) to use as a programmable material in which it is possible to change the characteristics using an external switching system (MEMS, PIN diodes ….). Dependently on the switch state (ON or OFF), the programmable material alternates between two different programmable behaviors: A connected cross type metamaterial (switches ON) behaving as an effective medium with a refractive index close to zero, and a disconnected cross type metamaterial (switches OFF) behaving as an effective medium with a refractive index greater than unity. Multiple agile metamaterial layers are stacked to obtain a 3D programmable metamaterial bulk. Using this 3D programmable metamaterial bulk, our goal will be the emulation of agile microwave devices such as rectangular and circular waveguides, pyramidal and conical horn antennas…

This work is divided into four chapters. The first one presents a state of art of metamaterials, in which definitions, characteristics, examples and applications are introduced.

The second chapter interests with the homogenization of metamaterials. It includes the criterion of homogenization and effective parameters (dielectric permittivity and magnetic permeability) extraction methods. Among them, we focus on the *S* parameters inversion method, also called “The Fresnel Inversion Method”, and the field summation method, also called “Field Averaging Method”. The *S* coefficients are obtained using a commercial software code which is based on finite element method in the frequency domain. Both methods (The Fresnel Inversion Method and the Field Summation method) are validated for some examples and data available in the published scientific literature.

The third chapter presents the agility techniques and gives a brief survey of agility applications: (frequency agile antennas, radiation pattern agile antennas, frequency agile filters…). Different agility techniques using MEMS, PIN diodes, ferroelectrics, ferromagnetic, liquid crystals etc are examine.

In the fourth and last chapter, we introduce a new concept of microwave device or component “functioning agility”. The device/component is a 3D programmable metamaterial bulk which has no pre-defined function. The metamaterial bulk “function” is defined and specified by programming different zones with the adequate shape size and refraction index in every layer constituting the 3D agile metamaterial bulk. So, it can behave, for example, as a waveguide (of any shape and any arbitrary size, in the limit of the bulk size), as a horn antenna (conical or pyramidal of any arbitrary size) or any other passive device. The 3D agile metamaterial bulk is said to be agile in “functioning” (functioning agility). We use the verb “emulate” which means “imitate”, “mimic” to express the idea of “behave as”. This terminology is brewed from computer science. A “printer X” emulator is a software which emulates the “printer X”. So, emulating a waveguide, for example, means that the agile metamaterial bulk is programmed to behave as a waveguide. We have emulated circular and rectangular waveguides, conical and pyramidal horn antennas. Simulation results show clearly that the emulated devices, using the a 3D agile metamaterial bulk, behave really as the simulated devices.

1. State of art

1.1 Introduction

New area is opened for metamaterial applications which did not exist in the few past years. Among the most important characteristics of meatmaterials that we will exploit in this work is the possibility to tailor their electromagnetic response. In other words, metamaterial offers the possibility to obtain the desired response in request. Often the electromagnetic responses of metamaterials can be determined analytically or numerically; with the desired accuracy and efficiency, but this operation is generally time consuming due to the increasing complexity of the metamaterial inclusion shapes. For that, to assure a desired metamaterial response, the metamaterial tailoring and engineering require methodic optimization. In this chapter, we present the definition and give historical works on metamaterials. We introduce also, the characteristics, classes and different applications of metamaterials.

1.2 Definition of metamterials

Metamaterials are man-made materials, composed of artificially structured unit cells that are designed of conventional materials and usually (but not necessarily) arranged in periodic fashion [1]. Although the matter is constituted of atoms and molecules (figure 1-1), the electromagnetic waves see the system like an electric and magnetic dipolar distributions which are the microscopic sources of the polarization and magnetization phenomena. We recall here briefly, the microscopic sources of these two phenomena. Generally, we have three microscopic mechanisms of polarization. The first one is the electronic polarization. It is related to the modification of the internal charges repartition of each atom or ion. It is constantly present whatever the state of the considered material. The second one is the atomic or ionic polarization. It concerns the displacements of atoms or ions compared to their equilibrium positions in the edifice where they belong. The third one is the orientation polarization. It arises when the atomic or molecular dipole moment is oriented under an electric field action. The origin of magnetization is the microscopic electric currents resulting from the motion of electrons and the spin of charged particles present in atoms.

Microscopically, to conceive a metamaterial, we can introduce inclusions like metal thin wires or split ring resonators (SRR) which behave like elementary electric dipoles or magnetic dipoles, respectively, in the conventional materials. If the size of the inclusions is very small compared to the wavelength of interest, then, the metamaterial is homogeneous.

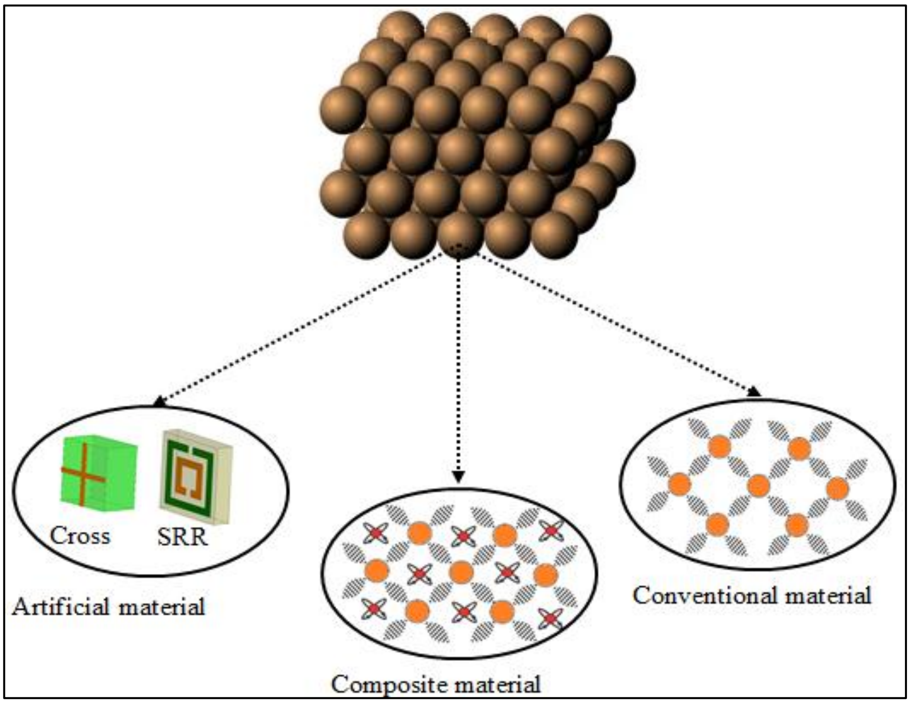

Figure 1-1 Unit cell types arranged in space compared to atomic scale in conventional materials

1.3 Historical points for metamaterials

The word ‘metamaterial’ first appeared in literature in 2000 when Smith et al. published their seminal paper on a structured material with simultaneously negative permeability and permittivity at microwave frequency. Other sources suggest that the term ‘metamaterial’ was first coined by Rodger M. Walser, a physics professor at the University of Texas in 1999 [1].

There are three fundamental papers that should be mentioned in metamaterial history. The first one is Veselago’s paper on left handed materials. This paper studied the unusual phenomena to be expected in a hypothetical left handed substance in which the field vectors $\vec{E}$, $\vec{H}$ and the wave vector $\vec{k}$ form a left handed system. The paper also explicitly presented the required material parameters to achieve the material simultaneously negative values of permittivity and permeability. The second one consists of the first experimental demonstration of a Veselago medium by Smith et al. which represents a passage from a theoretical prediction to experimental validation. The third paper is Pendry’s work on a perfect lens which represents the initial attempt to fill the gap between novel metamaterials and exciting applications [1].

1.4 Metamaterial characteristics

Metamaterial structural unit cell can be tailored in shape, size and their composition. The unit cells can be placed in a periodic or random manner to achieve a prescribed response.

The dependence of metamaterial properties on the unit cell architecture provides a great flexibility to tailor their electromagnetic responses, which are described by the effective constitutive parameters (effective dielectric permittivity and magnetic permeability). So, by varying different unit cell geometry parameters, we can design a metamaterial which responds to an electromagnetic field and can be tailored to meet a desired profile. Tailoring electromagnetic response is one of the important applications of metamaterials.

1.5 Metamaterial classes

There are several interesting classifications of metamaterials. In this work, we are interested by that based on the criterion of the effective (ε and μ) parameters signs. The figure 1-2 illustrates all possible properties that have a metamaterial in the ε– μ domain.

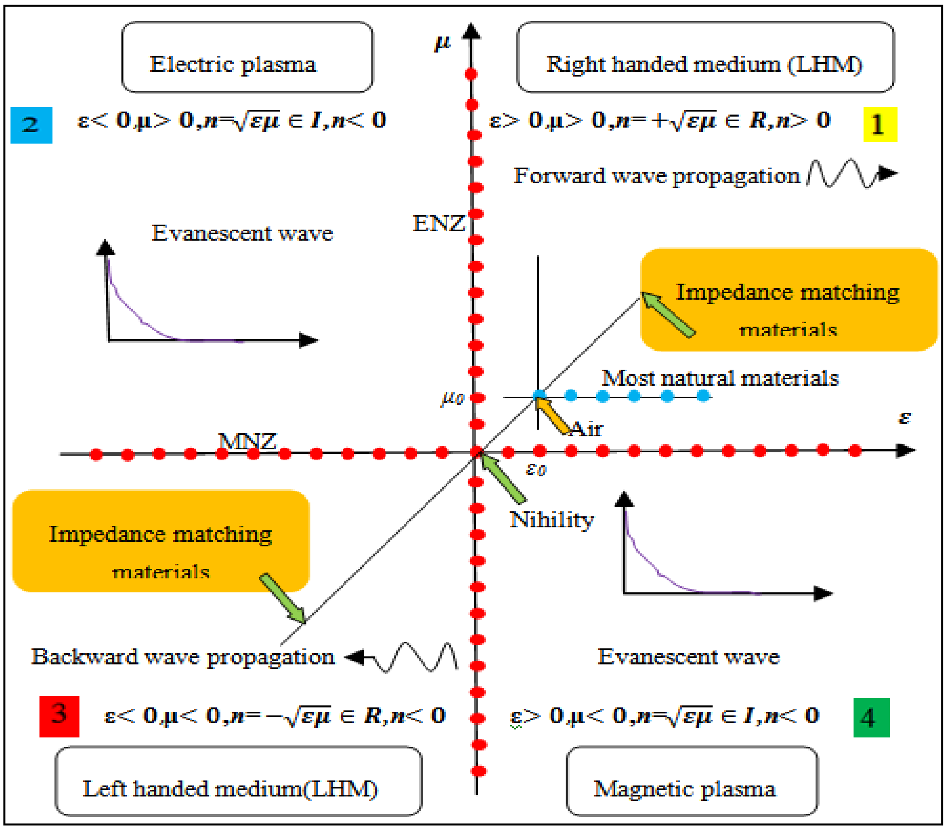

Figure 1-2 Metamaterial classes in the $\varepsilon - \mu$ domain.

The metamaterial constitutive parameters are the effective permittivity ε_r and permeability μ_r which are related to the refractive index n by:

$$n = \sqrt{\varepsilon_r \mu_r} \tag{1-1}$$

For simplicity, we consider a lossless medium ($\varepsilon_r'' = 0$, $\mu_r'' = 0$). So, depending on the signs of ε_r and μ_r, four possible couples can be considered.

- Case 1: $\varepsilon_r > 0$, $\mu_r > 0$

From equation (1-1), we have

$$n = \sqrt{\varepsilon_r \mu_r} > 0 \tag{1-2}$$

$$k = \omega\sqrt{\varepsilon_r \mu_r} = k_0 n \tag{1-3}$$

The expression of a propagating plane wave in such media is written as:

$$\vec{E} = \overrightarrow{E_0}\exp(-jkz) = \overrightarrow{E_0}\exp(-j\beta z) \tag{1-4}$$

Then, we have clearly a propagating waves (propagating medium). In figure 1-2, the first quadrant ($\varepsilon_r > 0$, $\mu_r > 0$) represents right handed materials (RHM), which support the forward propagating waves. From the Maxwell's equations, the electric field $\vec{E}$, the magnetic field $\vec{H}$, and the wave vector $\vec{k}$ form a right handed system.

- Case 2: $\varepsilon_r < 0$, $\mu_r > 0$

$\varepsilon_r < 0 \Rightarrow \varepsilon_r = -|\varepsilon_r|$ and $\mu_r > 0 \Rightarrow \mu_r = |\mu_r|$

From equation (1-1), we have

$$n = \sqrt{-|\varepsilon_r||\mu_r|} = j\sqrt{|\varepsilon_r||\mu_r|} \tag{1-5}$$

$$k = \omega\sqrt{\varepsilon_r \mu_r} = j\omega\sqrt{|\varepsilon_r||\mu_r|} \tag{1-6}$$

In general, we can write the complex propagation constant γ as:

$$\gamma = jk = j\omega\sqrt{\varepsilon_r \mu_r} = \alpha + j\beta \tag{1-7}$$

Replacing equation (1-6) in equation (1-7), we find:

$$\gamma = j\omega j\sqrt{|\varepsilon_r||\mu_r|} = \alpha + j\beta \tag{1-8}$$

By identification of (1-7) and (1-8), we find

$$\beta = 0 \text{ and } \alpha = -\omega\sqrt{|\varepsilon_r||\mu_r|} = \gamma \tag{1-9}$$

From equation (1-4), the expression of the propagating plane wave in such medium is:

$$\vec{E} = \overrightarrow{E_0}\exp(-\alpha z) \tag{1-10}$$

With ($\alpha < 0$), the last equation characterizes amplified evanescent waves inside left handed medium (LHM) which are discovered in 2000 by Pendry in his work on focusing and super resolution by LHM slab [2].

The second quadrant in figure 1-2 ($\varepsilon_r < 0$ and $\mu_r > 0$) when ($\alpha < 0$) denotes the electric plasma, which supports evanescent waves. For example, noble metals (gold and silver) have these properties in the infrared (IR) and visible frequency domains.

- Case 3: $\varepsilon_r < 0$, $\mu_r < 0$

$\varepsilon_r < 0 \Rightarrow \varepsilon_r = -|\varepsilon_r|$ and $\mu_r < 0 \Rightarrow \mu_r = -|\mu_r|$

From equation (1-1), we have

$$n = \sqrt{-|\varepsilon_r| \times -|\mu_r|} = \sqrt{|\varepsilon_r||\mu_r|} \tag{1-11}$$

$$k = \omega\sqrt{\varepsilon_r\mu_r} = \omega\sqrt{|\varepsilon_r||\mu_r|} \tag{1-12}$$

Comparing equations (1-7) and (1-12), then we obtain :

$$\alpha = 0 \text{ and } \beta = \omega\sqrt{|\varepsilon_r||\mu_r|} = \gamma \tag{1-13}$$

Then, the expression of the electric field corresponds to the propagating waves and can be written as:

$$\vec{E} = \overrightarrow{E_0}\exp(-jkz) = \overrightarrow{E_0}\exp(-j\beta z) \tag{1-14}$$

This third case is the well known left handed materials (LHM), which was proposed by Veselago in 1968, supporting the backward propagating waves (third quadrant in figure 1-2). In LHM, the electric field $\vec{E}$, the magnetic field $\vec{H}$, and the wave vector $\vec{k}$ form a left handed system.

- Case 4: $\varepsilon_r > 0$, $\mu_r < 0$

$\varepsilon_r > 0 \Rightarrow \varepsilon_r = |\varepsilon_r|$ and $\mu_r < 0 \Rightarrow \mu_r = -|\mu_r|$

From equation (1-1)

$$n = \sqrt{-|\varepsilon_r||\mu_r|} = j\sqrt{|\varepsilon_r||\mu_r|} \quad (1\text{-}15)$$

$$k = \omega\sqrt{\varepsilon_r\mu_r} = j\omega\sqrt{|\varepsilon_r||\mu_r|} \quad (1\text{-}16)$$

Comparing equations (1-7) and (1-16), we find

$$\beta = 0 \text{ and } \alpha = -\omega\sqrt{|\varepsilon_r||\mu_r|} = \gamma \quad (1\text{-}17)$$

From equation (1-4), the expression of the propagating plane wave in such medium is:

$$\vec{E} = \overrightarrow{E_0}\exp(-\alpha z) \quad (1\text{-}18)$$

With ($\alpha < 0$), the last equation characterizes also, the amplified evanescent waves in LHM.

The fourth quadrant (ε_r>0 and μ_r<0), in figure 1-2, represents magnetic plasmas like gyrotropic materials which support evanescent waves ($\alpha < 0$).

In figure 1-2 most natural materials only occur at certain discrete points on the line $\mu = \mu_0$ and $\varepsilon \geq \varepsilon_0$ and seldom natural electric plasma and magnetic plasma occur in very small parts in the second and fourth quadrants.

Most of material properties have to be realized using metamaterials, even for RHM. In a long period time, metamaterials, LHM, negative refractive index materials (NIM), double negative materials (DNG), and backward wave materials have been regarded as the same terms.

Metamaterials have much broader scope than LHM, as shown in figure 1-2. In the $\varepsilon - \mu$ domain, there are several special lines and points indicating special material properties. For example, the point $\mu = -\mu_0$ and $\varepsilon = -\varepsilon_0$ represents an antiair in the LHM region, which will produce a perfect lens; the point $\mu = 0$ and $\varepsilon = 0$ represents a nihility, which can yield a perfect tunneling effect, the line $\mu = -\varepsilon$ in both RHM and LHM regions represents impedance matching materials, which have perfect impedance matching with air, resulting no reflections. Also, the vicinity of $\mu = 0$ is called as μ near zero (MNZ) material, and the vicinity of $\varepsilon = 0$ is called as ε near zero (ENZ) material, which has special properties applied in perfect lens [2].

1.6 Artificial dielectrics

Artificial dielectrics, the first known metamaterials, usually consist of artificially created molecules: dielectric or metallic inclusions of a certain shape (figure 1-3). These • molecules can be distributed and oriented in space, either in a regular lattice or in a random manner.

The dimensions of the molecules and characteristic distances between neighboring ones are assumed to be very small, as compared to the wavelength. In artificial materials, the size of a single inclusion is usually much larger than those of real molecules and lattice periods of natural crystals. The electromagnetic waves see the inclusions as homogeneous medium. Then, we can describe it in terms of effective material parameters as well as apply the classic Maxwell's equations on these artificial dielectrics formed macroscopically.

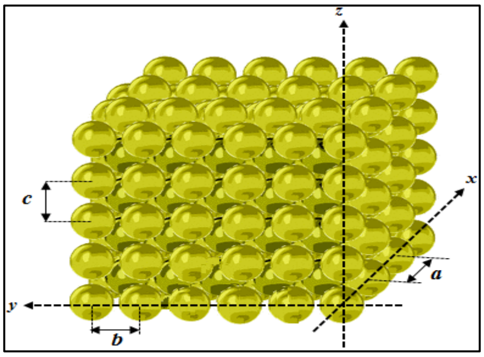

Figure 1-3 The geometry of a generic artificial dielectric.

The concept of artificial dielectrics was perhaps first introduced in [3], who used it to design low weight dielectric lenses at microwave frequencies. Metallic inclusions of various shapes with sizes that are small compared to the wavelength are used to artificially produce a high permittivity material. A very interesting example of artificial dielectrics is the wire medium, which has been known since 1950s. It is formed by a regular lattice of conducting wires.

1.7 Microscopic view of metal thin wire

Based on the effective medium theory, metamaterials can be characterized by effective electric permittivity and magnetic permeability. Pendry realized the artificial electric plasma using a metallic wire medium whose permittivity is negative [4] and the artificial magnetic plasma whose permeability is negative [5]. Metamaterials open a door to realize all possible material properties (desired electromagnetic properties tailoring) by designing different unit cells and using different substrate materials [6]. The various, usual and unusual material parameters provided by metamaterials ($\varepsilon_{eff} > 0$, $\mu_{eff} > 0$, $\varepsilon_{eff} < 0$, $\mu_{eff} < 0$, $\varepsilon_{eff} \approx 0$, μ_{eff} and $n \approx 0$ ...), lead to many interesting phenomena and applications.

The metal thin wire unit cell, presented in figure 1-4 (b), exhibits a plasmonic type permittivity frequency function of the form [7]:

$$\varepsilon_{reff}(\omega) = 1 - \frac{\omega_{pe}^2}{\omega^2 - j\Gamma_e\omega} \tag{1-19}$$

In real and imaginary parts, plotted in figure 1-4 (c), equation (1-19) becomes:

$$\varepsilon_{reff}(\omega) = 1 - \frac{\omega_{pe}^2}{\omega^2 + \Gamma_e^2} + j\frac{\Gamma_e\omega_{pe}^2}{\omega(\omega^2 + \Gamma_e)} \tag{1-20}$$

Where ω_{pe} and Γ_e are the electric plasma frequency and the damping factor due to metal losses respectively.

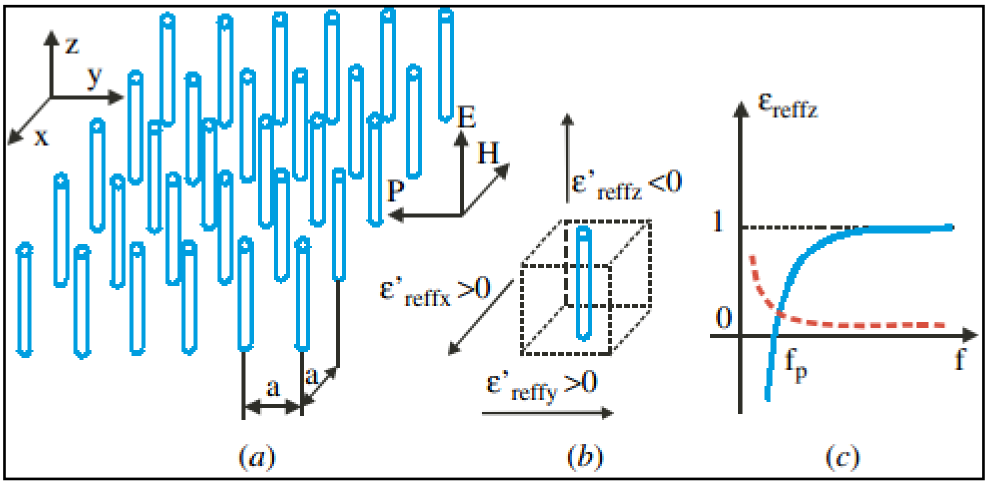

Figure 1-4 a) 2 D thin wires arrangement, b) Thin wire unit cell, and c) Real (solid blue) and imaginary (dashed red) parts of effective permittivity of metamaterial (a) [8].

The Drude parameters ω_{pe} and Γ_e are expressed in function of the geometric dimensions (the period $\boldsymbol{a}$ and the radius of the wire $\boldsymbol{r}$), the analytic procedure is detailed in [9]

$$\omega_{pe} = \sqrt{\frac{2\pi c^2}{a^2 \ln(a/r)}} \tag{1-21}$$

$$\Gamma_e = \varepsilon_0 \left(\frac{a\omega_{pe}}{\pi\sigma r^2}\right) \tag{1-22}$$

where c is the speed of light and σ is the conductivity of metals.

We observe from equation (1-20) that $Re(\varepsilon_{reff}) < 0$ for $\omega < \sqrt{\omega_{pe}^2 - \Gamma_e^2}$. It means that if there are no collisions, the free electrons movements are in phase of 180° with respect to the applied electric field. In this frequency band, the propagation is not possible and the wave is evanescent and it's completely reflected on the medium surface.

1.8 Artificial magnetic materials

Artificial magnetic materials are typically synthesized by using resonant elements, such as split ring resonators or Swiss rolls (as shown in figure 1-5). The split ring resonators are more widely used than the Swiss rolls since they can be manufactured using printed circuit technology. Artificial magnetic materials were known as far back as the early 1950s, and a book by Schelkunoff and Friis [10] provides expressions that can be used to calculate the magnetic flux of a split metallic wire loaded with a small capacitor, formed by a pair of parallel metallic plates. Schneider in [11] used a split metallic tube to produce an NMR probe, and in [12], Hardy proposed a Swiss roll resonator to achieve magnetic resonance at [200-2000] MHz. Kostin in [13] has synthesized an artificial magnetic material with frequency dependent positive permeability using a double circular ring resonators.

An artificial magnetic material, which is formed by split ring resonators, possesses negative permeability within a frequency band (bandwidth is typically narrow) near the resonant frequency of the single split ring resonator and it is widely used to create LHMs.

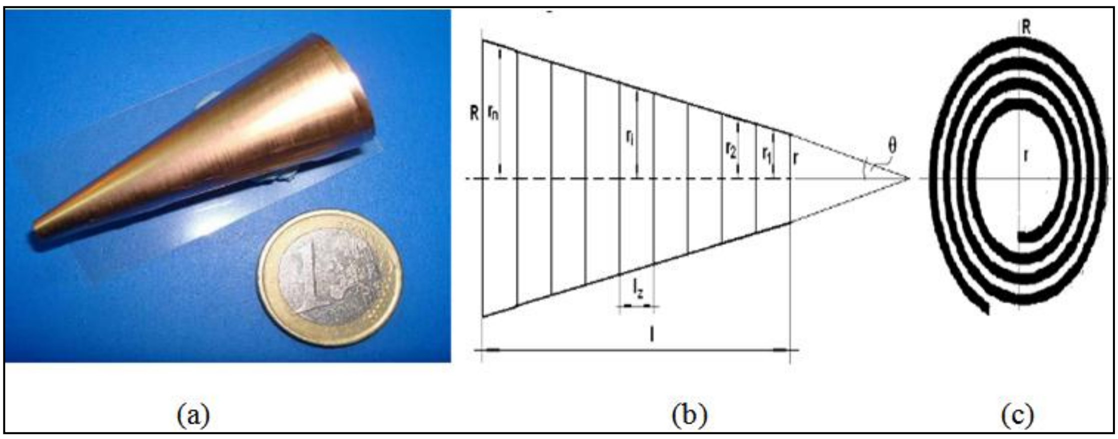

Figure 1-5 a) Conical Swiss roll unit cell, b) Transversal view, and c) Cross section.

1.9 Microscopic view of split ring resonator (SRR)

The SRR in figure 1-6 (b) exhibits a frequency dependent permeability of the form [7]:

$$\mu_{reff}(\omega) = 1 - \frac{\omega_{pm}^2}{\omega^2 - \omega_{0m}^2 + j\Gamma_m\omega} \qquad (1\text{-}23)$$

Where ω_{0m}, ω_{pm} and Γ_m are, respectively, the magnetic resonance frequency, magnetic plasma frequency and the damping factor due to metal losses.

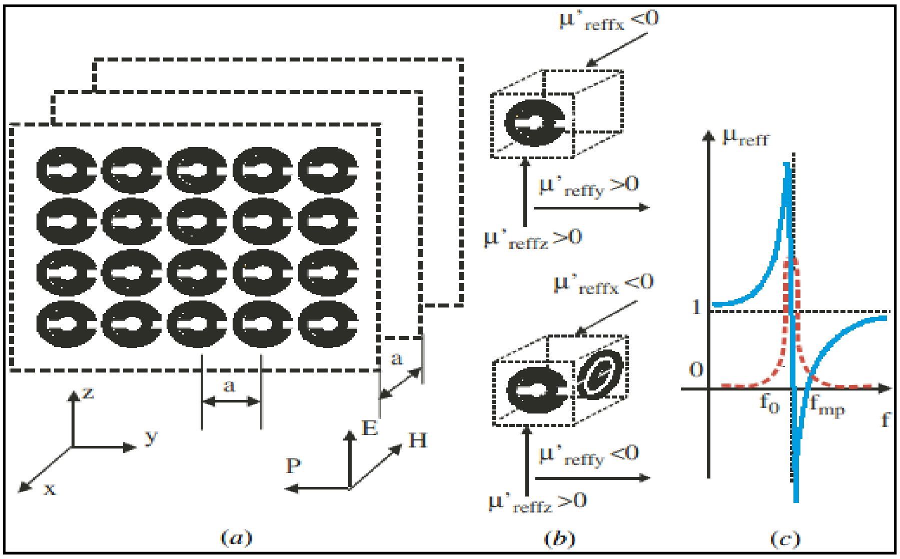

Figure 1-6 a) Array of SRR, b) SRR of 1 D and 2 D unit cells, and c) Re (μ_{reff}) (solid blue), Im (μ_{eff}) (dashed red) [8].

Equation (1-23) is divided in real and imaginary parts which are presented in figure 1-6 (c):

$$\mu_{reff}(\omega) = 1 - \frac{F(\omega^2 - \omega_{0m}^2)}{(\omega^2 - \omega_{0m}^2) + (\omega\Gamma_m)^2} + j\frac{\Gamma_m\omega_{pm}^2}{(\omega^2 - \omega_{0m}^2) + (\omega\Gamma_m)^2} \qquad (1\text{-}24)$$

Lorentz parameters are calculated in detailed manner in [5], they can be written as:

$$F = \sqrt{\pi({}^{r}/_{a})^2} \qquad (1\text{-}25)$$

$$\omega_{0m} = c\sqrt{\frac{3a}{\pi \ln 2\left({}^{2wr^3}/_{\delta}\right)}} \qquad (1\text{-}26)$$

Where $\boldsymbol{r}, \boldsymbol{w}$ and $\boldsymbol{\delta}$ are the inner radius for the smaller ring, width of the ring and radial spacing between the rings respectively.

We have also:

$$\Gamma_m = \frac{2aR'}{r\mu_0} \tag{1-27}$$

$\boldsymbol{R'}$ is the metal resistance per unit length.

We observe from equation (1-24) that $\mu_{reff} < 0$ for $\omega_{0m} < \omega < \frac{\omega_{0m}}{\sqrt{1-F}} = \omega_{pm}$. It means that if there are no collisions, the free electrons movements are in phase of 180° with respect to the applied magnetic field. In this frequency band, the propagation is not possible and the wave is evanescent.

1.10 Overview of metamareial applications

Due to the exciting and unusual features, metamaterials have found and are finding a lot of applications. Metamaterials can impact on communications, sensing and susceptibility across all wave types, but especially electromagnetics (radio waves to light) and acoustics

[14- 15], as it can be seen in figure 1-7.

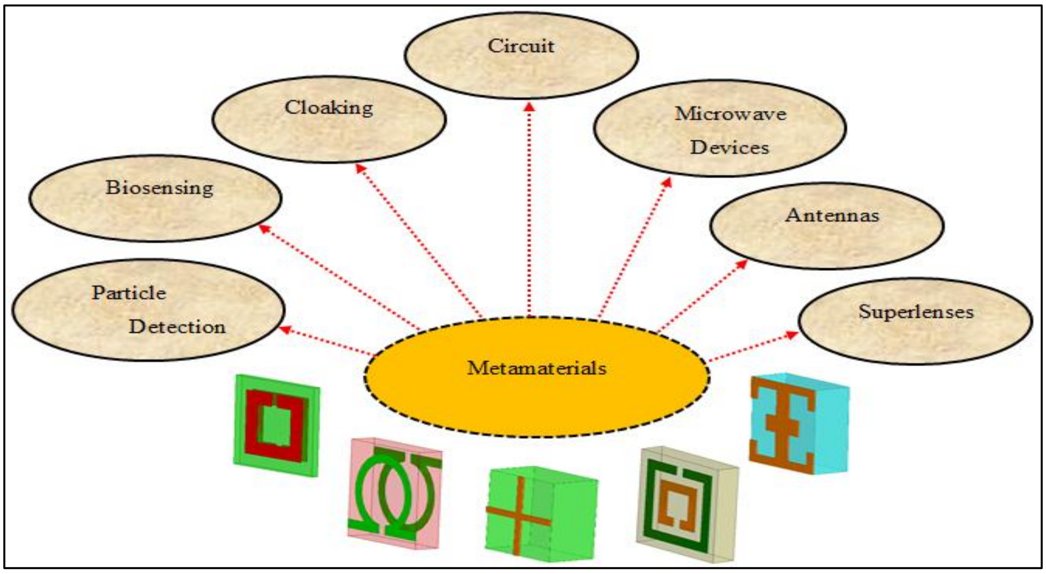

Figure 1-7 Some proposed metamaterials applications.

1.10.1 Superlenses

For LHM, the most attractive feature is the superlens, which can be widely used in super resolution medical imaging, optical imaging, and nondestructive detections [2]. A superlens or perfect lens is a lens which uses metamaterials to go beyond the diffraction limit [16]. The diffraction limit is an inherent limitation in conventional optical devices or lenses.

In 2000, a type of lens was proposed, consisting of a metamaterial that compensates for wave decay and reconstructs images in the near field and most importantly the both propagating and evanescent waves contribute to the resolution of the image (figure 1-8). In 2004, the first superlens with a negative refractive index provided resolution three times better than the diffraction limits and was demonstrated at microwave frequencies. In 2005, the first near field superlens which exceeded the diffraction limit was demonstrated [17]. The higher focusing resolution will be provided by flat LHM lens if compared to convex dielectric lens and elliptical reflector focusing system. The LHM lens has the potential to acquire higher imaging resolution and easy in depth scanning, which will simplify the detection system design.

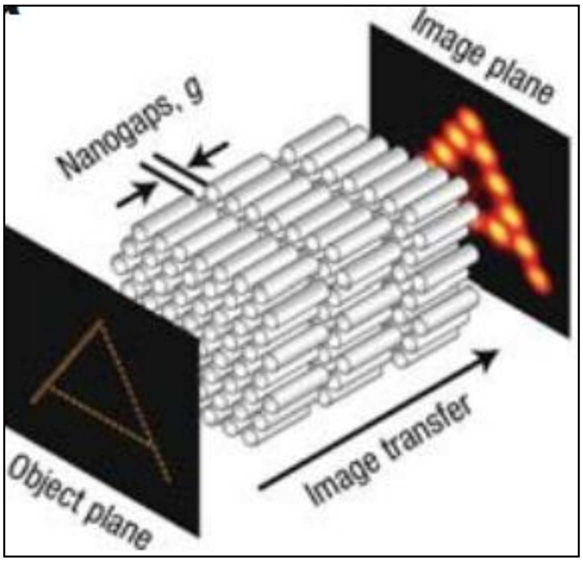

Figure 1-8 Super resolution imaging using a metamaterials nanolens.

For example in biological domain, microwaves are used to destroy or ablate diseased soft tissue by heating the tissue to a temperature that causes cell death. This is called hyperthermia. The generator produces microwave energy which is transmitted through the antennas into the patient. Elevating the temperature of tumor cells causes cell membrane damage, which leads to the destruction of the cancer cells. Hyperthermia treatment of cancer requires directing a carefully controlled dose of heat to the cancerous tumor and surrounding body tissue. The most prominent property of metamaterial lens is the ability of negative refractive index (NRI) to focus the electromagnetic field of a source. Hence it can generate appropriate focusing spot in biological tissue as required in microwave hyperthermia treatment. Flat metamaterial slab has been used as a lens to focus microwave energy emitted from the microwave source. In this application, a planar array of split-ring resonators placed between two parallel metallic plates and is fed by a small loop antenna to excite the split-rings. Recently, conformal microwave array applicators with proper source spacing and low loss LHM lens were used for hyperthermia treatment [17].

1.10.2 Antennas

Metamaterial antennas can enhance or increase performances of a system. It increases the radiated power of an antenna. Materials which can attain negative magnetic permeability provide many properties such as an electrically small antenna size, high directivity, and tunable operational frequency. Furthermore, metamaterials based antennas can demonstrate efficiency bandwidth performance.

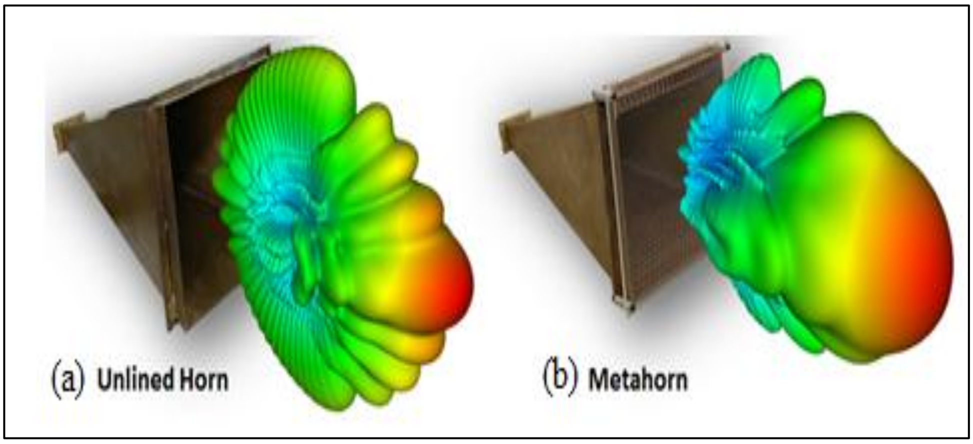

Figure 1-9 The rectangular horn antenna: a) alone, and b) with metamaterial.

Metamaterials employed in the ground planes surrounding the antennas offer improved isolation between radio frequency or microwave channels of Multiple-Input Multiple-Output (MIMO) antenna arrays. Metamaterial, high impedance ground planes can also be used to improve the radiation efficiency (figure 1-9), and axial radio performance of low profile antennas located close to the ground plane surface. They have also been used to increase the beam scanning range using both the forward and backward waves in leaky wave antennas. Various metamaterial antenna systems can be employed to support surveillance sensors, communication links, navigation systems, command and control systems [16].

The gradient refractive index metamaterials are also utilized to produce beam bending and beam focusing lenses. Based on such properties, high gain, and broadband gradient, planar lens and Luneberg like lens antennas have been proposed and realized [2]. The

Industrial, Scientific and Medical (ISM) radio bands are portions of the radio spectrum reserved internationally for the use of radio frequency (RF) energy for industrial, scientific and medical purposes other than communications. By using EBG (Electromagnetic Band Gap) structures in slotted microstrip antenna, increased efficiency and better return loss characteristics can be achieved. A patch antenna with slotted ground plane has been developed in which EBG structure is used as a metamaterial above the ground plane [17].

1.10.3 Microwave devices

Planar metamaterials which are composed of complimentary structures have been used to design microwave components like filters, power dividers, and phase shifters [8]. Narrowband and broadband polarizers have been realized using three dimensional (3 D) anisotropic metamaterials [2] (figure 1-10).

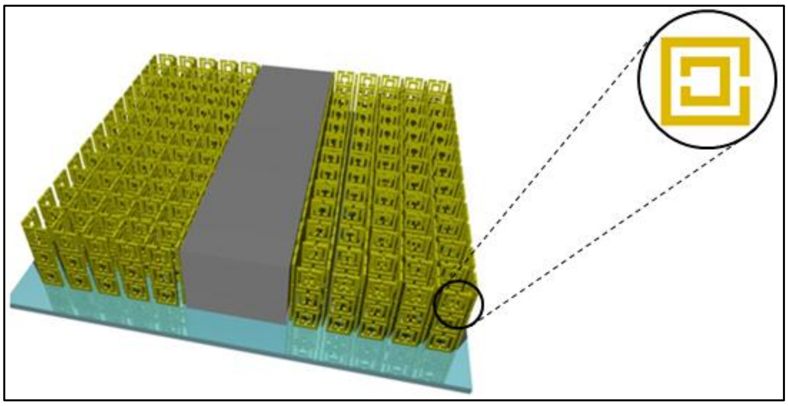

Figure 1-10 A planar waveguide with double SRR metamaterial.

Superconducting metamaterials have been achieved in addition to superconducting split rings and wires. They have been utilized to realize a number of unique applications [18]. The combination of left and right handed propagation media creates new type of resonant structures by laminating two materials with opposite senses of phase [8]. This material is used to design an ultra-compact resonator whose overall dimensions are unconstrained by the wavelength of the resonant wave. The proposed resonator consists of two flat conducting plates separated by a sandwich of left handed and right handed metamaterials. A wave propagating in the direction normal to the plates will suffer a combination of forward and reverse phase windings before reaching the other reflecting boundary. Under these conditions, the wave could undergo a net phase shift of zero radians and still create a resonance condition.

The net phase shift could also be a positive or negative multiple of 2π radians [18] as well, each creating a resonant condition.

Superconductors are particularly attractive for use in ultra-compact resonators and showed resonances with indices between +2 and -6, including zero, over the broad frequency range from about 5 to 24 GHz [18]. Quality factors of the negative order resonances were on the order of 3000 at 30 K, while those for positive order resonances were below 400.

1.10.4 Cloaking

Cloaking devices still attract more and more attention, particularly in the military field. The successful demonstrations of invisible cloaks experimentally in the microwave regime open the possibility to realize cloaking devices [2]. Metamaterials are a basis for attempting to build practical cloaking devices. The cloak deflects microwave rays, so they circumvent the object inside with little distortion (figure 1-11), making it appears almost as if nothing were there at all. Such a device typically involves surrounding the object to be cloaked with a shell which affects the passage of light near it [16].

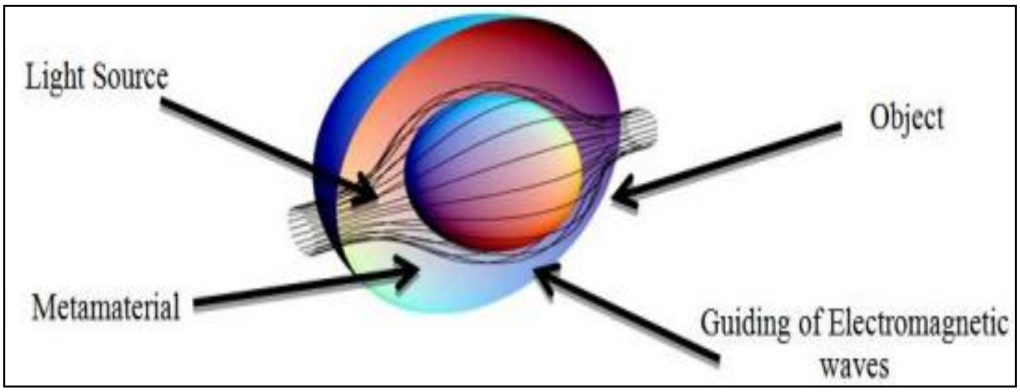

Figure 1-11 Invisibility cloaks.

1.10.5 Absorbers

Specific absorption rate is a measure of how much radiation is absorbed by human body. The basic principle behind the metamaterial absorbers (figure 1-12) is, when one of the effective medium parameter is negative and the other is positive, the medium will display a stop band. The stop band of metamaterials can be designed at operating bands of cellular phone. The unit cells are designed to operate at certain frequency band. The structure parameters of unit cells are chosen in order to behave as an effective medium with negative refraction index around this frequency band [17]. The metamaterials can be designed on circuit board, so it may be easily integrated to the cellular phones [17].

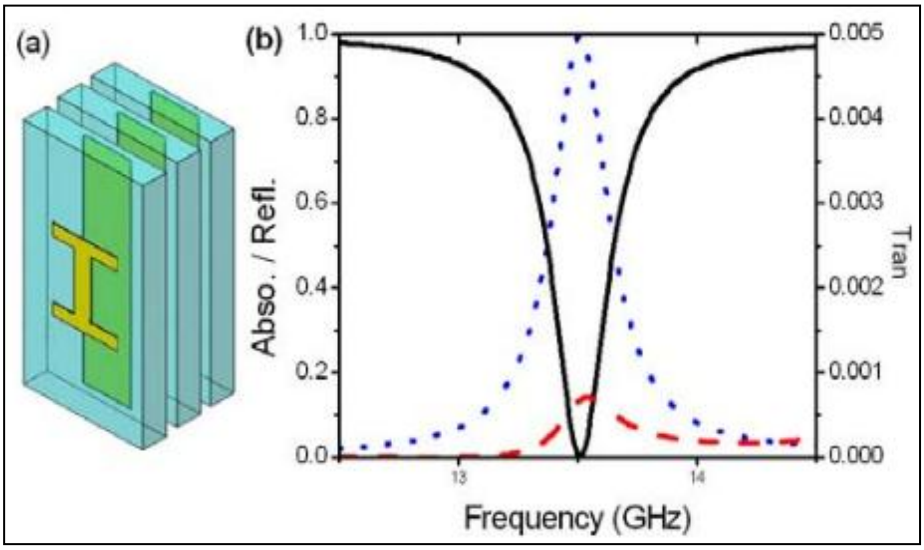

Figure 1-12 a) Three layer model of the simplified absorber structure, b) Properties of the perfect absorber structure: reflectance, absorbance, and transmittance (solid, dotted and dashed curves) [19].

1.10.6 Acoustic metamaterials

Acoustic metamaterials are designed to control, direct, and manipulate sound in the form of sonic, infrasonic, or ultrasonic waves (figure 1-13), as these might occur in gases, liquids, and solids [16]. They can be used to cloak objects or vehicles from radar, sonar, or other sound detection systems [20].

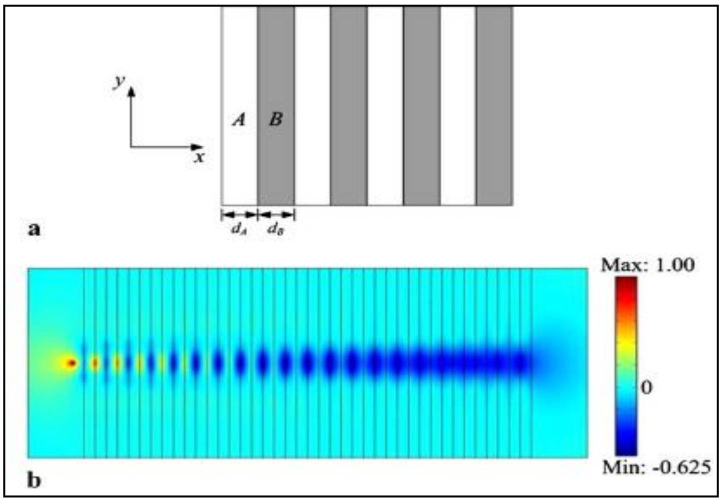

Figure 1-13 a) Alternating layered structure to implement the anisotropic material, b) Finite element simulation of acoustic straight waveguide consisting of the alternating layered structure [21].

1.11 Microwave filters

To design compact microwave filters, different resonant and non resonant metamaterial unit cells are useful for the tailoring of narrow and wide band pass filters [8] like the rectangular waveguide. The rectangular waveguide has a width ***d***, filled with general metamaterial. It has an isotropic permittivity and a uniaxial anisotropic permeability as shown in figure 1-14. Assuming that the propagating waves are TE modes and the filling material is lossless ($\varepsilon_r'' = 0 = \mu_r''$). The dispersion equation can be written as [8]:

$$\frac{k_x^2}{\mu_{lr}} + \frac{k_y^2}{\mu_{tr}} = \varepsilon_r k_0^2 \tag{1-28}$$

Then, the expression for the longitudinal propagation factor, in the lossless case, can be written as:

$$k_y = \pm k_0 \sqrt{\varepsilon_r^{'} \mu_{tr}^{'} \left[1 - \left(\frac{f_c}{f}\right)^2\right]} = \beta_y \tag{1-29}$$

Where: f, $f_c = \frac{f_{c_0}}{\sqrt{\varepsilon_r^{'} \mu_{lr}^{'}}}$ and $f_{c_0} = \frac{mc}{2d}$ are respectively, the frequency of the signal, the cutoff frequencies of an empty waveguide and the same one filled with matamterial.

$(m = 1, 2, 3 \ldots)$.

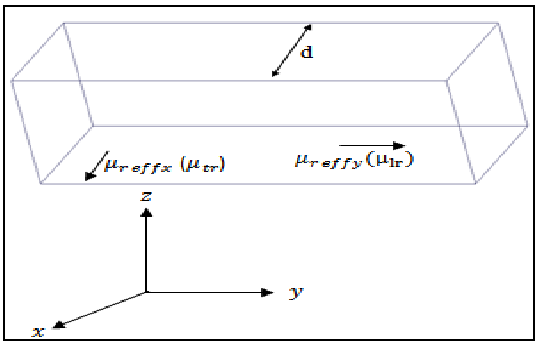

Figure 1-14 Waveguide filled with metamaterial.

Now, we analyze the influence of the effective parameters signs on the propagation of waves in the filled waveguide. There are four different cases:

- Case 1 ($\varepsilon_r' > 0, \mu_{tr}' > 0, \mu_{lr}' > 0$)

In the familiar case of an isotropic double positive (DPS) material, the physically meaningful solution ($\alpha_y > 0$) for $f > f_c$ is given by the positive sign of the square roots in equation (1-29) for lossless case. This solution has a positive phase factor ($\beta_y > 0$); hence, the propagation is described by forward waves. Below the cutoff frequency ($f < f_c$), the wave vector component k_y becomes imaginary in the lossless case; hence, there is no propagation.

One notices that a waveguide filled with anisotropic DPS material shows a high pass behavior as shown in figure 1-15.

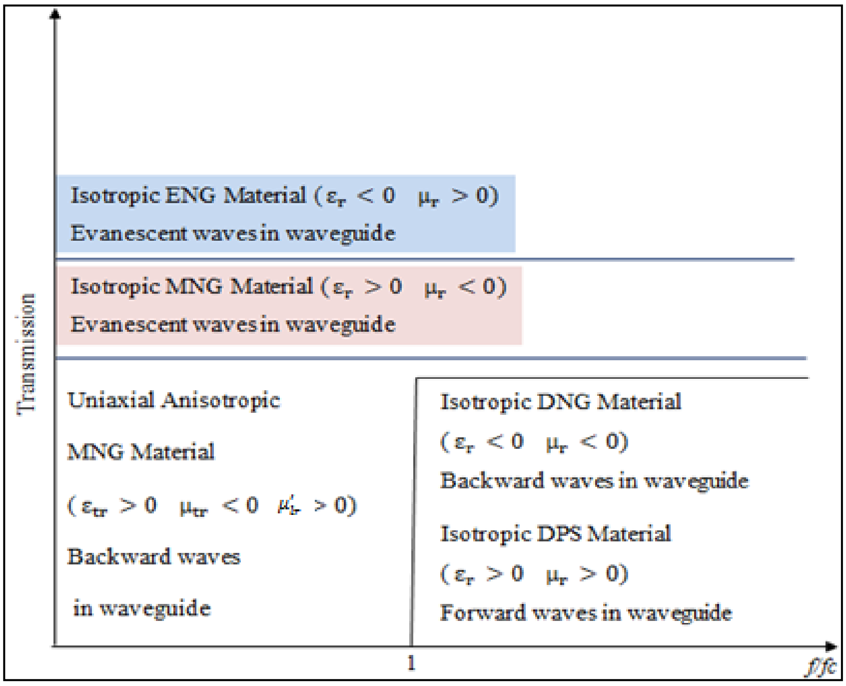

Figure 1-15 A metamaterial waveguide transmission bands for different material parameters sign.

- Case 2 ($\varepsilon_r' < 0, \mu_r' > 0$) or ($\varepsilon_r' > 0, \mu_r' < 0$)

A similar analysis shows that there is no wave propagation for all frequencies (both for $f < f_c$, and $f > f_c$) if a waveguide is filled either with an isotropic epsilon negative (ENG) material or with an isotropic mu negative (MNG) material (figure 1-15).

- Case 3 ($\varepsilon_r' < 0, \mu_r' < 0$)

In the case of an isotropic double negative DNG material, the solution of the wave vector component has a negative sign of the square root in the lossless case in equation (1-29) for frequencies above the cutoff frequency ($f > f_c$). The phase factor $\beta_y < 0$ in equation (1-29) indicates that the propagation is described by backward waves. Below the cutoff frequency ($f < f_c$), the sign of the square root is positive and the wave vector k_y is imaginary, in the lossless case (1-29). Thus, there is no wave propagation below the cutoff frequency and the waveguide again shows the high pass behavior (but with backward wave propagation above the cutoff frequency as shown in figure 1-15).

➢ Case 4 ($\varepsilon_r' > 0, \mu_{tr}' < 0, \mu_{lr}' > 0$)

A very interesting case occurs if the waveguide is filled with a uniaxial mu negative (MNG) material with negative transversal permeability. In the lossless case, the physically meaningful solution ($\alpha_y > 0$) above the cutoff frequency ($f > f_c$) is given by the negative sign of the square root in equation (1-29). The wave vector component k_y becomes imaginary. There is no wave propagation above the cutoff frequency. On the contrary, below the cutoff frequency ($f < f_c$), the solution of the square root in equation (1-29) has a negative $\beta_y < 0$ sign in the lossless case. Consequently, in this case, the wave propagation is now possible below the cutoff frequency. This propagation is in the form of backward waves. From figure 1-15, it is possible that the TE modes can propagate below the cutoff frequency. Hence, a waveguide filled with a uniaxial MNG material with negative transversal permeability exhibits a low pass behavior.

1.12 Frequency Selective Surface (FSS)

The frequency selective surfaces (FSS) (figure 1-16) are periodic structures in either one or two dimensions (singly or doubly periodic structures). Figure 1-17 illustrates some inclusion shapes used in FSS designing.

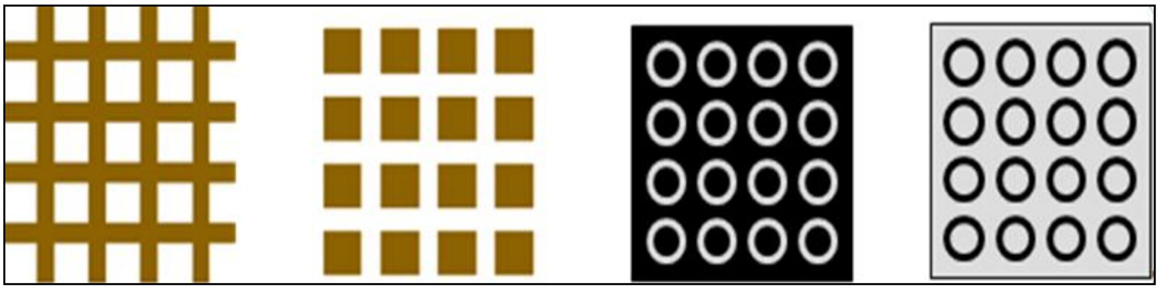

Figure 1-16 Different FSS structures [22-23].

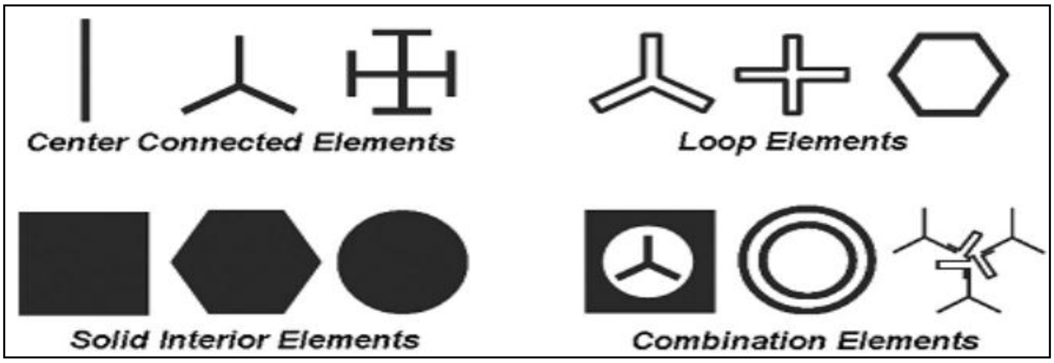

Figure 1-17 Different FSS inclusion shapes.

The FSS found their applications in radomes, reflectors, filters (figure 1-18 illustrates some frequency responses of different filter types based on FSS structures), absorbers and guiding TEM waves [24]. Also they are applied for [23]:

1- Selective shielding of the electromagnetic interference from high power microwave heating machines adjacent to wireless communication base stations,

2- Selective shielding of frequencies of communication in sensitive areas (military installations, airport, police.),

3- Protection from harmful electromagnetic radiation especially in the [2-3] GHz band in domestic environment, schools, hospitals etc. arising externally (wireless communication base stations) or internally (microwave ovens),

4- Control of radiation at unlicensed frequency bands (bluetooth applications, 2.45 GHz),

5- Picocellular wireless communications in office environments such as the Personal Handy phone System in offices where to improve efficiency each room needs to prevent leakage of radio waves into and of the room. This implies that windows, floor and ceiling need to be shielded. Kajima Research Institute is developing such a film to be applied to buildings,

6- Isolation of unwanted radiation. FSS windows can be incorporated in trains prevent mobile phone frequencies; around base station antennas to filter out unwanted radiation.

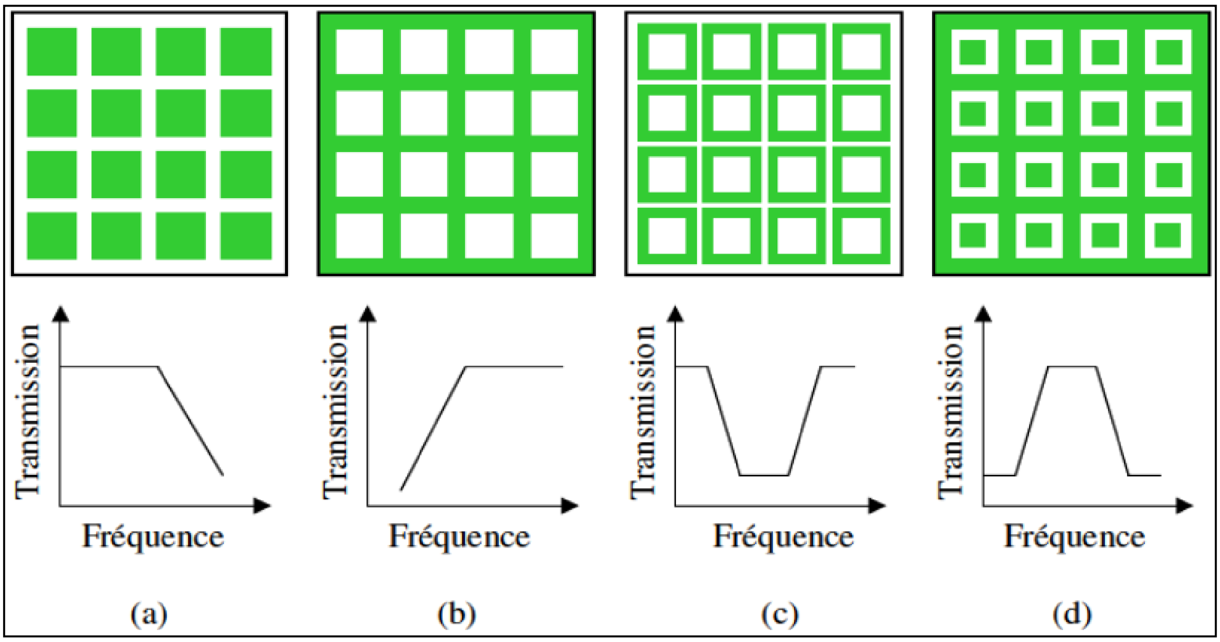

Figure 1-18 Filter types based on FSS [25].

1.13 Conclusion

Metamterials are artificial materials, their electromagnetic responses, which are the effective dielectric permittivity and effective magnetic permeability can be tailored and designed in request. These characteristics allow metamaterials to be useful. Consequently, metamaterials including FSS have many applications in different frequency domain such as: antennas, microwave devices, superlenses, absorbers, cloaks, filters and acoustics.

2. Effective parameters extraction of homogenized metamaterials

2.1 Introduction

The different applications and expected uses of metamaterials in electromagnetic engineering require a precise knowledge of their electromagnetic properties. So the metamaterial homogenization is an important step in the design process, because it is related to the environnemental scale and to the effective medium nature (isotropy, chirality …).

This chapter introduces the metamaterials homogenization. It is divided in two principal parts: the first one treats the effective medium properties and the homogenization criterion. The second one deals with the methods used to extract the effective electromagnetic parameters of the homogenized medium. This last is described by the effective dielectric permittivity ε, magnetic permeability μ and magnetoelectric coupling ξ_0. These effective parameters extraction methods use either the *S* parameters method or the field averaging (field summation) method in the material region of interest.

2.2 The effective media

All the electromagnetic phenomena are governed by Maxwell's equations, which are a set of equations describing the interrelationship between fields, sources, and material properties. Impinging fields in a system can influence the organization of electric and magnetic dipoles in a medium. Fields can induce polarization and magnetization to some degree, depending on the particular material involved. The electromagnetic properties of a material are described by the constitutive parameters which are the dielectric permittivity ε and the magnetic permeability μ. These physical quantities characterize the interaction between the matter constituting the medium, and the electromagnetic field in presence. Two other related parameters are the refractive index $n=\sqrt{\varepsilon\mu}$ and the wave impedance $z=\sqrt{\mu/\varepsilon}$. They are essentially macroscopic effective quantities because they are used to describe the overall average response of the material as a whole. Microscopically, a piece of crystal consists of atoms arranged in a periodic manner with a lattice constant of a few angstroms. On the atomic scale, in each atom or molecule, tiny electric dipoles can be excited by the electric component of incident wave, consequently the radiated energy in the dipoles occurs with a certain time delay. The excited dipoles create a periodic local field in the crystal, referred to as Lorentz local field; therefore the field distribution inside the crystal is certainly not uniform. However, the incident wave does not really feel the underlying inhomogeneity in the crystal, nor does it feel the processes of absorption and radiation. On the macroscopic scale, the detailed features and responses of the inhomogeneous structure are averaged, and relationships can be established between the macroscopic field vectors in Maxwell's equations, namely the electric field $\vec{E}$, the magnetic field $\vec{H}$, the electric displacement field $\vec{D}$, and the magnetic flux density $\vec{B}$. This is the origin of the permittivity and permeability parameters of materials. At different frequency range, this complicated physics is usually described using the transmittance and reflectance of waves with a certain retardation (delay). In addition, absorbed waves account for losses in the material and can be related to the imaginary parts of the complex constitutive parameters that are dielectric permittivity, magnetic permeability, and refractive index.

Similarly, the scale of inhomogeneities in a metamaterial is much smaller than the wavelength of interest, and the metamaterial design should ensure this. The inhomogeneity scale corresponds to the lattice constant of the artificial structure for the case of periodic metamaterial as shown in figure 2-1 (a). The size of the unit cell defines a new scale in the periodically structured metamaterial and substitutes the atoms and molecules of conventional materials[26-27].

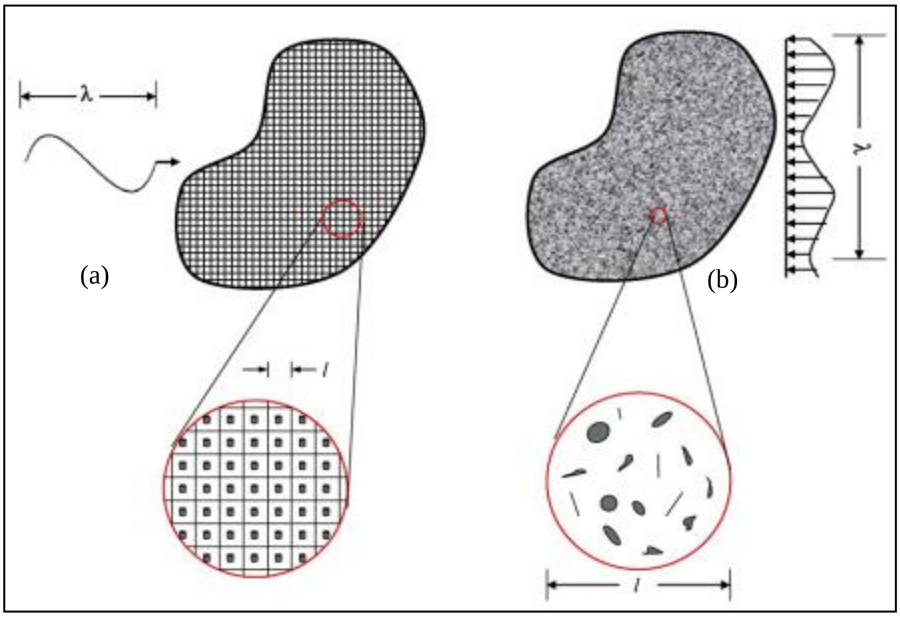

Figure 2-1 Composite material with: a). Periodic structure, b). Non periodic structure.

In the figure 2-1, the largest heterogeneity length scale ***l*** should be small enough compared to the smallest length scale λ. That is of physical importance. For a periodic medium, as shown in figure 2-1 (a), ***l*** is the unit cell size. For wave propagation problems, it is the smallest wavelength of interest. In a random medium as shown in figure 2-1 (b), it should be the smallest size of a sphere which at any position is a statistical representative of the entire body; a representative volume element (RVE). It may be defined as the smallest wavelength in the spatial Fourier expansion of the imposed excitation [28].

Then the key of homogenization is when the size of the unit cell is much smaller than the free space wavelength [26-29]. It is called the homogenization criterion: macroscopically, the metamaterial is seen as homogeneous medium as shown in (figure 2-2). Then, like in the treatment of conventional materials, the metamaterial electromagnetic response to external fields can be described using effective parameters including effective permittivity, effective permeability, refractive index and impedance.

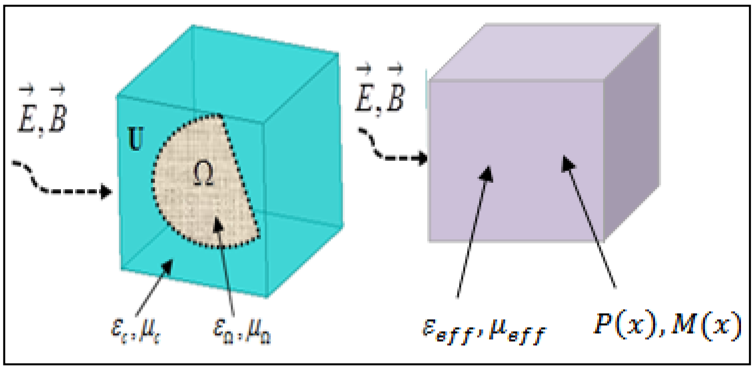

Figure 2-2 A two phase heterogeneous unit cell (left) and its equivalent to homogeneous unit cell with the imposed polarization fields P and M (right) [28].

This fact explains again why metamaterials made from basic constituents are identified as materials instead of devices [30]. From the point of view of Maxwell's equations, a material is a collection of sub wavelength units with global properties described by ε and μ. Through the dedicated design of meta-atoms, which is usually a metal dielectric structure, metamaterial research allows us to tailor the electromagnetic response of media in an unprecedented manner. Finally, there are cases such as bi-anisotropic media where the electromagnetic response is not described only with ε and μ tensors because of the complexity of the unit cells. Such structures may require additional material parameters like magneto-electric coefficients, which link the electric field vectors and the magnetic ones. Although some important metamaterial elements like split ring resonators are bi-anisotropic to some extent.

2.3Effective parameters extraction

If the spacing between scattering elements is much smaller than the operating wavelength, the metamaterial is homogenous and it responds to electromagnetic waves in a similar way [31]. It is possible to describe metamaterials as continuous materials [32]. In these conditions, they can be characterized by effective parameters without considering the local field distribution. This part of the chapter treats numerical homogenization approaches which are the *S* parameters extraction method (Fresnel inversion method) and the field summation method which is an averaging approach.

2.3.1The *S* parameters extraction (Fresnel inversion method)

The metamaterial effective parameters extraction requires two steps [36]:

1- Computation of the homogenized metamaterial forward and backward wave impedances (z^+, z^-) and complex refractive index (n) (figure 2-3),which are expressed in terms of reflection and transmission coefficients (S_{ij}).

2- Retrieval of the constitutive electromagnetic parameters (permittivity, permeability and magneto-electric coupling).

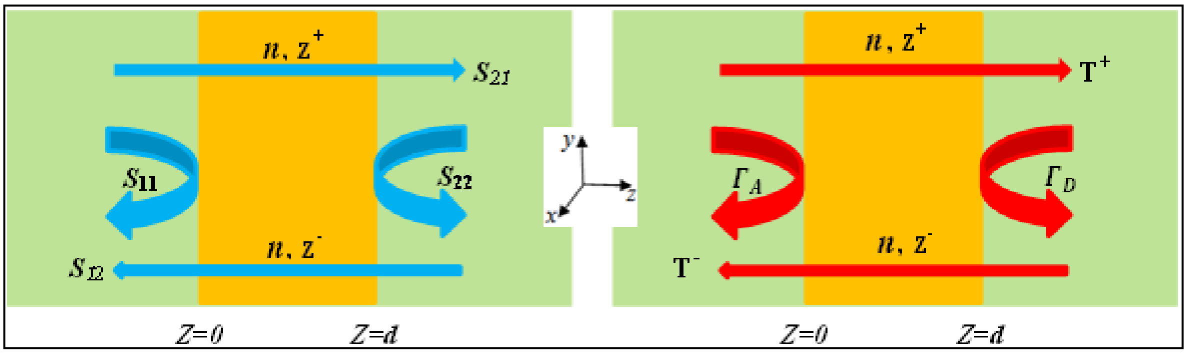

Figure 2-3 Transmission and reflection coefficients (S_{ij}) in the bianisotropic metamaterial.

2.3.2.1Metamaterial wave impedances and refractive index computation

In figure 2-3, a plane wave polarized in the *y* axis propagates along the *z* direction and is incident upon the structure. We suppose that the configuration in figure 2-3 has a bianisotropic property; the electric field in the *y* direction induces a magnetic dipole in the *x* direction, while the magnetic field in the *x* direction also induces an electric dipole in the *y* direction.

By assuming that the medium is reciprocal, and that the harmonic time dependence is $e^{-j\omega t}$, implying that $\varepsilon^{"} > 0$ and $\mu^{"} > 0$ simultaneously at all frequencies (we use primes and double primes for denoting real and imaginary parts of a quantity) the constitutive relations can be written ($\vec{E}$ - $\vec{H}$ or Tellegen representation) as:

$$\vec{D} = \overline{\overline{\varepsilon}}.\vec{E} + \overline{\overline{\xi}}\,\vec{H} \qquad (2\text{-}1)$$
$$\vec{B} = \overline{\overline{\varsigma}}.\vec{E} + \overline{\overline{\mu}}.\vec{H}$$

In equations system (2-1) $\vec{E}$, $\vec{H}$, $\vec{D}$, and $\vec{B}$ are, respectively, the electric and magnetic field intensities and flux densities. In these relations, the four material parameter tensors necessary to characterize the material are: the permittivity $\overline{\overline{\varepsilon}}$, the permeability $\overline{\overline{\mu}}$ and the magneto-electric coupling is expressed by two magneto-electric tensors $\overline{\overline{\xi}}$ and $\overline{\overline{\varsigma}}$. Note that the most general bi-anisotropic material requires 36 complex parameters for a full constitutive electromagnetic description. In reciprocal materials, the two magneto-electric tensors $\overline{\overline{\xi}}$ and $\overline{\overline{\varsigma}}$ are related by:

$$\overline{\overline{\xi}} = -\overline{\overline{\varsigma}}^{T} \qquad (2\text{-}2)$$

For bi-anisotropic and reciprocal media, the material constitutive parameters in equation system (2-1) can be written as:

$$\vec{D} = \overline{\overline{\varepsilon}}.\vec{E} + \left(\overline{\overline{\chi}}^{T} - j\,\overline{\overline{\zeta_0}}^{T}\right)\sqrt{\varepsilon_0\mu_0}\,.\vec{H} \qquad (2\text{-}3)$$
$$\vec{B} = \left(\overline{\overline{\chi}} + j\,\overline{\overline{\zeta_0}}\right)\sqrt{\varepsilon_0\mu_0}\,.\vec{E} + \overline{\overline{\mu}}.\vec{H}$$

where $\overline{\overline{\chi}}$, $\overline{\overline{\chi}}^{T}$, $\overline{\overline{\zeta_0}}$ and $\overline{\overline{\zeta_0}}^{T}$ are the magneto-electric and the chirality effect parameters . They define the real and imaginary parts of the complex magnet-electric coupling $\overline{\overline{\varsigma}}$ and $\overline{\overline{\varsigma}}^{T}$ .factors. The “T” denotes the transpose of a matrix. The magneto-electric $\overline{\overline{\chi}}$ and chirality $\overline{\overline{\zeta_0}}$ coefficients can be written as:

$$\bar{\bar{\chi}} = \frac{\bar{\bar{\varsigma}} + \bar{\bar{\xi}}^T}{2}, \bar{\bar{\zeta}}_0 = \frac{\bar{\bar{\varsigma}} - \bar{\bar{\xi}}^T}{2j} \quad (2\text{-}4)$$

It is clear that the substitution of (2-2) in (2-4) leads to the following values:

$\bar{\bar{\chi}} = 0$ and $\bar{\bar{\varsigma}} = j\bar{\bar{\zeta}}_0\sqrt{\varepsilon_0\mu_0}$.

The different tensors parameters $\bar{\bar{\varepsilon}}$, $\bar{\bar{\mu}}$, $\bar{\bar{\xi}}$ and $\bar{\bar{\varsigma}}$ can be now written as:

$$\bar{\bar{\varepsilon}} = \varepsilon_0 \begin{pmatrix} \varepsilon_{xx} & 0 & 0 \\ 0 & \varepsilon_{yy} & 0 \\ 0 & 0 & \varepsilon_{zz} \end{pmatrix}, \bar{\bar{\mu}} = \mu_0 \begin{pmatrix} \mu_{xx} & 0 & 0 \\ 0 & \mu_{yy} & 0 \\ 0 & 0 & \mu_{zz} \end{pmatrix} \quad (2\text{-}5)$$

$$\bar{\bar{\xi}} = \frac{1}{c} \begin{pmatrix} 0 & 0 & 0 \\ \text{-j}\zeta_0 & 0 & 0 \\ 0 & 0 & 0 \end{pmatrix}, \bar{\bar{\varsigma}} = \frac{1}{c} \begin{pmatrix} 0 & \text{j}\zeta_0 & 0 \\ 0 & 0 & 0 \\ 0 & 0 & 0 \end{pmatrix} \quad (2\text{-}6)$$

In equations (2-5) and (2-6) ε_0 and μ_0 are, respectively, the permittivity and permeability of the vacuum, *c* is the speed of light in vacuum. The other quantities such as ε_{xx} , ε_{yy} , ε_{zz} , μ_{xx} , μ_{yy} , μ_{zz} and ζ_0 are dimensionless and are unknowns. In the present case, we will only deal with the determination of forward and backward wave impedances entailed by ε_{yy} , μ_{xx} , and ζ_0 . The other four unknown quantities (ε_{xx} , ε_{zz} , μ_{yy} and μ_{zz}) are not related to the bianisotropic structure of the figure 2-3 when a plane wave with a polarization in the *y* direction is incident in the *z* direction.

The wave equations are obtained when the equations system (2-1) are substituted into Maxwell curl equations, they are written as:

$$\frac{\partial^2 E_y}{\partial z^2} + \omega^2\varepsilon_0\mu_0(\varepsilon_y\mu_x - \zeta_0^2)E_y = 0 \quad (2\text{-}7)$$

$$\frac{\partial^2 H_x}{\partial z^2} + \omega^2\varepsilon_0\mu_0(\varepsilon_y\mu_x - \zeta_0^2)H_x = 0 \quad (2\text{-}8)$$

where: E_y and H_x are the electric and magnetic fields in *y* and *x* directions respectively.

These equations can be written in the form:

$$\frac{\partial^2 E_y}{\partial z^2} + k_z^2 E_y = 0 \quad (2\text{-}9)$$

$$\frac{\partial^2 H_x}{\partial z^2} + k_z^2 H_x = 0 \quad (2\text{-}10)$$

If the wave number in equations (2-9) and (2-10) is given by:

$$k_z = nk_0 \quad (2\text{-}11)$$

Where n and k_0 are the complex refractive index of the bi-anisotropic metamaterial and free space wave number. Then, by identification with equations (2-7) and (2-8), the complex refractive index n can be written as:

$$n = \pm\sqrt{\varepsilon_y \mu_x - \zeta_0^2} \quad (2\text{-}12)$$

The normalized forward and backward wave impedances (z^+ and z^-) are given by:

$$z^+ = Z^+ / Z_0 = \frac{-E_y^+}{H_x^+ Z_0} = \frac{\mu_x}{(n + j\zeta_0)} \quad (2\text{-}13)$$

$$z^- = Z^- / Z_0 = \frac{+E_y^-}{H_x^- Z_0} = \frac{\mu_x}{(n - j\zeta_0)} \quad (2\text{-}14)$$

where Z_0 is the impedance of vacuum.

Now, the purpose is to express the effective parameters (ε_y, μ_x and ζ_0) in terms of (S_{ij}), assuming that the electric field $\vec{E}$ and magnetic field $\vec{H}$ are in the y and x directions. From the figure 2-3, the reflection and transmission S parameters can be written as [37-38]:

$$S_{11} = \frac{\Gamma_A(1 - T^2)}{1 - \Gamma_B T^2} \quad (2\text{-}15)$$

$$S_{21} = S_{12} = \frac{\Gamma_C T}{1 - \Gamma_B T^2} \quad (2\text{-}16)$$

$$S_{22} = \frac{\Gamma_D(1 - T^2)}{1 - \Gamma_B T^2} \quad (2\text{-}17)$$

where Γi are the reflection coefficients at points ($i = A, B, C$ or D) and T is the transmission coefficient. They are given by:

$$\Gamma_A = \frac{z^+ - 1}{z^+ + 1} \quad (2\text{-}18)$$

$$\Gamma_B = \Gamma_A \Gamma_D \quad (2\text{-}19)$$

$$\Gamma_C = 1 - \Gamma_B \quad (2\text{-}20)$$

$$\Gamma_D = \frac{z^- - 1}{z^- + 1} \quad (2\text{-}21)$$

$$T = e^{jk_0 nd} \quad (2\text{-}22)$$

By substituting equations (2-15) to (2-17) into equations (2-18) to (2-22), we obtain the expressions of the forward and backward wave impedances and the complex refraction index:

$$z^+ = \frac{-\Lambda_2 \pm \sqrt{\Lambda_2^2 - 4\Lambda_1\Lambda_3}}{2\Lambda_1} \quad (2\text{-}23)$$

$$z^- = \frac{\Lambda_4 z^+ + 1}{z^+ + \Lambda_4} \quad (2\text{-}24)$$

$$n = \frac{1}{k_0 d}\left[\mp(\ln T)'' \mp 2\pi m - j(\ln T)'\right] \quad (2\text{-}25)$$

where:

$$\Lambda_1 = S_{21}^2 - (1 - S_{11})(1 - S_{22}) \quad (2\text{-}26)$$

$$\Lambda_2 = 2(S_{11} - S_{22}) \quad (2\text{-}27)$$

$$\Lambda_3 = (1 + S_{11})(1 + S_{22}) - S_{21}^2 \quad (2\text{-}28)$$

$$\Lambda_4 = \frac{S_{11} + S_{22}}{S_{11} - S_{22}} \quad (2\text{-}29)$$

The prime $(')$ and double prime $('')$ denote the real and imaginary parts, and the integer $m = 0,1,2,\ldots$ is the branch index values. Note that the correct sign of z^+, z^- and n correspond to those who satisfy the passivity conditions ($(z^+)' > 0$, $(z^-)' > 0$ and $(n)'' \geq 0$) considering that $n = n' - jn''$ with e^{-jwt} notation.

2.3.2.2The electromagnetic parameters computation

From equations (2-23), (2-24), (2-25) and (2-18) to (2-22), we deduce the effective parameters expressions:

$$\zeta_0 = \frac{(2-\Gamma_C)^2 - (4\Gamma_A^2 + \Gamma_C^2)}{4i\Gamma_A\Gamma_C / n} \tag{2-30}$$

$$\mu_x = \frac{\Gamma_C(n^2+\zeta_0^2)}{n(2-\Gamma_C) - 2n\Gamma_A - i\Gamma_C\zeta_0} \tag{2-31}$$

$$\varepsilon_y = \frac{n^2+\zeta_0^2}{\mu_x} \tag{2-32}$$

2.3.2The *S* parameters inversion method results

The metamaterial effective constitutive parameters are extracted using the *S* parameters inversion method detailed above. The results are compared with those obtained in [39]. The used metamaterial structure, shown in figure 2-4, consists of two types of conducting elements, a split ring resonator and wire. Both are made of copper (thickness 17 um) and positioned on opposite sides of a 0.25 mm thick FR4 dielectric board (ε_r = 4.4 and loss tangent of 0.02).

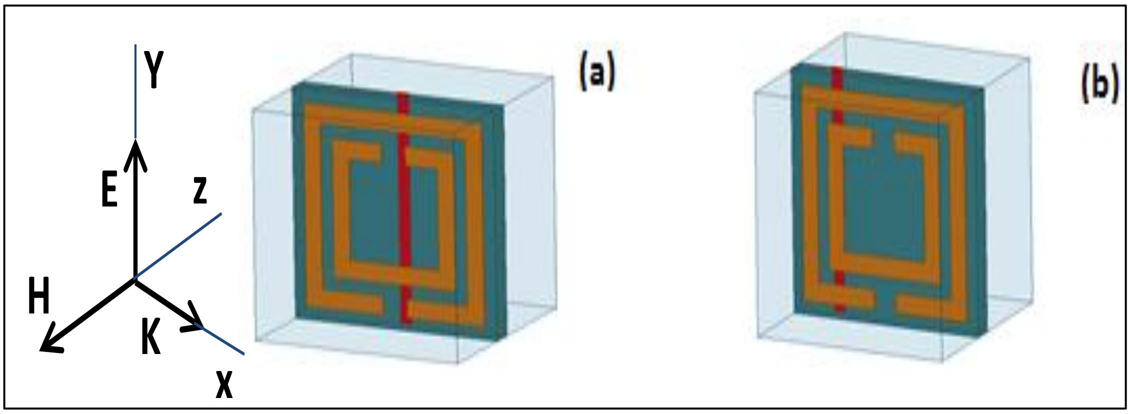

Figure 2-4 The split ring resonator SRR: a) Symmetric, b) Asymmetric (the wire has been shifted 0.75 mm away from its centered position).

The extracted electromagnetic parameters of the symmetric and asymmetric unit cell metamaterials are shown in figure 2-5 and figure 2-6 respectively. We observe from figures 2-6 and 2-5, the good agreement between our results, if they are compared to those obtained in [39] for the symmetrical and asymmetrical unit cell metamterials. The asymmetrical unit cell metamaterial is obtained by shifting the conductor wire 0.75 mm away from its centered position of the symmetrical one.

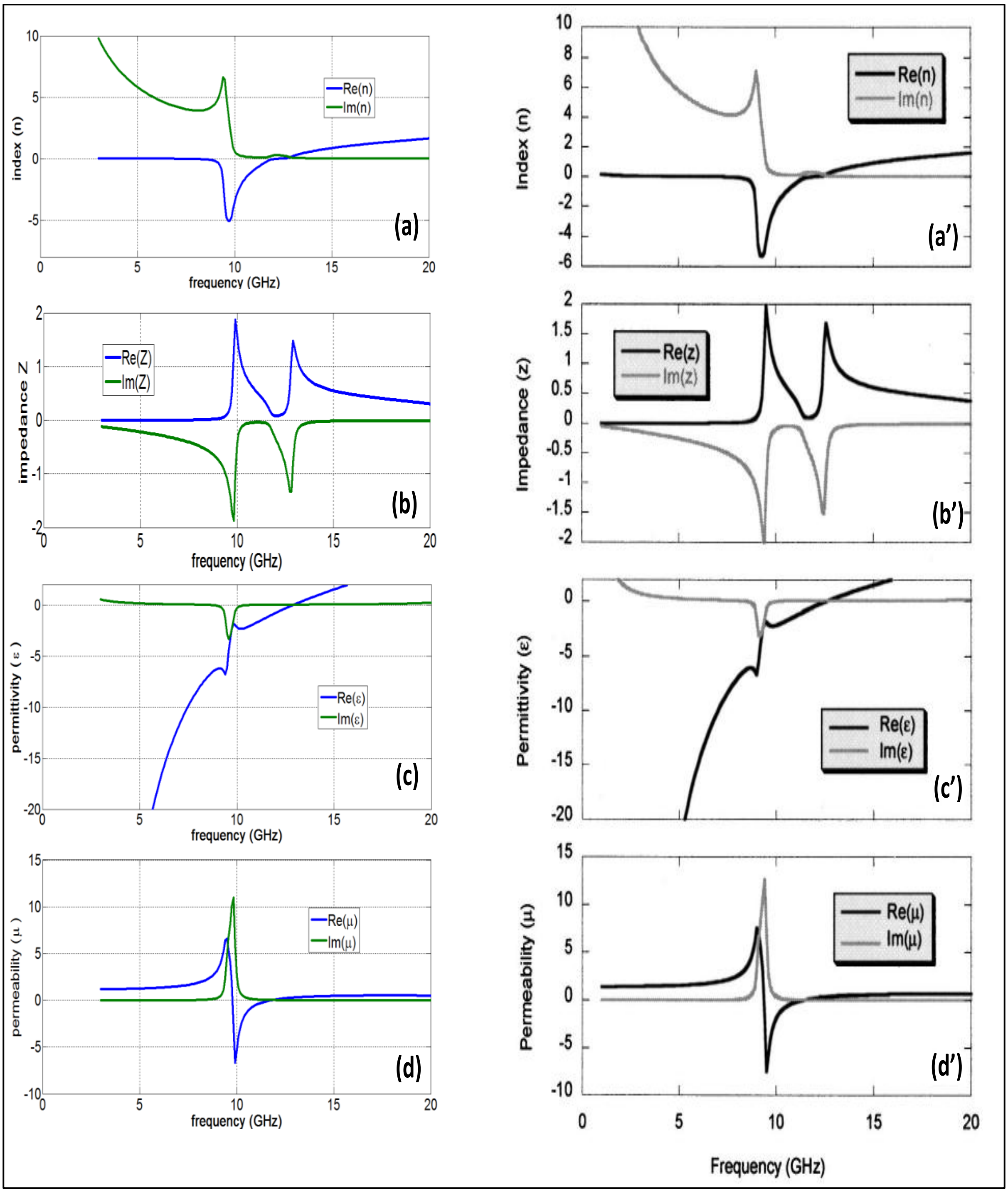

Figure 2-5 Comparison between our extraction program results (left: with colors) and those obtained from [39] (right) for symmetric unit cell metamaterial. (a)-(a'). Index (n). (b)-(b'). Impedance (z).

(c)-(c'). Relative dielectric permittivity (ε). (d)-(d'). Relative magnetic permeability (μ).

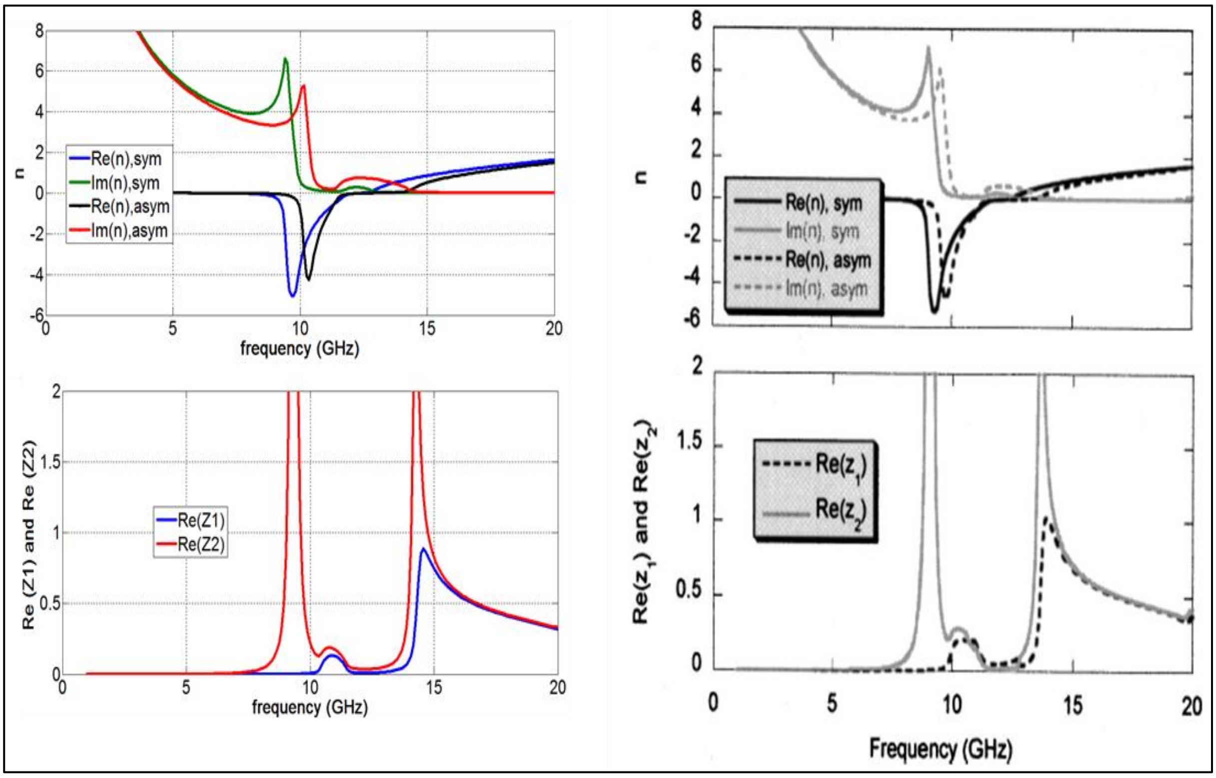

Figure 2-6 Comparison between our extraction program results (left) and those obtained in [39] (right) for the asymmetric unit cell metamaterial.

2.3.3Field summation extraction method

Another way to validate our simulated results is to use a method based on a completely different physical concept: the field summation method. This last one is based on the electromagnetic field cards distribution within the unit cell metamaterial.

We use the Maxwell's curl equation, the distributions $\vec{D}$ and $\vec{B}$ fields can then be calculated from those of the electric $\vec{E}$ and the magnetic $\vec{H}$ fields:

$$\begin{aligned} \vec{\nabla} \wedge \vec{E} &= -j\omega \vec{B} \\ \vec{\nabla} \wedge \vec{H} &= j\omega \vec{D} \end{aligned} \qquad (2\text{-}33)$$

In the quasi-static regime, when the size ***d*** of the unit cell is small compared to the wavelength and the inclusion volume is small, it is possible to calculate the effective permittivity and permeability. We start by integrating over an appropriate volume (V) and a surface (S), the field variables ($\vec{E}$ and $\vec{H}$). The constitutive relations for Tellegen representation in the equations (2-1) can now be written as [40]:

$$\vec{D}_y = \varepsilon_0 \varepsilon_{yy} \vec{E}_y - j\zeta_0 \sqrt{\mu_0 \varepsilon_0}\, \vec{H}_x \qquad (2\text{-}34)$$

$$\vec{B}_x = \mu_0 \mu_{xx} \vec{H}_x + j\zeta_0 \sqrt{\mu_0 \varepsilon_0}\, \vec{E}_y \qquad (2\text{-}35)$$

The equations (2-34) and (2-35) involve three remaining unknowns $(\varepsilon_{yy}, \mu_{xx}, \zeta_0)$, so we need one more equation to solve this last system equation. It is obtained from the wave impedance in the backward and the forward directions given by the equations (2-13) and (2-14). The constitutive parameters can then be written as:

$$\varepsilon_{yy} = \frac{< D_y >_p}{\varepsilon_0 < E_y >_V} + j\zeta_0 \sqrt{\mu_0 \varepsilon_0} \frac{< H_x >_p}{\varepsilon_0 < E_y >_V} \qquad (2\text{-}36)$$

$$\mu_{xx} = \frac{< B_x >_V}{\mu_0 < H_x >_p} - j\zeta_0 \sqrt{\mu_0 \varepsilon_0} \frac{< E_y >_V}{\mu_0 < H_x >_p} \qquad (2\text{-}37)$$

where:

$$\zeta_0 = \frac{j(F.z_0^2 + N^2.A)}{-2.N.z_0 + d.z_0^2 + N^2.b} \qquad (2\text{-}38)$$

$$F = \frac{< B_x >_V}{\mu_0 < H_x >_p}, z_0 = 120\pi, N = \frac{< E_y >_V}{< H_x >_p}, A = \frac{< D_y >_p}{\varepsilon_0 < E_y >_V} \qquad (2\text{-}39)$$

$$d = \frac{\sqrt{\mu_0 \varepsilon_0}}{\mu_0} \frac{< E_y >_V}{< H_x >_p}, b = \frac{\sqrt{\mu_0 \varepsilon_0}}{\mu_0} \frac{< H_x >_p}{< E_y >_V}, < K_i >_\Omega = \frac{1}{\Omega} \int K_i(\vec{r})\, \vec{dr} \qquad (2\text{-}40)$$

To validate our extraction procedure based on the field summation method, we compare the obtained results with those obtained for a test structure, shown in figure 2-7, which is a Broadside coupled SRR [41]. In the field summation method, the electromagnetic material properties of periodic composites are calculated using the expressions (2-36), to (2-38). The averaged $\vec{E}$ and $\vec{H}$ fields are calculated in the volume (V), the other two electromagnetic fields $\vec{D}$ and $\vec{B}$ are averaged appropriately on the surfaces (P) normal and parallel to the common axis ($\vec{k}$) of the SRR (figure 2-7). These average fields are substituted in the constitutive equations, which are then solved together with the dispersion relation for the bianisotropic medium defined in the equation (2-12) to give the overall electromagnetic properties of the periodic composites.

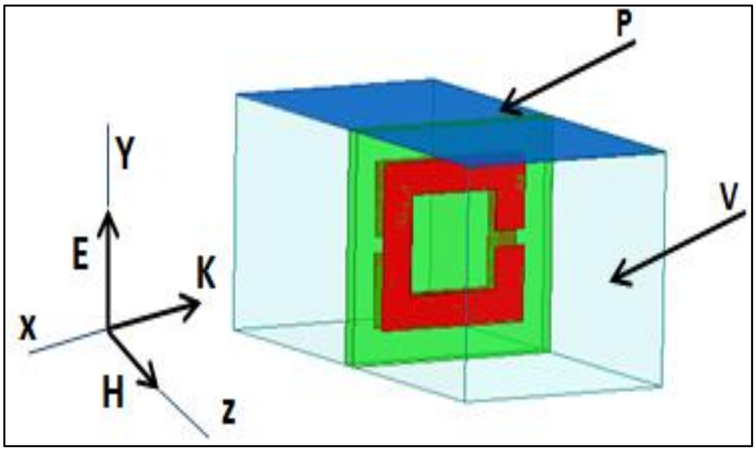

Figure 2-7 The split ring resonator SRR type (Broadside-coupled SRR) metamaterial.

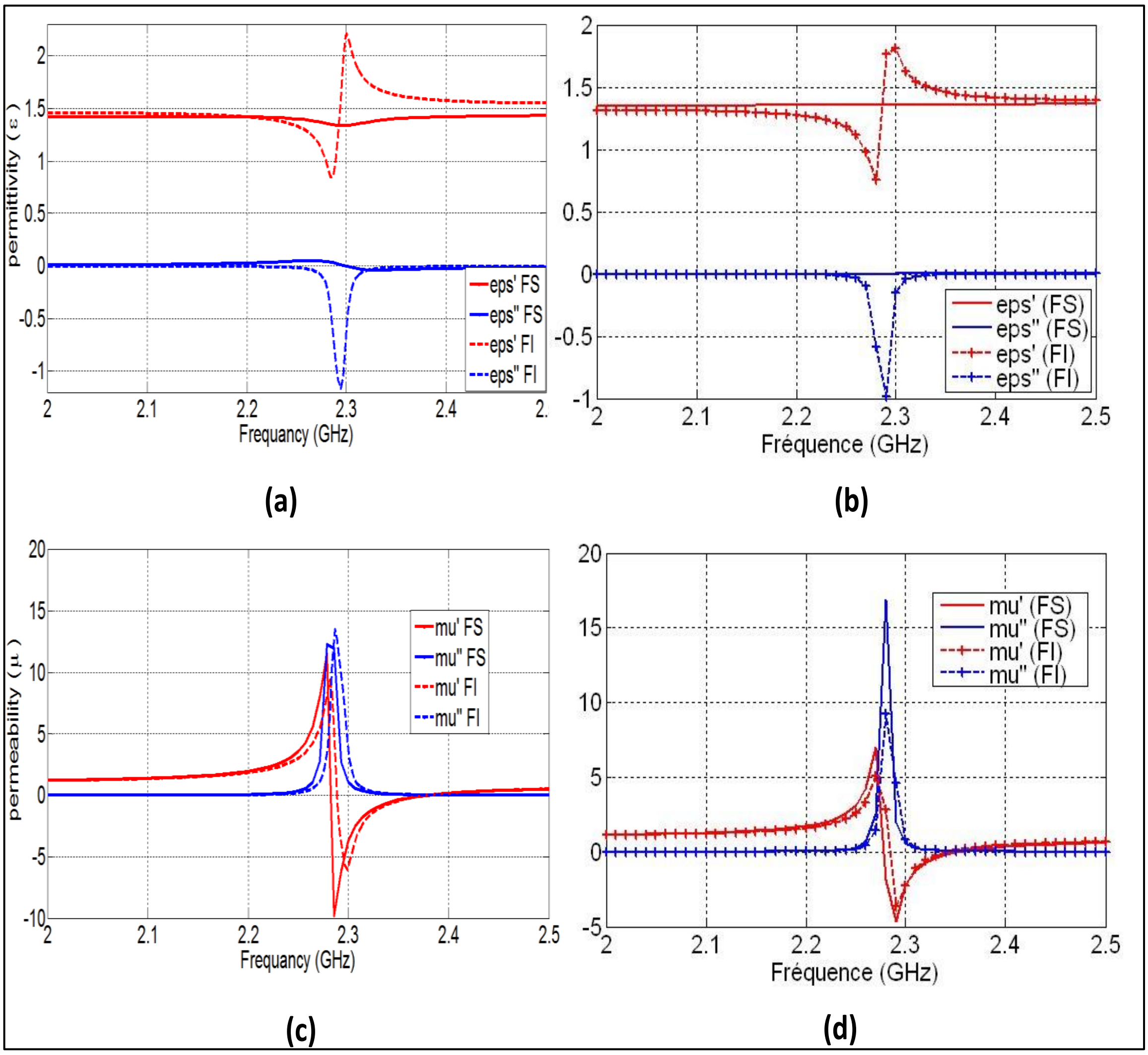

Figure 2-8 Results comparison between our extraction programs (Fresnel inversion (FI) and field summation methods (FS) (left)) and those obtained in [41] (right).

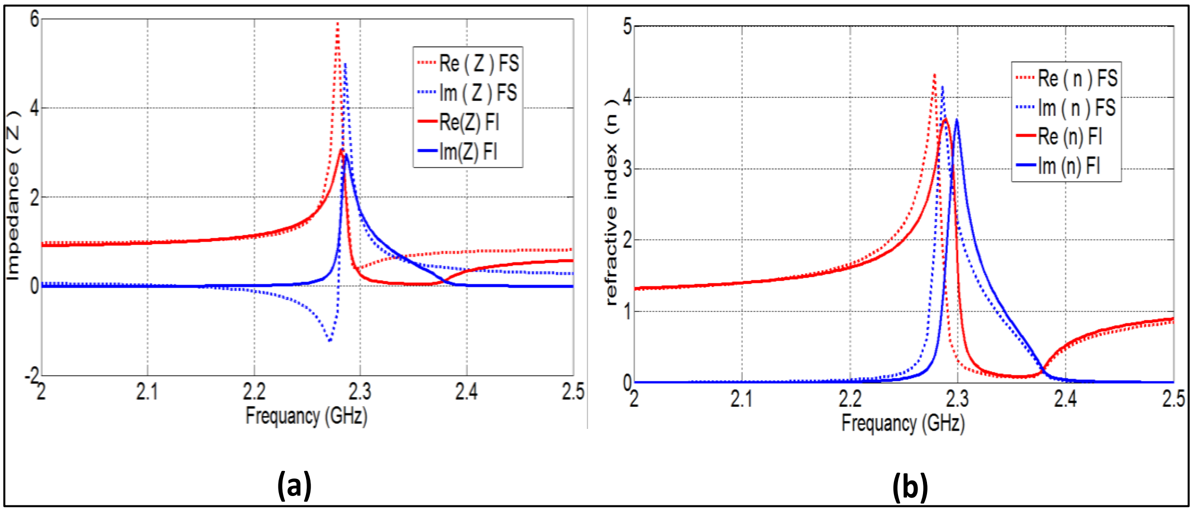

Figure 2-9 a) Complex refractive index, b) impedance with Fresnel inversion (FI) and field summation methods (FS).

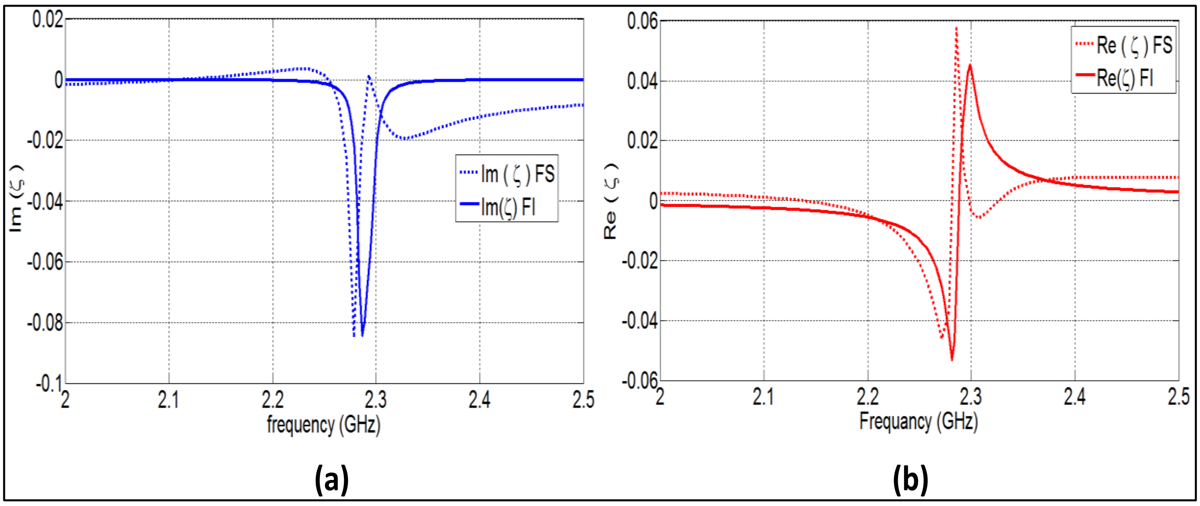

Figure 2-10 Retrieved electromagnetic coupling coefficient by Fresnel inversion (FI) and field summation methods (FS).

In figure 2-8 to figure 2-10 are compared our extracted effective parameters (ε, μ, n, z, and ζ_0), using FS and FI methods, with those obtained in [41]. We note a good agreement in one hand, between results obtained by the FS and FI methods and in the other hand, with those of reference [41]. Note that for the effective permeability μ_{eff} our results obtained by the FI and FS present a better concordance, compared to those in [41]. Indeed, this best agreement is due to the fact that our parameters extraction procedure tack into account the magneto-electric coupling effect, which is ignored in reference [41]. The good agreement between the results obtained by two different methods based on completely different physical concepts, gives a numerical validation to our extraction parameters procedure.

2.4Conclusion

A metamaterial is seen as homogeneous material if the period of the unit cells constituting it, is much smaller than the wavelength of interest. Metamaterials can be described by the effective constitutive parameters: the effective permittivity ε_{eff}, the effective permeability μ_{eff} and the magneto-electric coupling ξ_0. The effective constitutive parameters can be extracted by using the *S* parameters inversion method (Fresnel Inversion Method) and the field averaging method (Field Summation method). This latter is based on field card distributions. These both methods exhibit results that are in good agreement compared to those obtained in the literature [39-41].

3. Agile and programmable metamaterial

3.1 Introduction

In electronics, performing several functions or for different operating range through a single apparatus or instrument is called agility or tuning depending on the desired function. Apparatus can take different system forms (devices, materials, metamaterials…). Research in agile systems became a necessary procedure in the production chain because it offered many advantages to these functions. As examples, we present agile antennas and filters. In this chapter, firstly, a general view is presented on the technical solutions which exist to perform agility. Then, we introduce examples of agile metamaterials which use these agility techniques. Finely, the main focus of interest in this chapter concerns our agile metamaterial that is based on the agile cross unit cell type metamaterial we designed for this purpose. This latter is characterized and optimized to give the desired behavior required to design agile microwave devices.

The starting point in metamaterials fabrication is their elementary particle (constituent element), also called the unit cell. It can be designed in different forms with different arrangement periods depending on the operating conditions. Although, multiple types of unit cells can be used, the choice is decisive in the electromagnetic responses, applications, and also the ease of processing and fabrications.

We are interested by the designing of an agile unit cell controlled by an external switching system and which exhibits two different behaviors depending on the switches states (ON or OFF). In an earlier works, we have used the Jerusalem cross [42-44], connected and disconnected cross type unit cell metamaterials to conceive a metamaterial superstrate to enhance a microstrip patch antenna gain or to control its radiation pattern. The behavior of the connected and disconnected cross type unit cell metamaterials has drawn our attention. In one hand, the connected cross type metamaterial behaves like a medium with a close to zero refractive index, while the disconnected cross type metamaterial behaves like an epsilon positive medium. In another hand, the connected and disconnected unit cell metamaterials can be gathered in single unit cell by using an adequate switching system. The result is an agile metamaterial unit cell, which has two different behaviors depending on an external command system. This agile metamaterial unit cell is mainly arranged in 2 D to obtain an agile metamaterial layer where one of the challenges will be the miniaturization of the cross unit cell to give meaning to metamaterials homogenization and then, to the programmable matrix sections in the agile metamaterial layer.

3.1.1 Tunable antennas

Antennas are crucial element in any wireless communication system and like another function, it is highly evolved. Patch antennas are more compact and easier to integrate in industrial process. Today, antennas miniaturization via various techniques (synthesis, industrial progress, use of metamaterials…) achieves significant proportions while maintaining high performance.

Currently, it is difficult to realize wide band antennas. The multi band antennas have important dimensions when they come to covering three, four or five frequency bands. Agile frequency antennas can constitute a solution to reduce congestion in multi standard terminals. Beam antennas reconfiguration for example is an active domain of research. It interests anticollision RADAR, GPS localization or LAN systems. The most common solution is to command the beam direction by phase signals feeding the different antenna elements

(figure 3-1) [45].

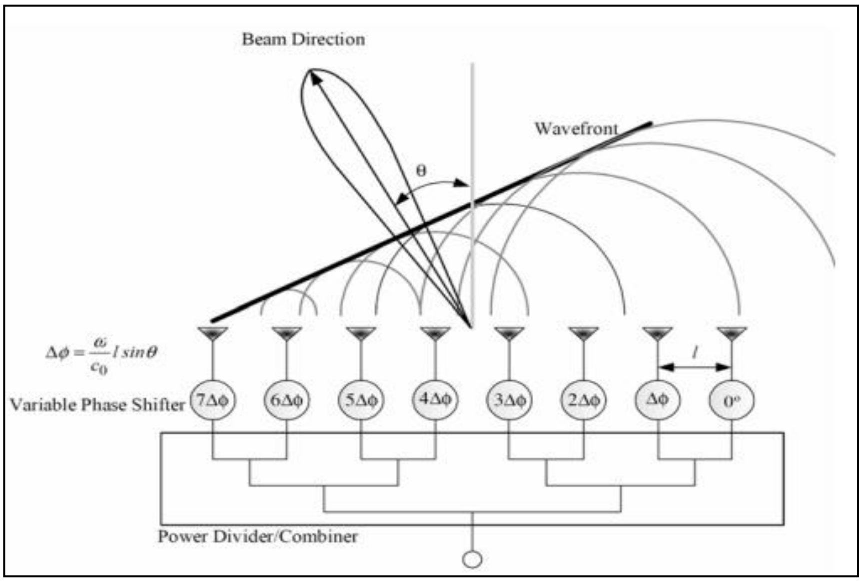

Figure 3-1 Phase command network antennas using agile phase shifter.

3.1.2 Agile filters

Agile filters should not be agile only in frequency, but also in bandwidth. For example in figure 3-2, Doppler radars are limited in their applications by the filter bandwidth following the mixer. Make tunable such a device, via the replacement of the post mixer filter by an agile filter, allows to measure very fast speed of objects (aircraft). In military applications, agile filters are used in miniaturized communicating systems (drones). Tunable phase shifters, agile impedance adapters, and oscillators are also other functions that have potential applications in electronic systems.

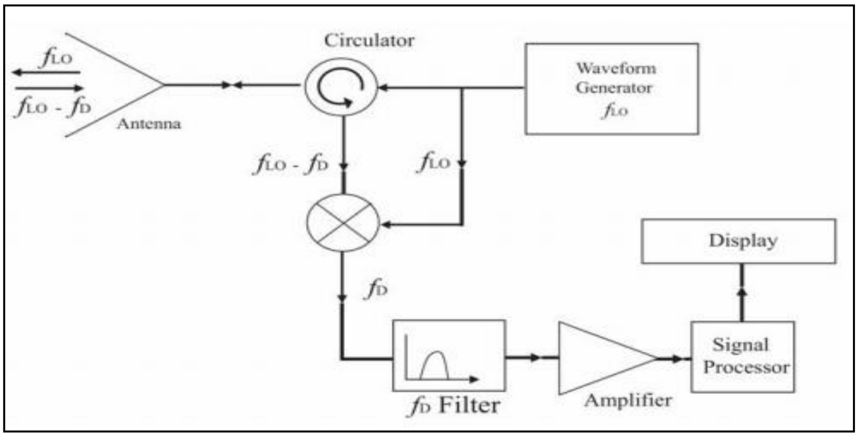

Figure 3-2 Simplified scheme of Doppler radar [45].

3.2 Technical solutions for tunability (agility)

Many solutions have imagined realizing agile functions. Generally they can be divided in two large families: agility devices and agile materials.

3.2.1 Localized elements

Function agility based agility devices consists of the association of classic variable elements as diodes, transistors, or MEMS

3.2.1.1. PIN diodes

They are made of semiconductors and composed of two doped layers P and N respectively and intrinsic undoped layer. In direct polarization, the voltage across the diode is constant and presents a resistance, inversely proportional to the current flow. This variable resistance can be used to realize attenuators. In reverse bias, the diode behaves as constant capacitor with parallel resistance which corresponds to power dissipation when it is blocked. For microwave applications, it is important that this parallel resistance is larger to limit losses.

In microwave applications, PIN diodes are used as switches. Placing the diode on the way of the propagating wave (figure 3-3), it is possible that the signal passes (direct polarization) or reflects (reverse polarization). Remaining in the direct polarization, attenuator is released via the varying of the diode series resistance.

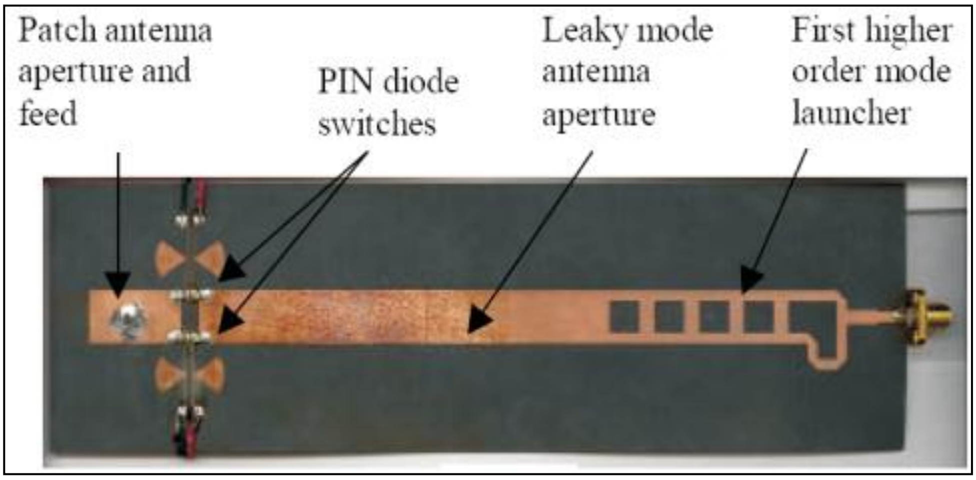

Figure 3-3 Example of agile antenna PIN diode [46].

3.2.1.2. Varactor diodes

Varactor diodes are PN heterojunction type diodes. When they are reversely polarized, the charge displacements between two doped regions create a zone empty of any charge which behaves as a dielectric of a capacitor. When the reversely voltage is increased, the size of this region is increased. As the capacity is inversely proportional to the region size, then the series diode capacity decreases via the voltage augmentation (figure 3-4).

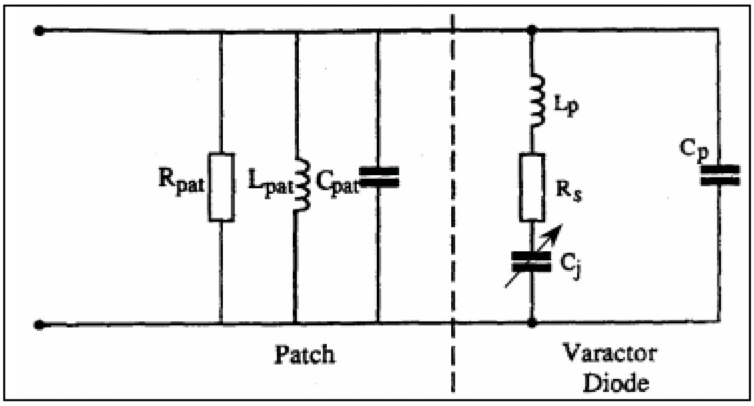

Figure 3-4 Equivalent circuit of agile antenna using varactor diode [46].

3.2.1.3. (Micro Elector Mechanical System) MEMS

For years, engineers have worked to eliminate mechanical devices by replacing them with electronic or “solid state” devices. Recently, there has been resurgence back to moving micro-machines or Micro-Eectro Mechanical Systems (MEMS) technology. Built in ways similar to integrated circuits, MEMS devices are fabricated on silicon wafers by patterning various layers of materials and releasing (underetching). After releasation, these tiny structures are capable of motion (figure 3-5).

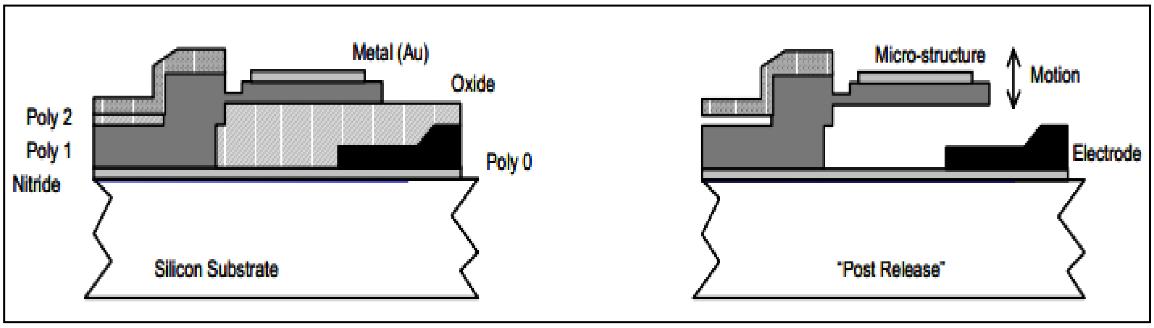

Figure 3-5 Surface micromachined MEMS device (Pre and Post release) [47].

MEMS are micro circuits fabricated of very small dimensions such as the mechanism can be actuated by a force of different origins. Now, MEMS are found in many sectors like automotive, aerospace, medicine and telecommunications.

To move these tiny structures, several methods exist. Most common ways include electrostatic, electromagnetic and thermal actuation (or some combination of the three). Each has their pluses and minuses.

A. Electromagnetic actuation

Electromagnetic control requires one or more coils and a permanent magnet on the microstructure. The big disadvantages are size, weight and power dissipation. The size of the coils and the magnets make fabricating dense arrays very difficult. The size and weight of the actuated microstructures can result in potentially low resonant frequency structures (making high speed control more difficult) and make fabricating dense arrays very difficult.

B. Electrostatic actuation

By applying a differential voltage between the microstructure and a fixed electrode, one can make a device move. Unfortunately, these forces are relatively weak requiring high voltages. As with other methods, there is a danger of snapdown (when the device exceeds 1/3 the distance to the electrode). Unless properly designed, snapdown can cause damage to the devices. The major advantage with electrostatic actuation is the very low power consumption and the small size. Once a device is moved to its position, no additional power is required.

C. Thermal heating actuation

A third actuation method is mechanical expansion and contraction through thermal heating and cooling. Regarding telecommunications, the MEMS are mostly used as switches (ohmic mode) like in figure 3-6 or variable capacitors (capacitive mode) as shown in the figure 3-7. In the ohmic mode, the contact is direct between the two electrodes but in the capacitive mode, a dielectric layer is inserted between them which allow the creation of variable capacitor.

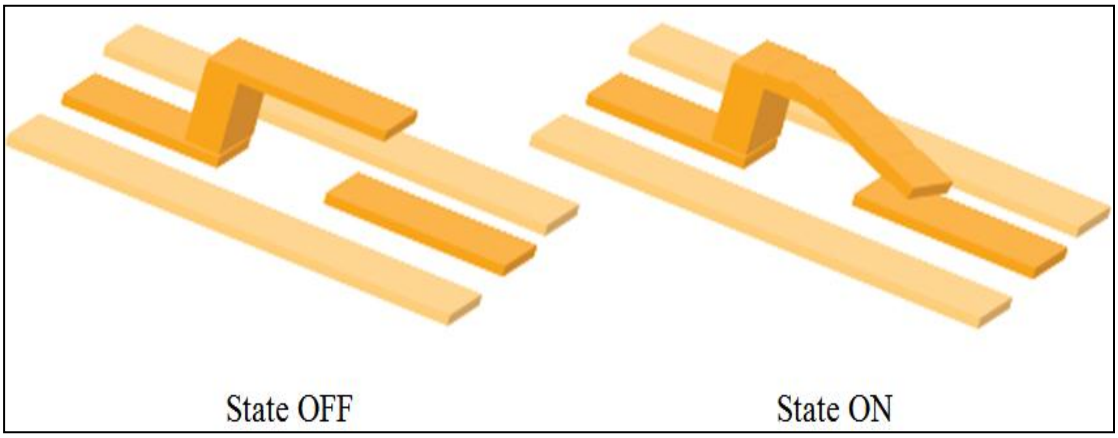

Figure 3-6 Ohmic switch [47].

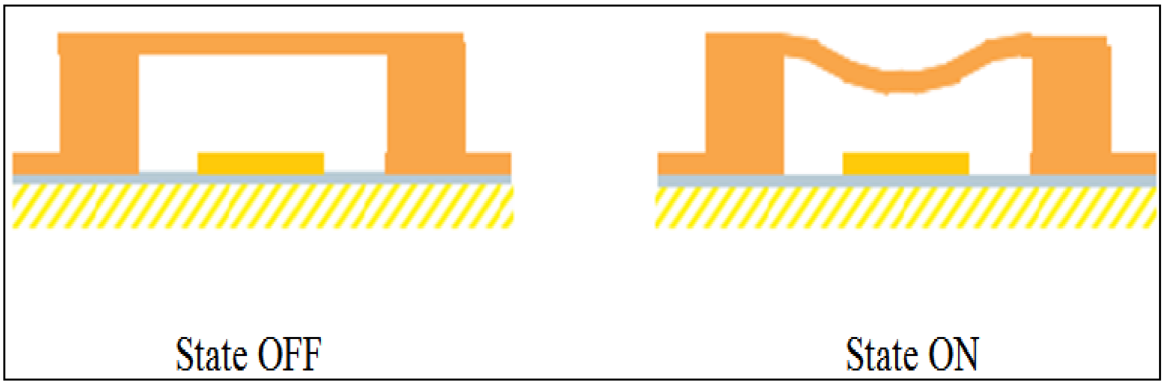

Figure 3-7 Capacitive switch [48].

The MEMS actuation principle is very easy and simple. The mechanic deformation and the micro commutator moving require external force action. Through an actuation system (electrodes and polarization line), this force is applied to the deformable zones of the component. The most common actuation mode is that of electrostatic command. This last require only two conductor electrodes, one fixed and the other movable. When a voltage is applied between the electrode terminals then an electric force is generated which flexes the moveable electrode toward the fixed one. Large agile functions have been realized based on MEMS such as filters, phase shifters, and antennas. They prove interesting potential to agility applications.

A particular challenge is properly releasing and handling such small and often fragile devices. Once they are released or etched, it is extremely difficult to separate chips out without contaminating or damaging them (traditional wafer sawing sends particles everywhere). New methods are being developed now to allow for volume packaging at the chip and wafer level. Depending on the function, it is desirable to package devices in a sealed package with a window to reduce contamination (particle or moisture).

3.2.2 Agile materials

To achieve tuned functions, another solution consists to exploit the properties of agile materials. These later have the property to modify their dielectric permittivity, permeability, or both under an external command action. These materials are often used as substrates where microwave devices are realized. Agile materials and technologies based on nonlinear materials like ferromagnetic, ferroelectrics materials or liquid crystals offer a line of passive tunable microwave components such as varactors, filters and phase shifters, suitable as key components in phased array antennas for automotive radar sensors and in future reconfigurable (frequency agile) RF frontends in mobile communication systems with multiband operation [49].

In this chapter, three agile materials are presented: ferromagnetic, liquid crystals (LC), and ferroelectrics.

3.2.2.1.Ferromagnetic materials

Ferromagnetic materials can modify their permeability depending on the magnetic field action. At gyromagnetic frequency their dielectric losses become more important. In microwaves, the intended properties of these materials are: low conductivity, low coercive field, strong saturation magnetization and good temperature stability.

3.2.2.2.Liquid crystals

They are constituted of molecules of elongated form which introduce polarizable part with high sensitivity to the electric field. Liquid crystals (LC) pass through intermediate phases, or mesophases, between liquid and crystal state. Liquid crystals come in two basic classifications: thermotropic and lyotropic. The phase transitions of thermotropic liquid crystals depend on temperature, while those of lyotropic liquid crystals depend on both temperature and concentration.

Tunable passive microwave materials, such as nematic liquid crystals (LC) are very promising for tunable passive components in microwaves and millimeter wave regions (frequency tuned phase shifters and antennas). We are mainly interested on the nematic phase (figure 3-8 (a)) which is characterized by molecular disorder where their average orientation keeps a well defined direction.

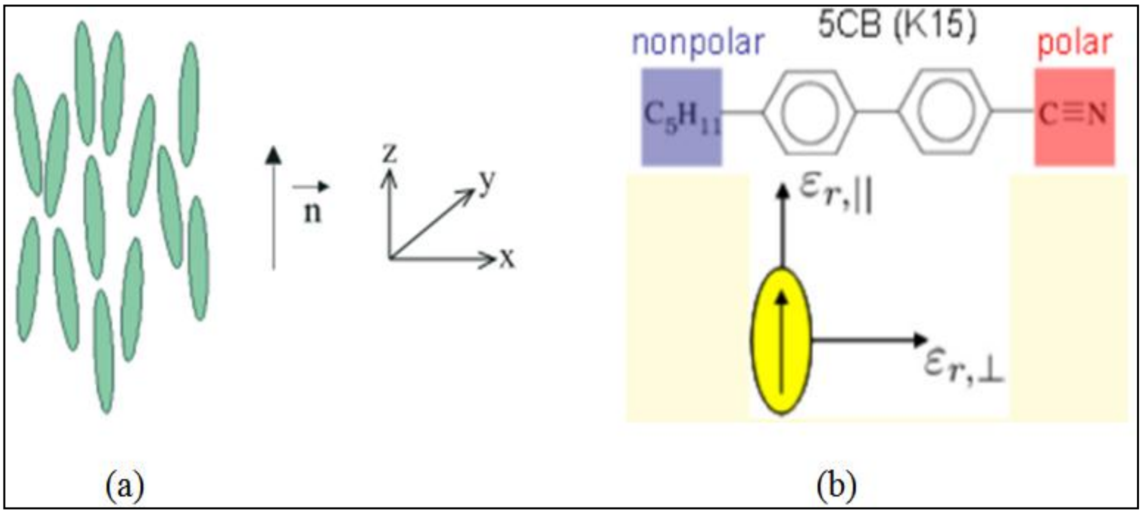

Figure 3-8 a) The LC molecule of the 5CB, and b) Tunable permittivity at high frequencies [49].

These dielectric materials offer a tunable permittivity when the molecules are aligned by an external electro or magnetostatic field (figure 3-9). For a microwave signal, when a sufficient voltage is applied, the molecules overbalance according to the field command then the material is anisotropic; the gap between their parallel and perpendicular permittivity depend on the used liquid crystal (figure 3-8-(b)).

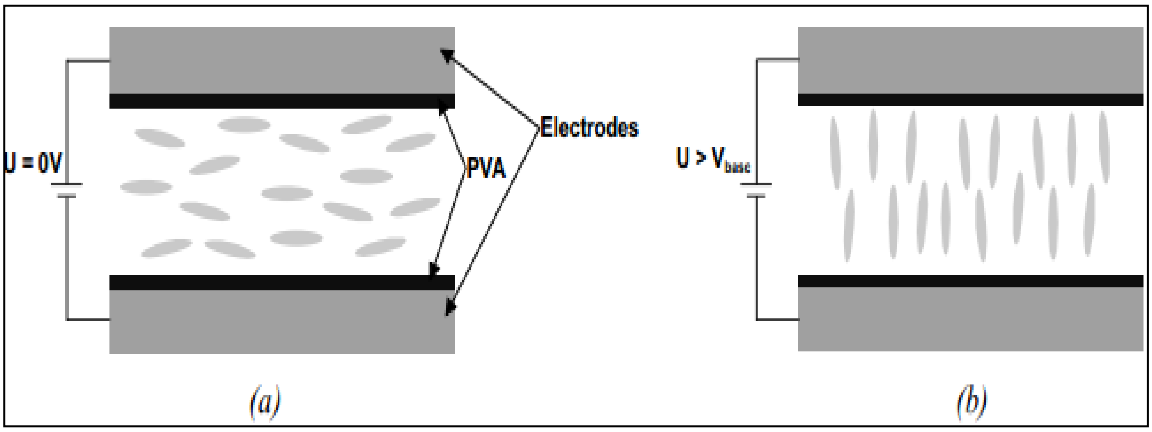

Figure 3-9 Liquid Crystal reorientation bias DC voltage.

3.2.2.3.Ferroelectric materials

Ferroelectrics are truly multifunctional materials and widely used in electronic, optical, acoustic and magnetic components. In the past, most of the developed microwave devices have been based on bulk ceramics which demonstrate a spontaneous electric polarization at temperatures below a critical value known as the Curie temperature. In the subcurie temperature region of operation, application of a DC electric field, normally on the order of kV cm^{-1}, causes a non linear change in the material's complex permittivity. When they are used as a thin film layer, to reduce bias voltage requirements, this enables the production of tunable filters and resonators [50].

Ferroelectrics, as high permittivity materials, are widely used in high density commercial decoupling capacitors. Acoustoelectronic transducers are the other traditional components where the ferroelectric piezoelectrics are used. On the other hand the DC electric field dependent dielectric permittivity is the most important feature of some perovskites that makes them attractive for agile microwave components, such as varactors, tunable delay lines, phase shifters, tunable filters ….. For these applications the complex metal oxides, known as perovskites, such as Titanates (CaTiO3, BaTiO3 ….), Tantalates (KTaO3 ….).

Niobates (KNbO3) are the most considered ferroelectrics. They are characterized by a common chemical formula, ABO3, and have the same crystal structure (figure 3-10-(a)). Above the polar to non-polar phase transition (Curie) temperature Tc (Curie temperature), their crystal lattice has a cubic structure. In this phase the crystal has no spontaneous polarization. Its permittivity is rather high DC field temperature and strain dependent. Below Curie temperature the centers of the positive and negative charges shift, and the crystal is characterized by spontaneous polarization. One of the surfaces of a macroscopic crystal is charged positively, while the opposite surface is charged negatively. Below Curie temperature the crystal is in a polar phase characterized by hysteresis loop (figure 3-10-(b)) and piezoelectric effect. In this phase the DC dependent permittivity has butterfly shape (figure 3-10-(e)), and the ferroelectrics are used in nonvolatile memory cells and piezoelectric transducers. Above Curie temperature the crystal is in a paraelectric phase with a bell shaped dependence of the permittivity on the applied DC field (figure 3-10-(f)). This phase is preferable for most of the agile microwave applications since it has no hysteresis, (figure 3-10-(c)), and the permittivity of the crystal may be given clearly via the applied DC field.

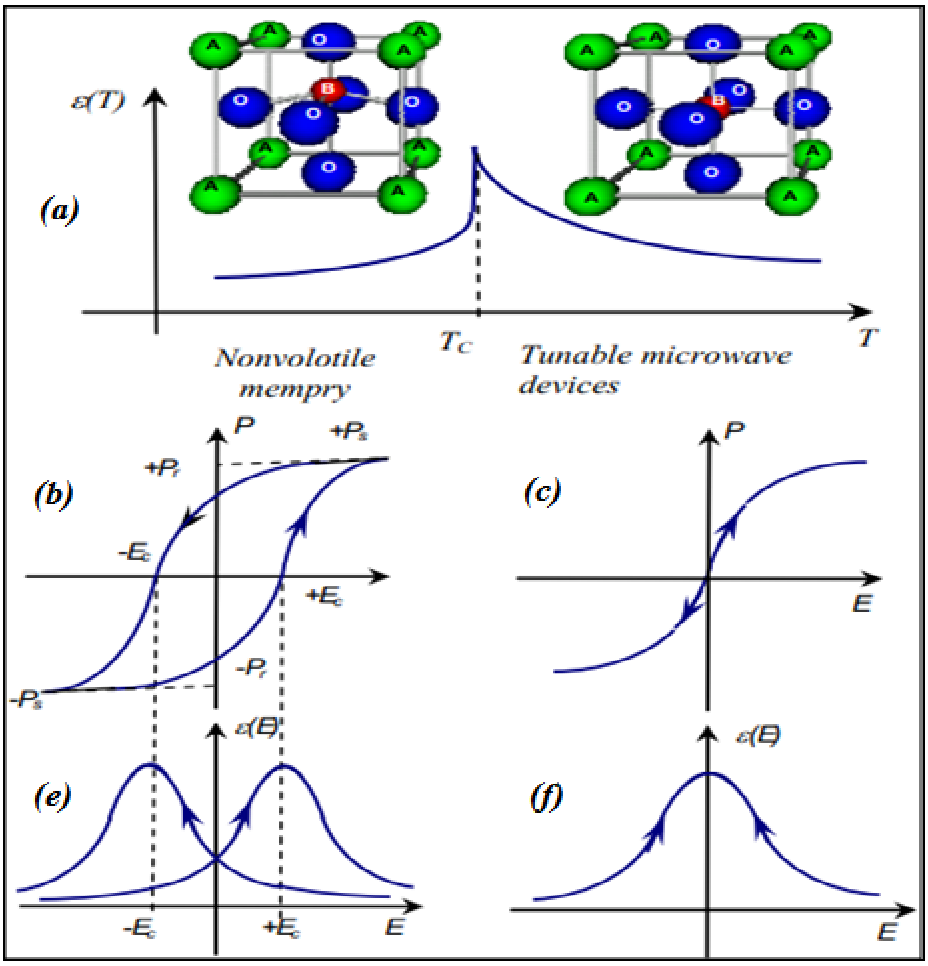

Figure 3-10 a) Temperature dependences of the permittivity, and b), c) DC field dependent polarization. e), f) Permittivity of a typical ferroelectric below and above the Curie temperature [51].

Varactors are the basic microwave components where ferroelectrics in paraelectric phase are used. They may be based on ceramic (bulk, film) and single crystal (bulk, epitaxial film) films, and may have parallel plate and coplanar plate designs (figure 3-11) [51].

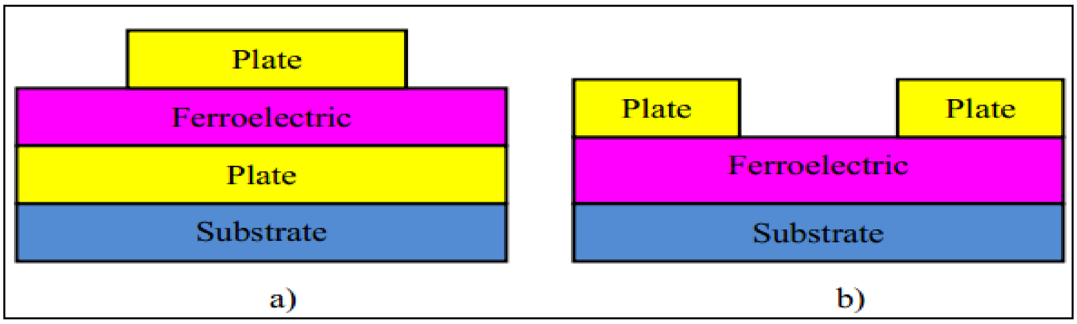

Figure 3-11 a) Parallel plate, b) Coplanar plate ferroelectric varactors.

The thin (epitaxial and ceramic) films have better performances in comparison with the bulk ceramics and thick films and they offer integration flexibility. The parallel plate varactor offers higher tunability at low applied DC voltages but has more complex fabrication process as compared with the coplanar plate design.

The recent research activities have been focused on the development of microwave devices and circuits based on new materials physical phenomena. It includes synthesis of the thin films, modeling, fabrication and experimental characterization of components and circuits based on ferroelectrics. Figure 3-12 (a) shows a circuit application example of parallel plate varactors, while the figure 3-12 (b) shows the dependence of the varactor Q factor on the composition of the used ferroelectric $Ba_xSr_{1-x}TiO_3$ films. The varactors of this type are used in different microwave devices. An example of Voltage Controlled Oscillator (VCO) based on these varactors is considered below.

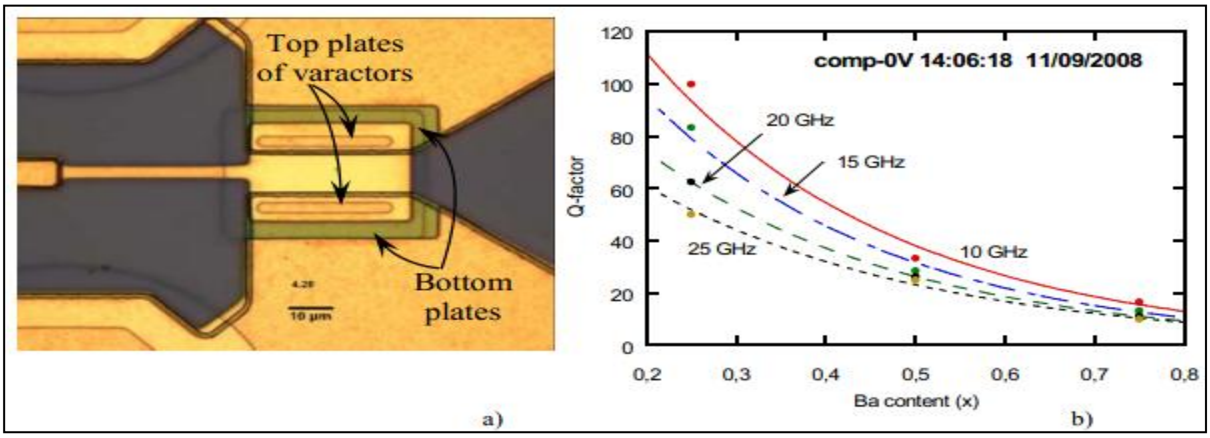

Figure 3-12 a) Micro-photo of three terminal ferroelectric varactors, b) Composition (*x*) dependence of the$Ba_xSr_{1-x}TiO_3$ based varactors at zero DC bias and for different frequencies [51].

Some comparative parameters are summarized in table-1 for competing technologies. It is apparent that there are pluses and minuses for each technology, and therefore the choice depends strongly on the particular application. BST dielectrics are favored for applications:

1) Which require rapid, continuous tuning, and 2) frequency conversion devices, that exploit the fast capacitive non-linearity. Neither of these applications can be addressed by MEMS varactor and LC devices, which are too slow. In both categories, BST based components can be designed for much higher capacity than a comparable GaAs based varactor at higher frequencies. On the other hand, applications demanding very high Q factors such as narrowband tunable filters for communications, or even phase shifters if lowest possible

insertion loss is an important objective are not yet appropriate for implementation with BST components, due to persistently high material losses in the microwave range. This might be overcome by strained relieved BST thin films, which achieved significantly high dielectric quality factors In comparison to semiconductors, BST devices promise to be extremely competitive in terms of cost, in particular at mm waves.

Technology [1-40] GHz	**Tunability**	**Q at 10 GHz**	**Power consumption**	**DC control voltage**	**Response time (speed)**	**Cost**
Semi Cond **PIN/Schottky** **GaAs FET** **GaAs Varac**	High	Moderate [30-60]	Poor 1-5 mW 1-5 mW 100-300 mW	 1-10 V 1-10 V 10-40 V	Fast 1-5 ns 2-10 ns 1-5 µs	Moderate to High
MEMS **Varactor**	Low	V good 100-1000	Excellent <<1 µW	10-100v	Slow >5 µ s	Low to Moderate
Ferroelectrics **Thin film** **Thick film**	Moderate to High	Moderate <30;100 <20	Excellent <<1 µW <<1 µW	<20 V 10-100 V	Very fast <1 ns <1 ns	Low
LC	Moderate	-	<<100 µW	<30 V	>10 ms	Low

Tab. 1 Some parameters for microwave components for competing technologies [52].

3.3 Agile metamaterials

3.3.1 Tunable Omega type structure

The example of figure 3-13 shows the possibility of tuning the electromagnetic properties via a change of the operating frequency [53]. However, in many practical applications, it is interesting to vary the operating point at a fixed frequency. This can be done by changing the dielectric properties of the constituent materials. In the following, such a change is exemplified via the use of LC technology.

Indeed, it is well known that LCs such as nematic compound is birefringent. This means that they exhibit different index values along the long and short axes of the ellipsoidal shaped molecules. The LC molecules can be oriented primarily, but also, reoriented using an external stimuli such as electric or magnetic field. The idea for tuning the properties of metamaterials is to reorientate the LC films that are infiltrated within the back to back of C shaped motifs of omega particles.

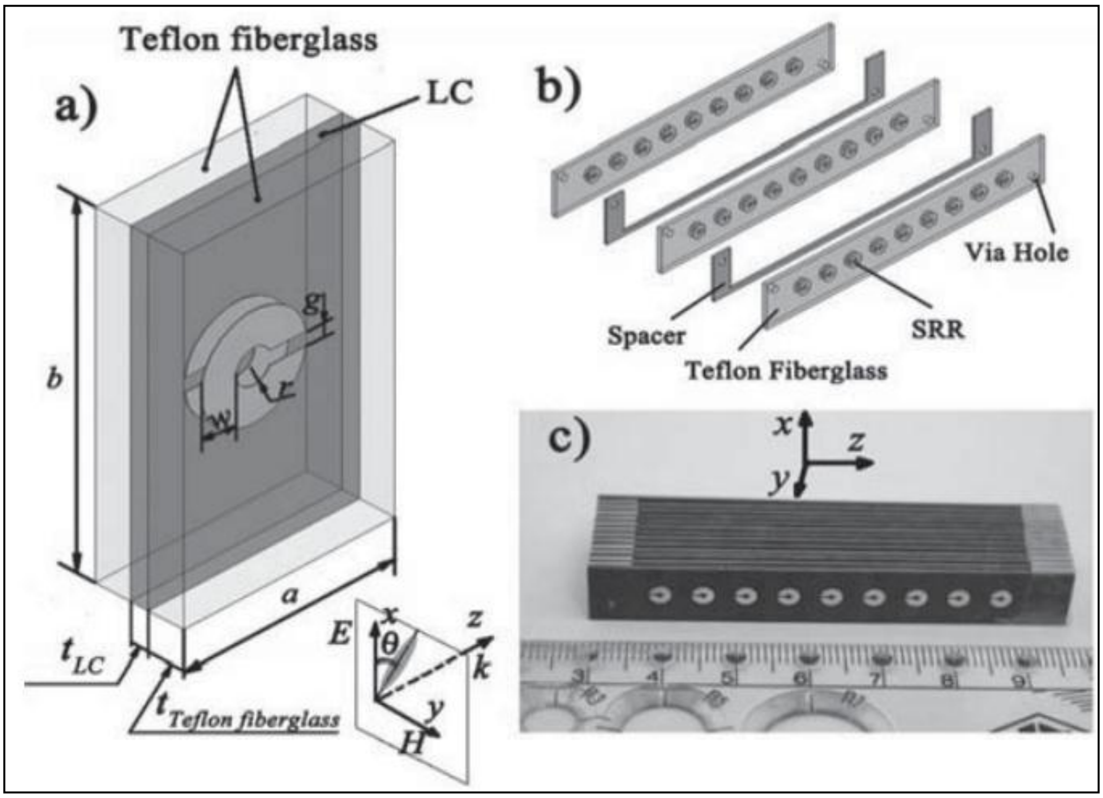

Figure 3-13 Experimental demonstration of the tunability of single negative media using liquid crystal (LC) where ellipsoidal shaped nematics are reoriented with permanent magnets [53].

The basic metamaterial unit cell of the magnetic negative medium is presented in the figure 3-13-(a). The fact of using back to back gap configuration is motivated by the search of pure magnetic response by cancelling the electric field induced currents. Under the condition of a single negative medium, the index is purely imaginary. In terms of propagation properties, this corresponds to evanescent waves in the frequency band where μ_{eff} is negative. As a result, a stop band is expected rather than passband transmission characteristics. For tunability purposes, LCs are infiltrated between the two metal C shaped unit cells by means of spacer layers as illustrated in figure 3-13-(b). Their reorientation (θ

angle) as a function of the electric field polarization is controlled experimentally via permanent magnets.

In figure 3-14, the frequency dependence of the transmission coefficient, measured (figure 3-14-(a)) through a “Vector Network Analyzer” and calculated by full wave analysis (figure 3-14-(b)) is compared [53]. Similar trends are obtained for calculated and measured data in agreement with frequency shift predicted when θ is increased between 0° and 90°.

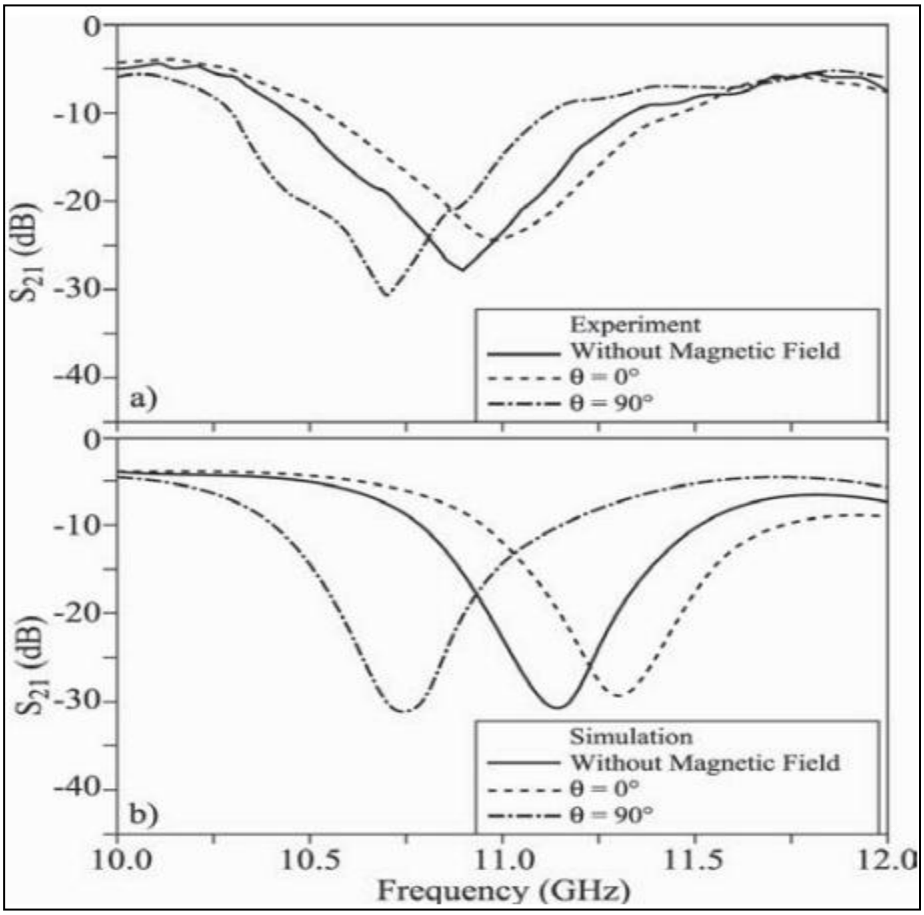

Figure 3-14 A comparison between simulated and measured single negative permeability metamaterial scattering parameters S_{21} [53].

3.3.2 Tunable fishnet

Figure 3-15 shows schematic views of tunable fishnet metamaterial structure. It is composed of three layers; a layer of fishnet topologies patterned on the surface of Teflon fiberglass slabs with void in between designed to be infiltrated with a nematic LC [53]. The idea for tuning the left hand (LH) passband is to change the substrate effective permittivity via LC molecular reorientation, by applying a DC voltage between the top and bottom metal layers. To achieve all angles LC reorientation between 0° and 90°, a thin layer of Polymide

(PI) was spanned on the surface of the Teflon substrate and cooper element to force nematic LC to align parallel to the metal surface. The combination of electrical dipoles and current loops provides simultaneously negative permittivity and permeability.

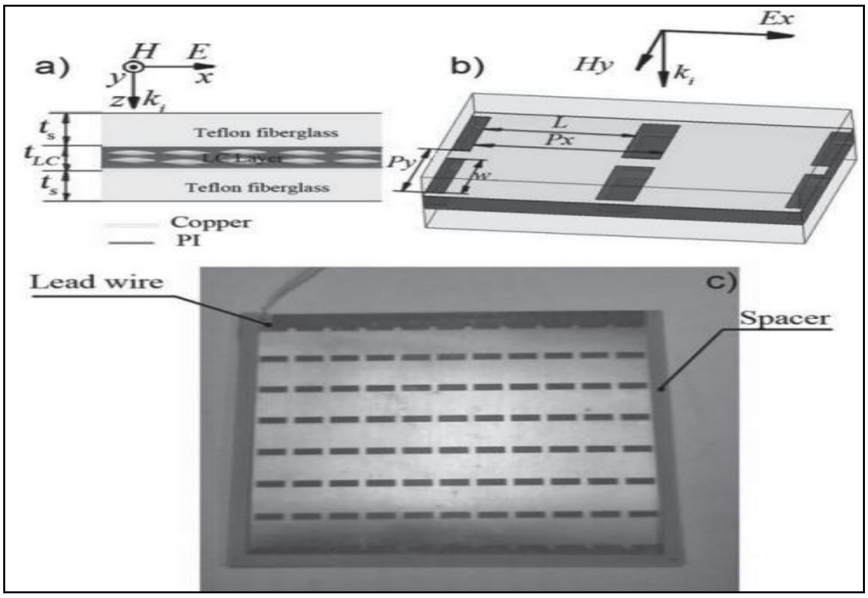

Figure 3-15 Schematic of the basic unit cell of fishnet metamaterial operating at microwaves and consisting of two staked rectangular aperture arrays: a) side view, b) 3D view and c) image [53].

The frequency dependence of the transmission, measured under various bias voltages has been compared with full wave calculation (figure 3-16).

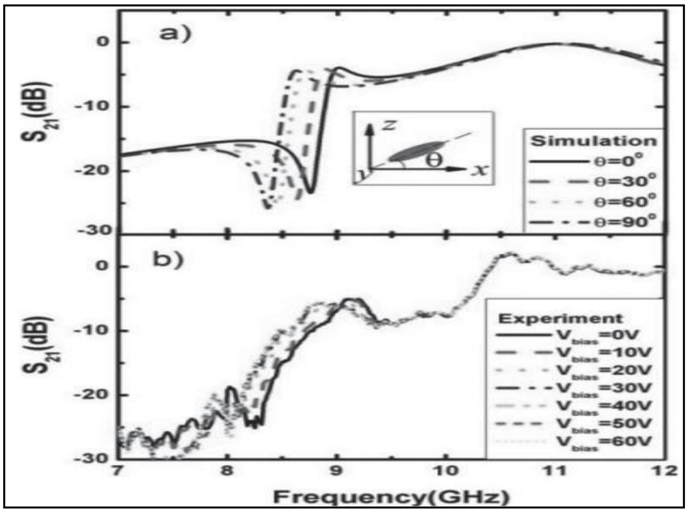

Figure 3-16 Frequency dependence of the transmission coefficient: a) Calculated. b) Measured [53].

As shown in figure 3-16, for the initial alignment with the LC director parallel to the fishnet surface, there is a peak with high intensity transmission around 9.01 GHz. As the LC director is oriented from 0° to 90°, it is shown that the ground transmission peak is shifted downward 8.6 GHz, accounting 400 MHz frequency variation.

3.3.3 Tunable phase shifter

As an illustration of the CRLH properties, we present a study results that make use of the coplanar waveguide technology.

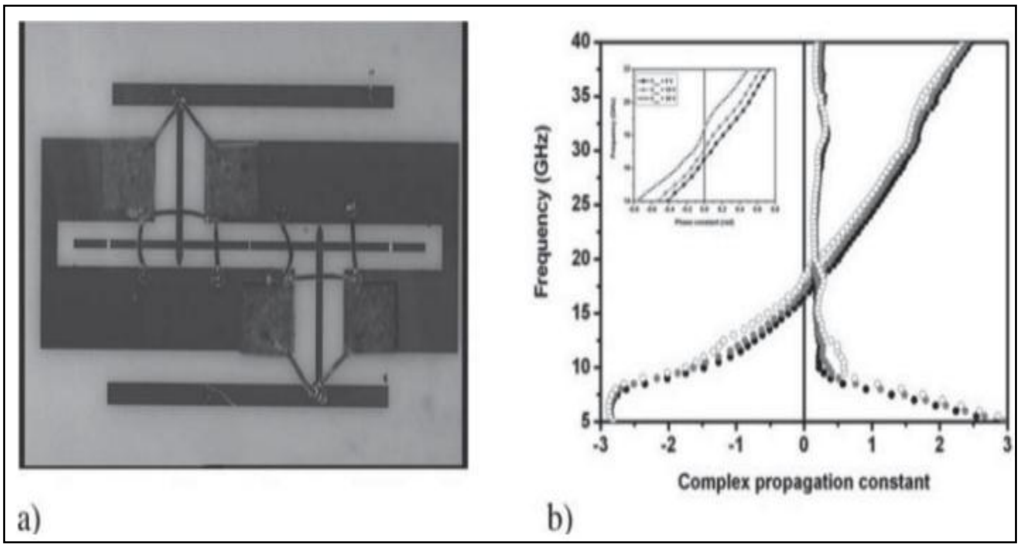

Figure 3-17 a) Image of prototype based on CPW transmission line loaded with series capacitances and shunt inductances based in thin ferroelectric film, b) Dispersion characteristics for various DC voltages controlling the ferroelectric film permittivity [53].

The series capacitance C_{LH} is designed by means of an interdigited pattern. The shunt inductances are realized with stub like unit cells. A thin ferroelectric film is deposited onto the substrate prior to the metallization for tenability purposes [53]. The inductance metal strips are also used for biasing electronically controlled capacitance through the variation of the permittivity of the ferroelectric films.

The measured dispersion characteristics can be retrieved from the complex scattering parameters measurement and are shown in figure 3-17 (b). There is a transition between the left handed dispersion branch (negative values of k) and the right handed dispersion branch. The varactors or MEMS allow shifting between the left and right handed bands.

3.4 Agile cross type unit cell metamaterial

3.4.1 Design of the agile cross type unit cell

As already mentioned in section 3.1, our metamaterial layer is a periodic arrangement of cross unit cells, it has two equal periods ***a*** in the *x* and *y* directions as shown in figure 3-18 (a). The cross type unit cell is made of dielectric substrate of thickness ***d*** on which a metallic cross like conductor is printed. This cross like conductor a length ***L*** such as $L \leq a$, a width ***w*** and a thickness ***t*** as shown in figure 3-18 (b).

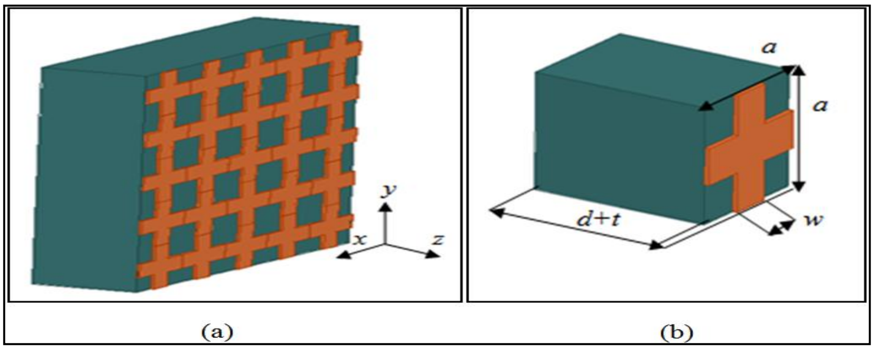

Figure 3-18 a) Metamaterial layer, b) Cross unit cell.

3.4.2 Description of the agile cross type unit cell

The agile cross unit cell has two configurations: the first one consists of a connected cross as shown in figure 3-19-(a), it is characterized by: $L = a$, the second one represents a disconnected cross where a gap ***g*** is produced inside or outside the conductor cross as shown in figure 3-19 (b) and (c).

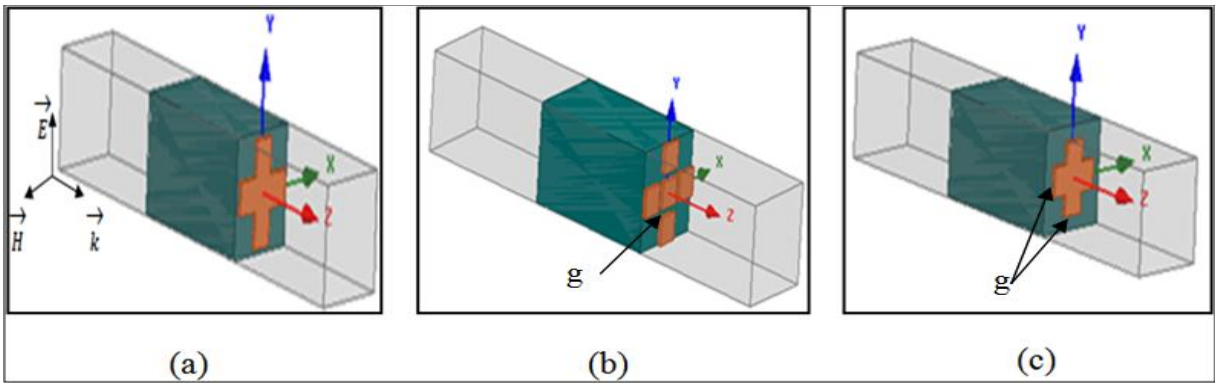

Figure 3-19 Different cross unit cells: a). Connected cross unit cell, b) Disconnected cross unit cell: model 1 and c) Disconnected cross unit cell: model 2.

To describe the behavior of the agile metamaterial layer, the metamaterial unit cell *S* parameters are calculated using a commercial code based on the finite element method. The imposed conditions on the unit cell are: i) perfect electric conductor (PEC) on the planes parallel to the *(xz)* plane (figure 3-19), ii) perfect magnetic conductor (PMC) in the planes parallel to the (*yz*) plane (figure 3-19) and iii) the electric and magnetic fields $\vec{E}$, $\vec{H}$ are, respectively, in the *y* and *x* directions. The wave propagation is in the *z* direction (wave vector $\vec{k}$ axis) (figure 3-19).

PEC/PMC can be seen as special cases for Bloch's boundary condition (periodic boundary condition) where the $\vec{k}$ vector is set to zero in the corresponding directions. The waves or the fields in Bloch's state are in an infinite periodic structure (metamaterial layer) and can be calculated by using the elementary unit cell approach and the image theory. Using the image theory, the electric and magnetic fields $\vec{E}$, $\vec{H}$ of the adjacent unit cells are also in the *y* and *x* directions as the elementary unit cell. Then, a 2D periodic metamaterial layer is structured. Consequently the effective constitutive parameters of 2D periodic metamaterial layer are equal to that of the elementary unit cell.

The agile cross unit cell metamaterial has two different configurations as presented in the figure 3-20 (a-b). We can flip between the desired behaviors by external commutation systems (using MEMS, PIN diodes…). The agile cross unit cell metamaterial is simulated over the [25 – 50] GHz frequency band where the operating frequency f_o = 40 GHz. We use e^{-jwt} harmonic time dependence

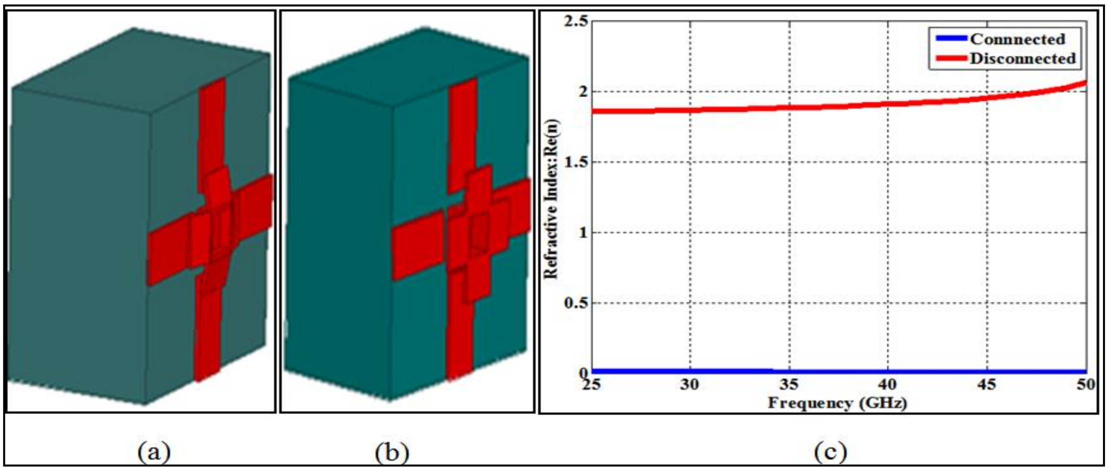

Figure 3-20 Agile cross unit cell controlled by MEMS switch: a) Switch ON, b) Switch OFF, andc) Refractive index contrast.

When the commutator is switched to ON as shown in figure 3-20 (a), the cross unit cell is said connected and the obtained effective medium has low and close to zero refractive index as presented in figure 3-20 (c) (blue solid line:$Re(n) \approx 0$). When the commutator is switched to OFF (figure 3-20 (b)), the cross unit cell is said disconnected and the obtained effective medium has a refractive index greater than unity over the frequency band (red solid line as shown in figure 3-20 (c)).

3.4.3 Bianisotropic metamaterial analysis

The electromagnetic response of the agile cross unit cell depends upon the direction of the applied electric and magnetic fields. This fact is related to the symmetry of the unit cell (position of the conductor cross in the unit cell). As depicted in figure 3-18 (b), our cross unit cell is asymmetric ($S_{11} \neq S_{22}$) and is qualified as a bianisotropic structure. It presents a magnetoelectric coupling effect: the magnetic field interacts with matter and introduces electric dipoles (polarization) in the medium and inversely the electric field introduces magnetic dipoles (magnetization). This effect is quantified by the coefficients $\bar{\bar{\xi}}$ and $\bar{\bar{\zeta}}$ in equations (2-6). The constitutive relations describing the cross unit cell are:

$$\begin{aligned} D_y &= \varepsilon_0 \varepsilon_y E_y - j\frac{1}{c}\xi_0 H_x \\ B_x &= \mu_0 \mu_x H_x + j\frac{1}{c}\xi_0 E_y \end{aligned} \qquad (3\text{-}1)$$

We note that ε_y, μ_x and ξ_0 are dimensionless quantities. ε_0, μ_0 D_y and H_x are respectively; the permittivity, the permeability of vacuum, the electric, and the magnetic flux densities.

3.4.4 Effective parameters extraction using FI and FS methods

3.4.4.1. Connected unit cell type metamaterial

In the case where the spacing between scattering elements is much smaller than the operating wave length, the metamaterial is seen as homogenous and it responds to electromagnetic waves in a similar way as continuous materials. In these conditions, metamaterials can be characterized by effective parameters without considering the local field distribution. The homogenization approach is based on the S parameters extraction and it is explained in the second chapter.

The connected cross unit cell to be characterized will be made of Rogers / Duroid 5880 (tm) dielectric substrate with ε_r =2.2 and the following physical dimensions (***a*** = 0.948 mm, ***w*** = 0.3 mm, ***d*** = 1.27 mm, ***t*** = 0.035 mm) as shown in figure 3-21 (a) where $f_0 = 40$ GHz.

First, we observe that the operating wavelength $\lambda_0 = c/f = 7.5$ mm. Then, the minimum homogenization ratio is $\lambda_0/(d+t) = 5.747$.

The extracted effective parameters ε_{eff} and μ_{eff} of the symmetric connected cross unit cell type metamaterial shown in figure 3-21 (a) using FI and FS methods are presented in figure 3-22. In the FS extraction method, the integration surface (purple color) is normal to the electric field direction, as shown in figure 3-21 (b-c). When the cross is continuous such as it intersects with the integration surface, as shown in figure 3-21 (a), the extraction procedure fails. This is due to the lost information present in the integration surface. This information is affected by the conduction current.

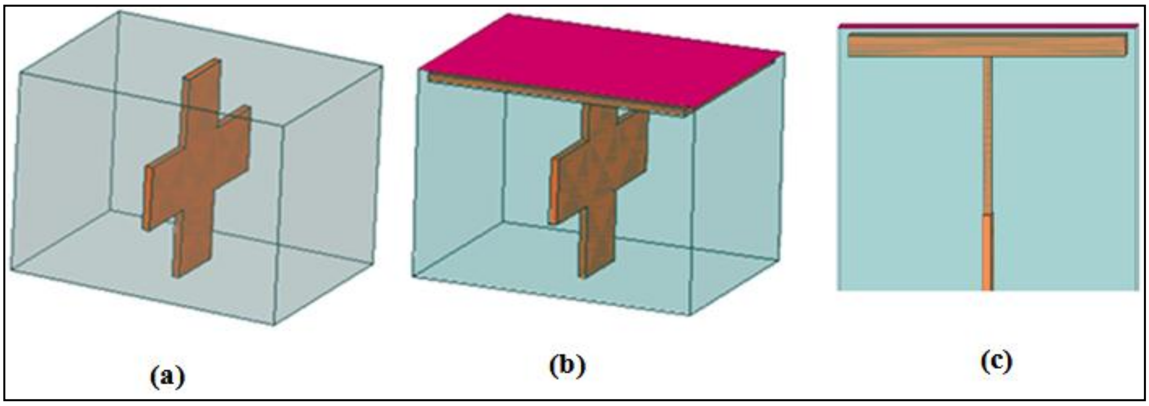

Figure 3-21 (a) Connected unit cell. (b) Integrated capacitor used in the field summation method. (c) The gap between the conductor plate and the integration surface.

The challenge in the connected unit cell is type metamaterial; how do we recuperate the conduction current, distributed in the integration surface? As a solution, a capacitor is introduced, which allows replacing the conduction current with a displacement current. Its effect depends on varying the geometrical dimensions such as the gap between the plate and the integration surface, the plate thickness, its length and width as shown in figure 3-21 (b-c). The choice of this capacitor dimensions is critical and very sensitive; the gap must be extremely reduced to ensure the recuperation from large point number on integration surface. Generally, the dimensions are varied in graduate manner to obtain the desired behaviors of effective permittivity and permeability. For example the capacitor of figure 3-21 (c) has a gap of 15 µm, the conductor plate has of a thickness of 35 µm, a width of 0.94 mm, and a length of 1.18 mm.

From the figure 3-22 (a), we note a good agreement between results obtained by the FI and FS methods for the effective permittivity. Otherwise, in the figure 3-22 (b), we note a good agreement between them for the imaginary part values, but the real part values of the effective permeability are less accurate.

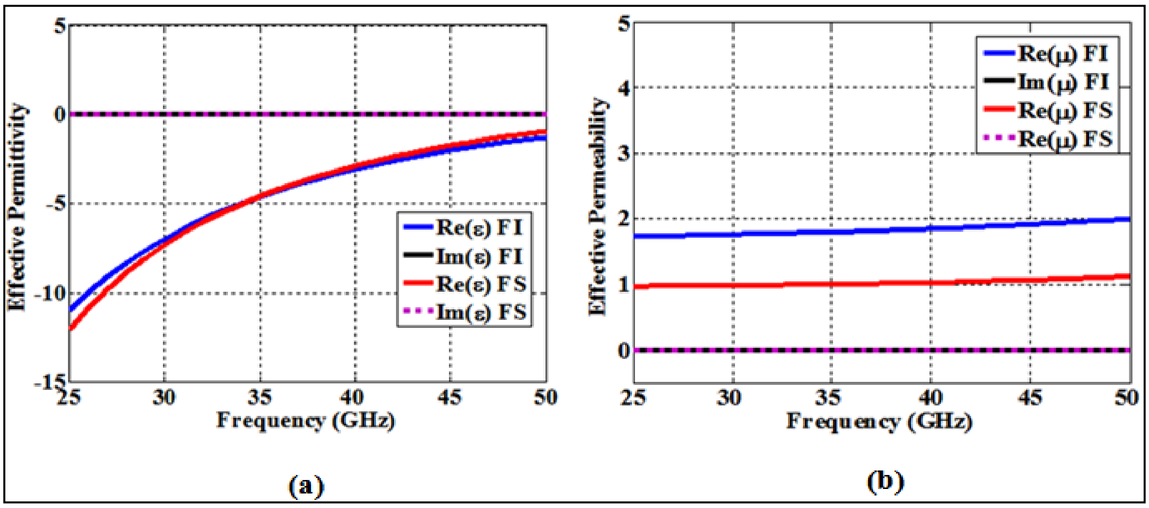

Figure 3-22 Comparison of the connected unit cell type metamaterial effective constitutive parameters between field summation (FS) and Fresnel inversion (FI) methods: a) ε_{eff} and b) μ_{eff}.

3.4.4.2. Disconnected unit cell type metamaterial

The simulated disconnected cross unit cell has the same physical dimensions as the connected one presented in figure 3-23 (***a*** = 0.948 mm, ***w*** = 0.3 mm, ***d*** = 1.27 mm, ***t*** = 0.035 mm) with a gap ***g*** = 0.14 mm.

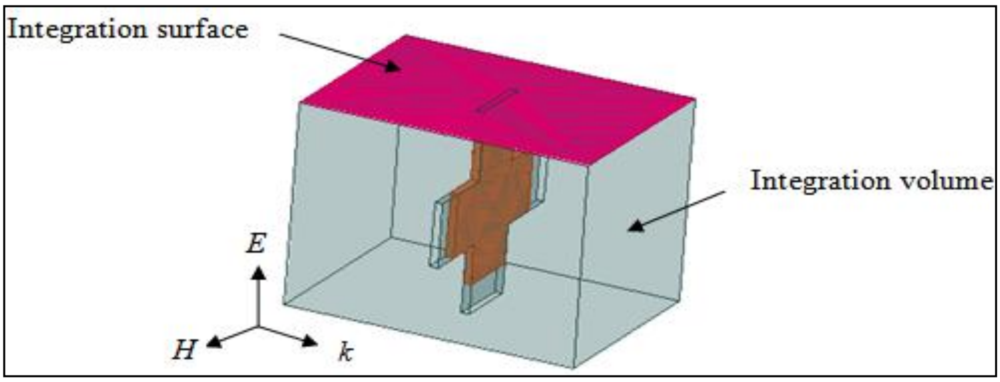

Figure 3-23 Surface and volume of integration in the field summation method.

The effective parameters ε_{eff} and μ_{eff} of the symmetric disconnected cross unit cell type metamaterial shown in figure 3-23 (***a*** = 0.984 mm, ***w*** = 0.3 mm, ***d*** = 1.27 mm, ***t*** = 0.035 mm and ***g*** = 0.14 mm) are presented in figure 3-24.

From the figure 3-24 (a-b), we observe that FS and FI methods are in good agreement for a wide frequency band [25-40] GHz where the values of the effective permittivity and permeability are very similar either for FS or FI methods.

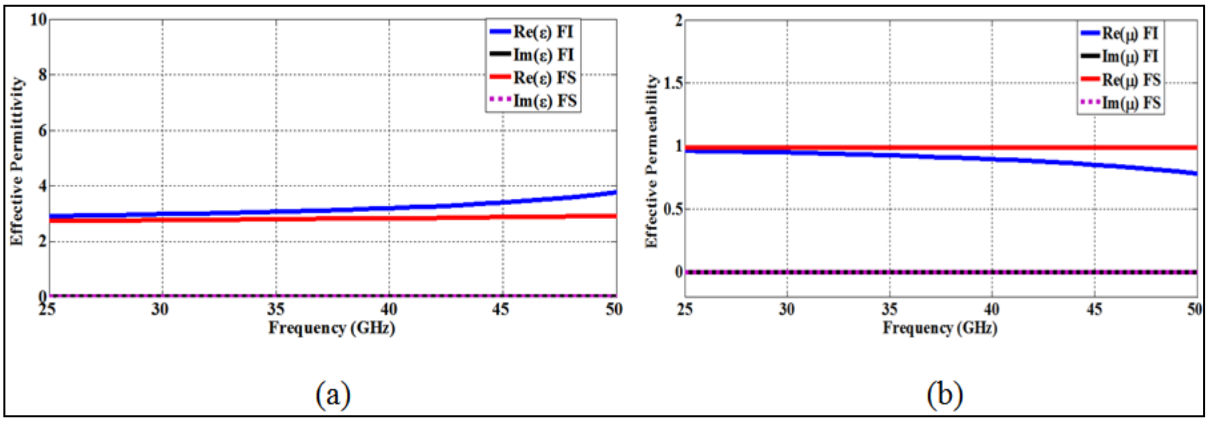

Figure 3-24 Disconnected cross type metamaterial effective parameters comparison between field summation (FS) and Fresnel inversion (FI) methods: a) ε_{eff}, b) μ_{eff}.

3.4.5 Periodic structures and metamaterial slab

Another possible applications of our bianisotropic metamaterial, is to design a metamaterial slab which is composed of a 3 D stacking of several cross type metamaterial layers (2 D structures) designed in section 3.4. For this, we use a new unit cell composed of an arrangement of several periodically spaced cross unit cells as shown in figure 3-25 (b).

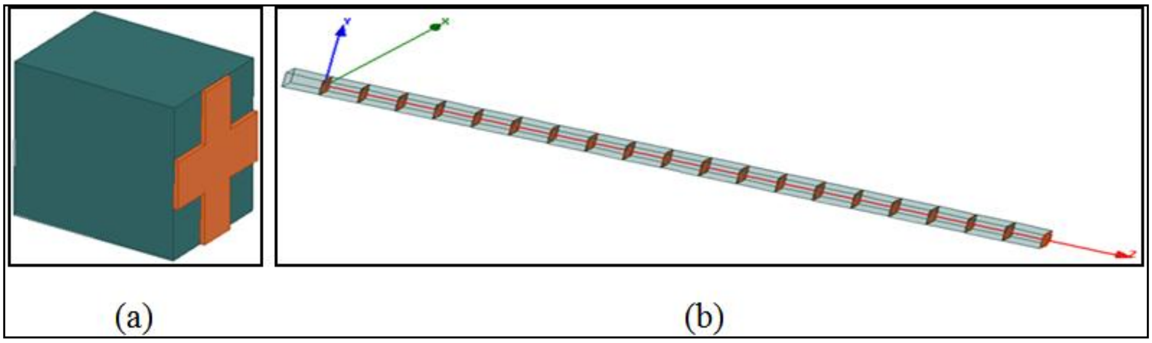

Figure 3-25 a) Asymmetric connected unit cell (a = 0.711 mm, w = 0.35 mm, d = 1.27 mm and t = 0.035 mm), b) Metamaterial slab having a length of 26.1 mm (20 unit cells).

Under the homogenization condition, the new metamaterial slab structure can be seen as a homogenous material. It can be also described by their effective constitutive parameters.

The figure 3-26 represents a comparison between effective parameters of a metamaterial slab (several connected cross unit cells) and a metamaterial layer (single cross unit cell).

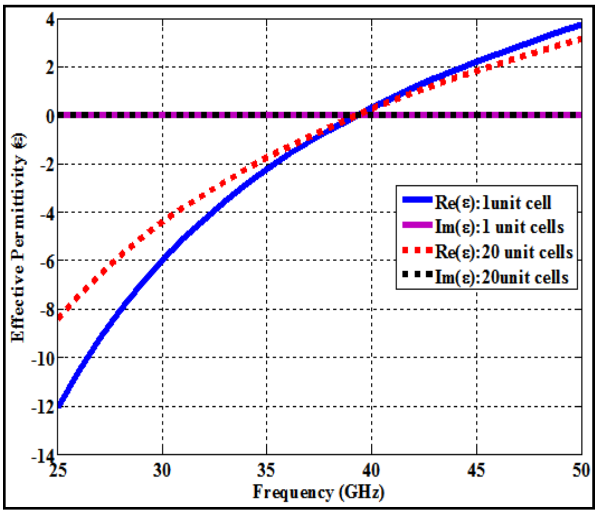

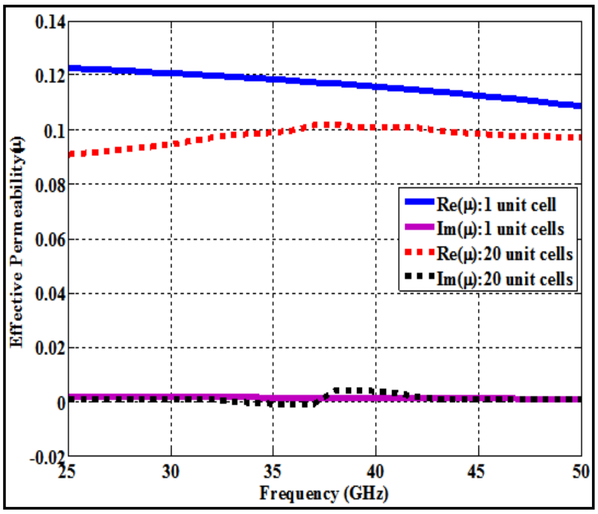

(a) (b)

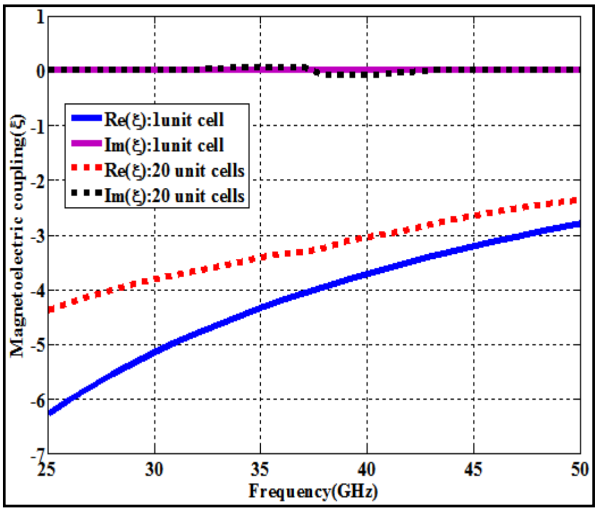

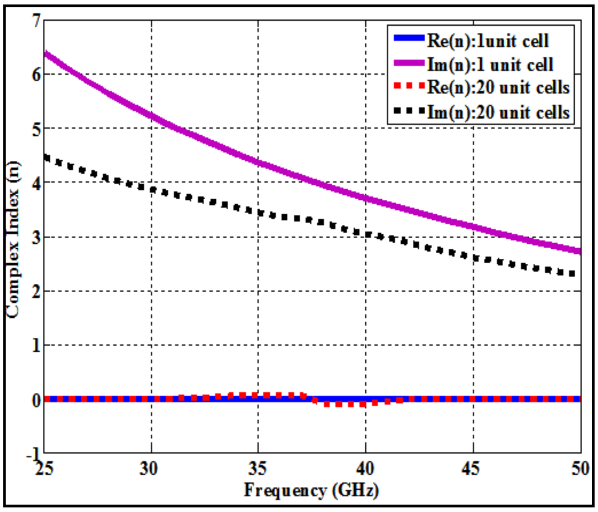

(c) (d)

Figure 3-26 Comparison of effective parameters between single metamaterial layer and metamaterial slab: real (blue solid and red dashed lines) and imaginary (magenta solid and dashed black lines) parts.

We observe from the figure 3-26 that the connected cross type metamaterial slab and the connected cross type metamaterial layer have almost the same effective parameters principally in the operating frequency range [40-50] GHz. We notice, in the low frequency region, a slight difference for the real part of effective permittivity and for the imaginary part of the refractive index. Note that the two connected cross type metamaterials (slab and layer) present the same plasma frequencies $f_p = 39.3$ GHz (figure 3-26-a). The most important difference concerns the magnetoelectric coupling factor. The slab presents a higher magnetoelectric coupling compared to the layer. The permittivity and the permeability imaginary parts are identical for the slab and the layer (figure 3-26 (a) and (b)) but we observe that for the refractive index, the slab has a lower imaginary part (figure 3-26- (d)). This fact must be explored and clarified. Indeed, the refractive index imaginary part accounts for losses in the medium and we expect to have more losses in the slab. Over all, we can consider that the connected cross type metamaterial slab can be described by the same constitutive parameters as the connected cross type metamaterial layer.

For the disconnected metamaterial slab shown in figure 3-27 (b), the structure length in the wave propagation direction is greater than the wave length, the phase of complex quantities exceeds 2π which results on a phase ambiguity $\left(\theta = \theta_0 + m\pi, \quad m = 1,2, \ldots\right)$, where m is the branch index to be determined. As it is corrected, consequently, the effective parameters are also corrected. A proposed correction over the frequency range is shown in figure 3-27 (c).

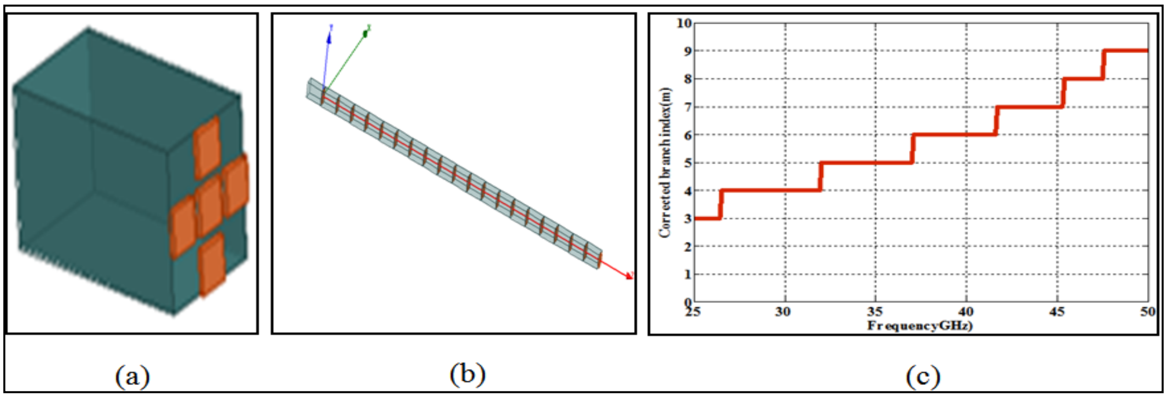

Figure 3-27 a) Disconnected unit cell ($a = 0.711$ mm, $w = 0.35$ mm, $d = 1.27$ mm, $t = 0.035$ mm and $g = 0.02$ mm), b) Association of 20 unit cells, and c) Corrected branch index m over the frequency range [25-50] GHz.

After the correction, the obtained results of effective parameters of disconnected metamaterial slab are compared and presented in figure 3-28.

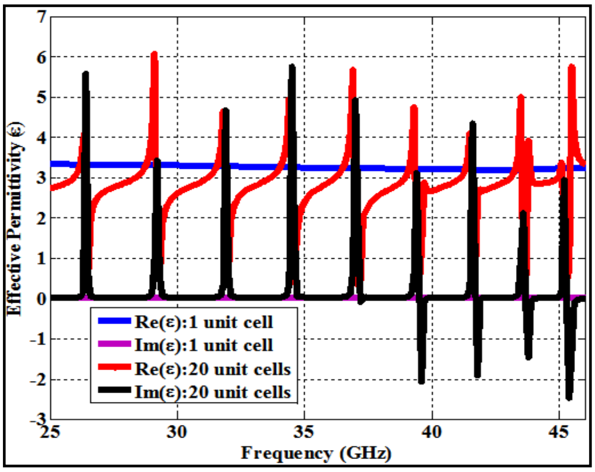

(a)

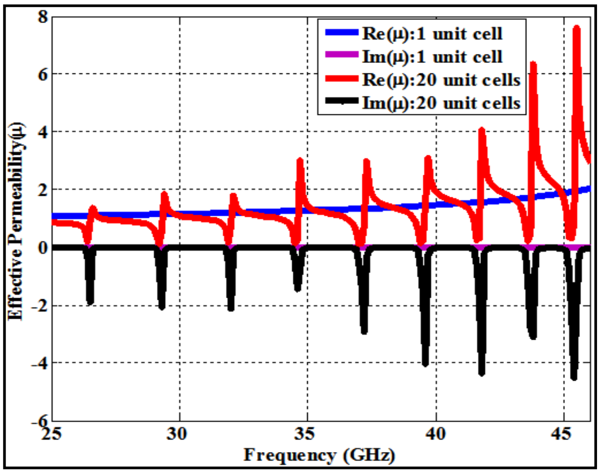

(b)

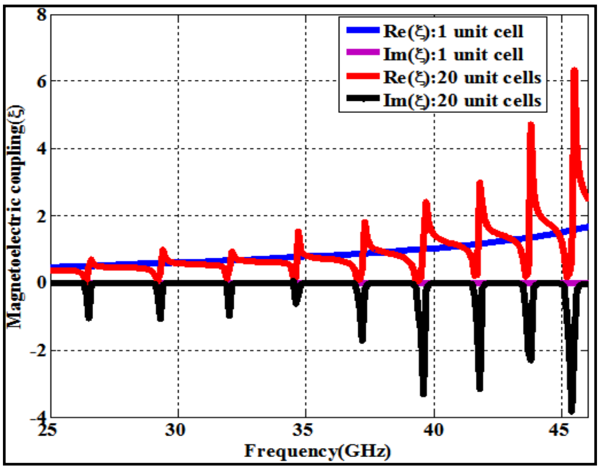

(c)

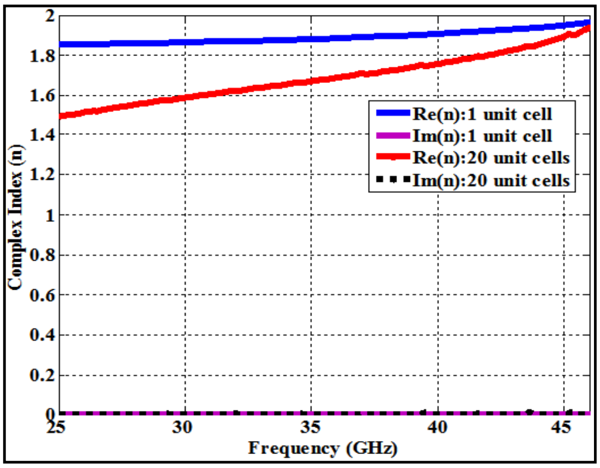

(d)

Figure 3-28 Comparison of corrected effective parameters of disconnected cross type metamaterial plane and slab: Real part (blue and red solid lines) and imaginary part (magenta and black solid lines).

We begin with the corrected complex refractive index shown in figure 3-28 (d), the metamaterial slab and the metamaterial layer have the same behavior: we observe the same imaginary parts (positive close to zero). The real parts of refractive index for the metamaterial layer and slab are very comparable ($Re(n) = 1.85$ for a metamaterial layer and 1.5 for a slab at 25 GHz). Consequently, the effective permittivity ε_{eff}, permeability μ_{eff} and magnetoelectric coupling coefficient ξ_0 are corrected, and calculated from the corrected complex index, the forward and backward wave impedances (z^+, z^-). For example at 25 GHz, $Re(\varepsilon_{eff}) = 3.3$ for one unit cell and it is 2.7 for a slab, $Re(\mu_{eff}) = 1.1$ for a disconnected unit cell metamaterial and 0.86 for the metamaterial slab, $Re(\xi_0) = 0.47$ for one unit cell and 0.38 for the slab. All the imaginary parts are positive and close to zero. Finally, the metamaterial slab behaves like a disconnected cross type metamaterial layer.

In fact, the discontinuities, in the extracted parameters of the slab of 20.1 mm, appear at frequencies where the metamaterial slab length is multiple of one half wavelengths in the material. These divergences appear at points corresponding to the multiple of one half wavelengths, the *S* parameters are very small, and then certain uncertainty will exist.

In the figure 3-29, a comparison of effective parameters of a symmetric disconnected cross type metamaterial slab (***a*** = 0.984 mm, ***w*** = 0.3 mm, ***d*** = 1.27 mm, ***t*** = 0.035 mm and ***g*** = 0.14 mm) between the FI and FS extraction procedures is presented.

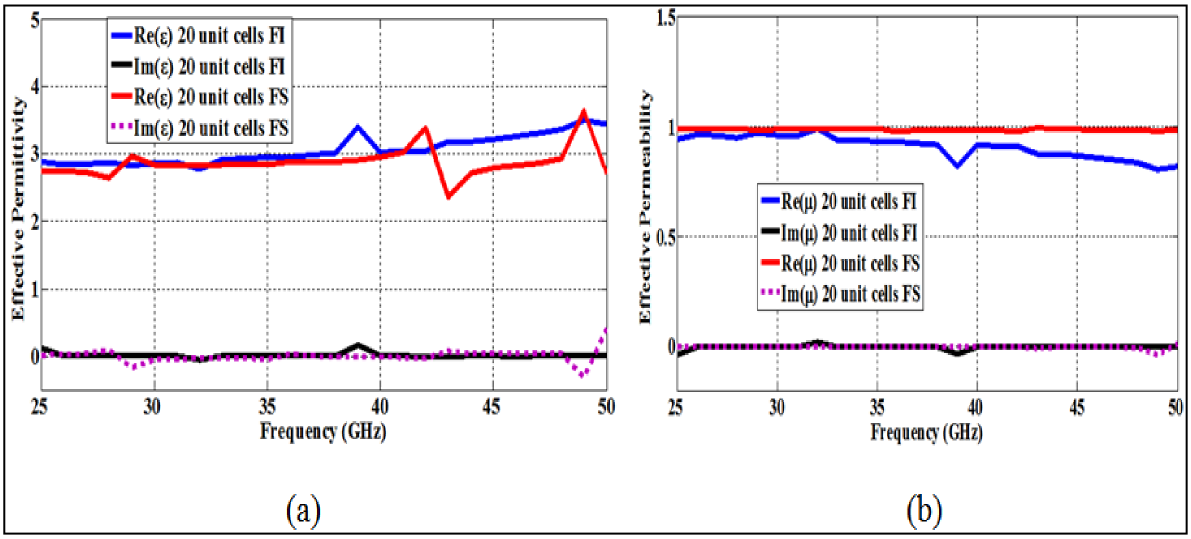

Figure 3-29 Effective parameters comparison between field summation (FS) and Fresnel inversion (FI) methods: a) ε_{eff} (1 unit cell), b) μ_{eff} (1 unit cell), c) ε_{eff} (20 unit cells) and d) μ_{eff} (20 unit cells).

From the figure 3-29, we note a good agreement for a wide frequency band [25-40] GHz between results obtained by FS and FI methods except for the frequencies where the metamaterial slab length is a multiple of one half wavelengths ($l = p\lambda/2$). Consequently the metamaterial slab is considered as behaving like a single unit cell and the numerical extraction methods (FS and FI) establish the same behaviors for the effective permittivity and permeability often the great difference concepts that they are based on.

3.5 Agile cross unit cell design

The electromagnetic properties of the cross unit cell type metamaterial depend strongly on its physical dimensions: the period ***a***, the dielectric subsrate thikness ***d***, the conducting strip width ***w***, the gap ***g*** and the dielectric permittivity $\boldsymbol{\varepsilon_r}$. These are key parameters for metamaterial tailloring (connected and disconnected cross type)

3.5.1 Effect of the period *"a"*

The period optimization is a fundamental concept in the homogenization. Then, to obtain more homogenized metamaterial, a few period values are available and their effect is presented in the figure 3-30.

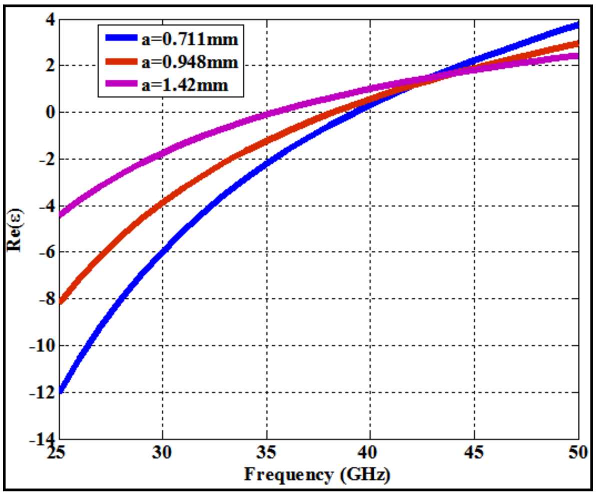

(a)

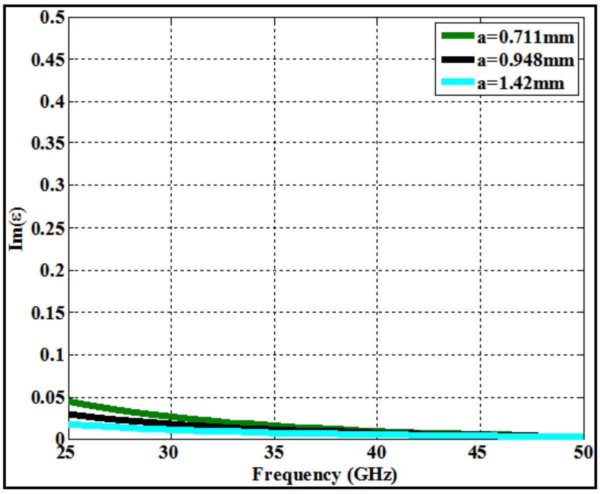

(b)

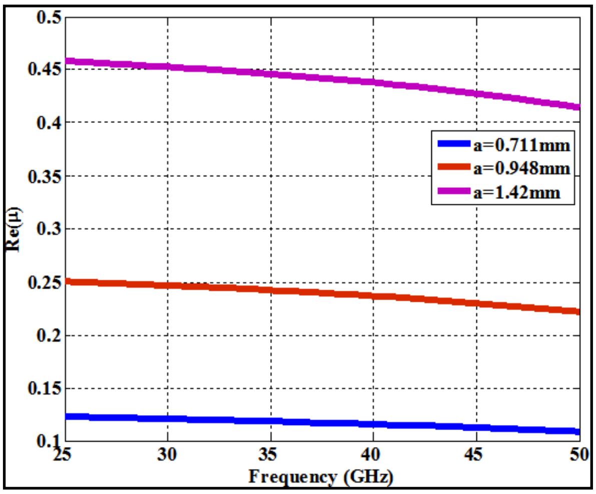

(c)

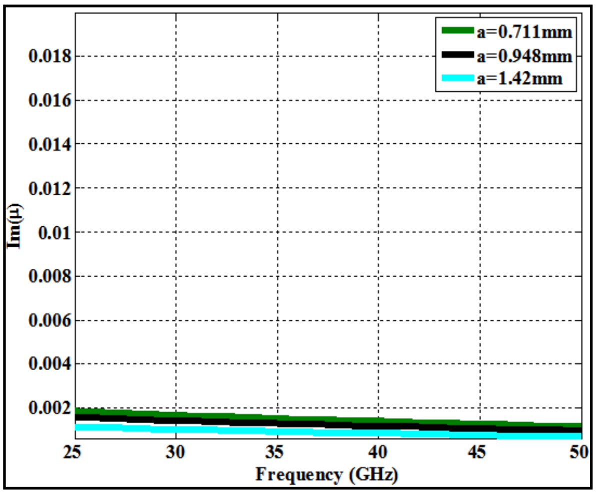

(d)

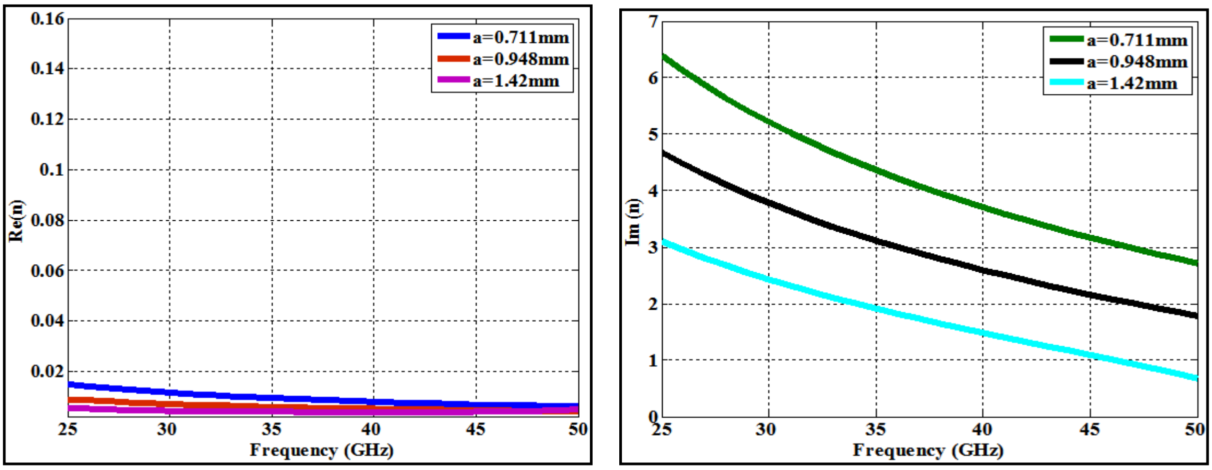

(e) (f)

Figure 3-30 Real and imaginary parts of the effective parameters when the period a is varied (known that d = 1.27 mm, w = 0.35 mm, ε_r = 2.2).

Figure 3-30, shows that the behavior of the metamaterial can be tuned by aging on the period value. The period $\boldsymbol{a}$ acts strongly on the metamaterial frequency plasma which is shifted to lower frequencies when $\boldsymbol{a}$ is increased. Even if the relative variation of the real part of the permeability is important when the period is increased, its amplitude varies slowly and stay very small than unity. We can also observe that the real part of the refraction index isn't very sensitive to the period variation, but the imaginary part does. That means losses in the metamaterial are sensitive to the period variation. When the period is increased, losses in the metamaterial are decreased. When choosing the period value, we need to keep in mind to respect the homogenization condition. To get a more homogenized metamaterial, the period must be a small fractionnal of the wavelengh. With a substrate thikness $\boldsymbol{d}$ = 1.27 and $\boldsymbol{a}$ = 1.42 mm the homogenization ratios are 5.747 and 5.28 times respectively. So, the metamaterials with $\boldsymbol{d}$ = 1.27 mm and ($\boldsymbol{a}$ = 0.711 mm or 0.948 mm) are more homogenized than the case where $\boldsymbol{d}$ = 1.27 mm and $\boldsymbol{a}$ = 1.42 mm.

3.5.2 Effect of the dielectric thickness "*d*"

The dielectric thickness $\boldsymbol{d}$ values are limited due to the homogenization criterion. Their effect on the effective constitutive parameters is shown in the figure 3-31.

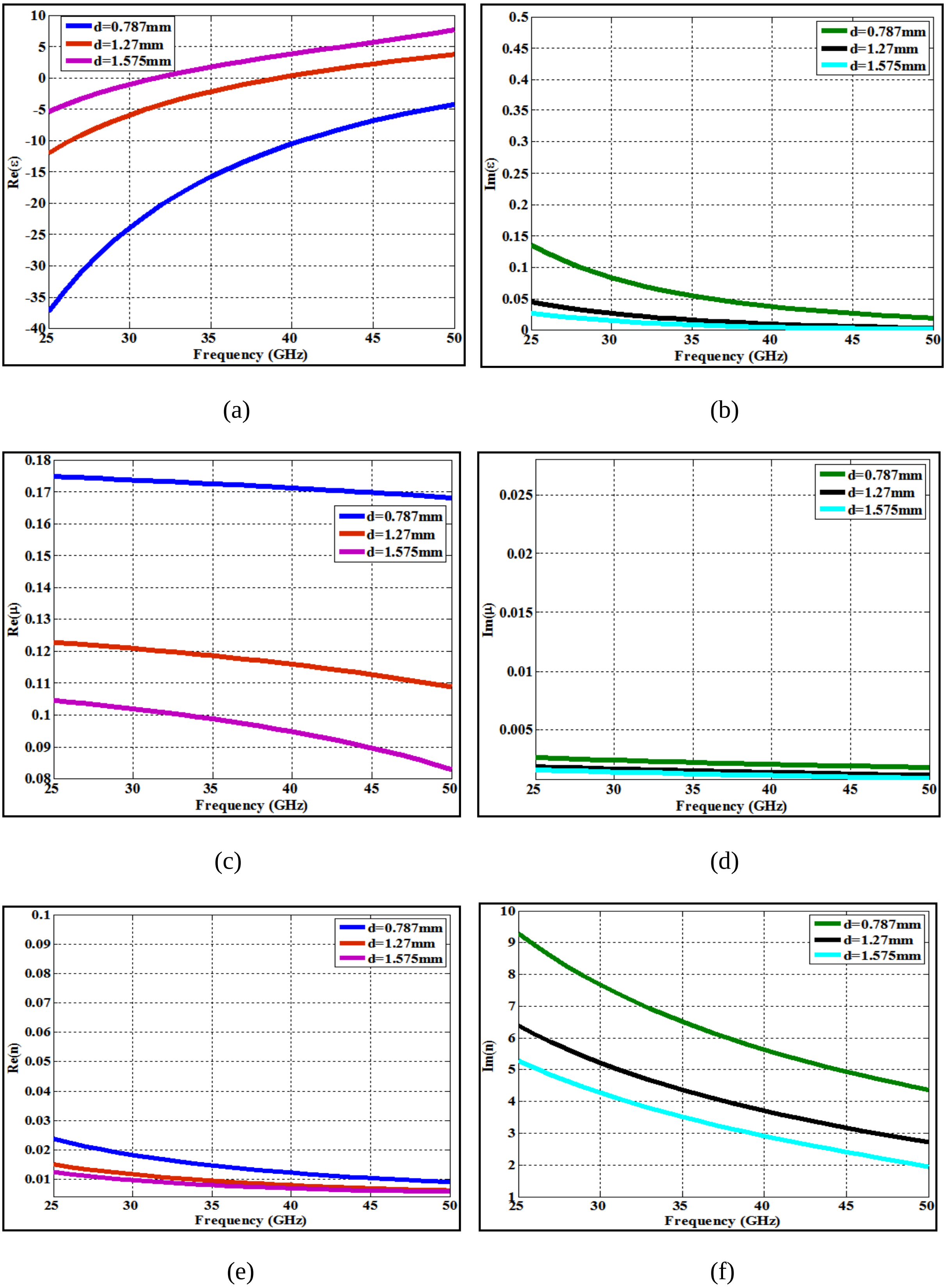

Figure 3-31 Real and imaginary parts of the metamaterial effective parameters when the dielectric thickness d is varied (such as a = 0.711 mm, w = 0.35 mm, ε_r = 2.2).

With these dielectric thickness values, the homogenization ratios are respectively (9.124, 5.747, and 4.658) times, this implies that metamaterial with $\boldsymbol{d} = 0.787$ mm is more homogenized. From the figure 3-31 (a to f), we observe that the increasing of $\boldsymbol{d}$ shifts the plasma frequency f_p to the lower frequencies and decreases losses in the metamaterial. Indeed the imaginary parts of the metamaterial complex parameters $Im(\varepsilon_{eff})$ and $Im(\mu_{eff})$ and $Re(n)$ are close to zero.

3.5.3 Effect of the width "w"

The effect of the width $\boldsymbol{w}$ on the effective constitutive parameters is shown in figure 3-32. From The figure 3-32, when $\boldsymbol{w}$ is increased then, we observe that the f_p and index imaginary part are increased. We have also $Im(\varepsilon_{eff})$, $Im(\mu_{eff})$ and $Re(n)$ close to zero.

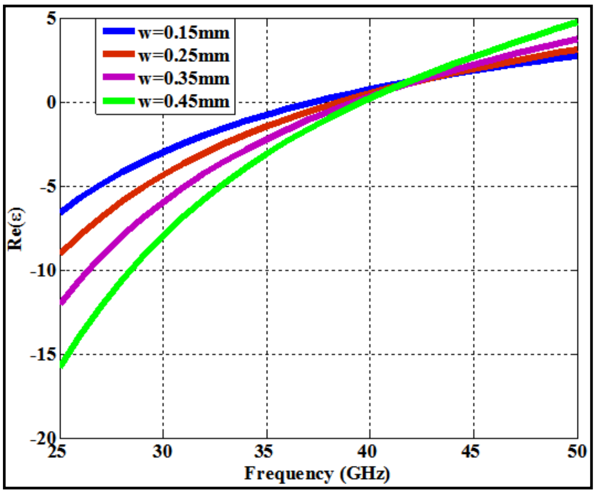

(a)

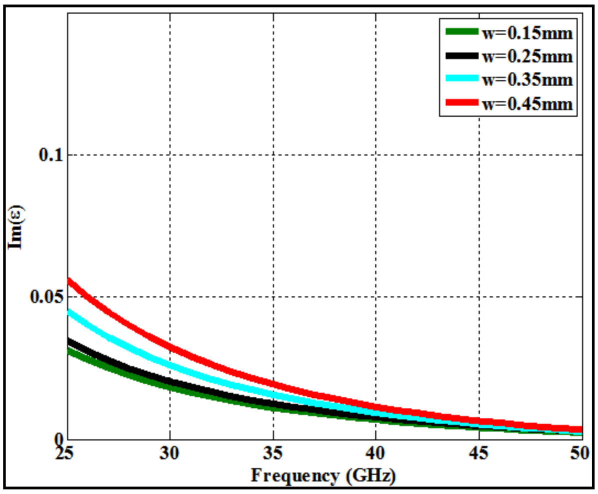

(b)

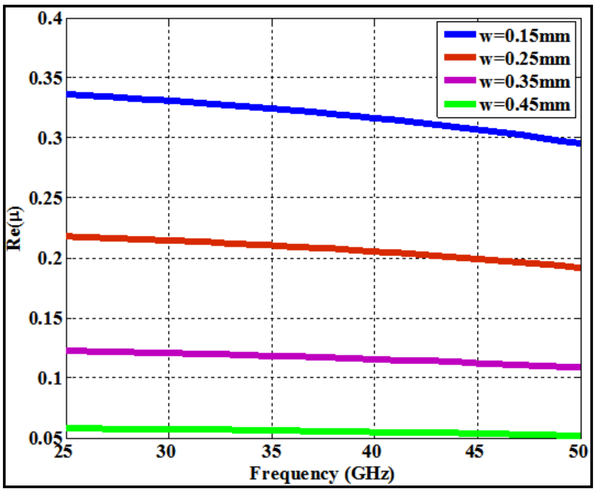

(c)

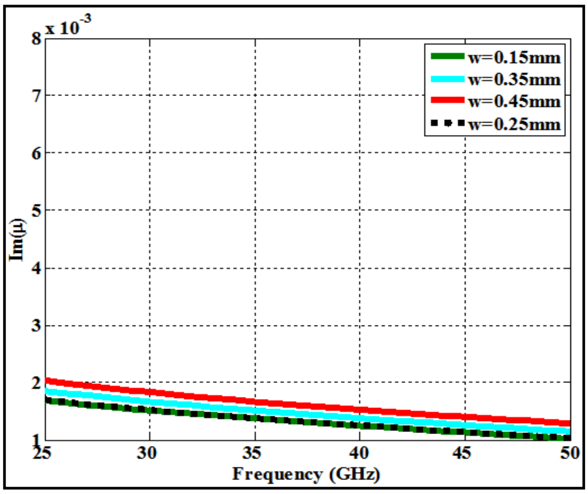

(d)

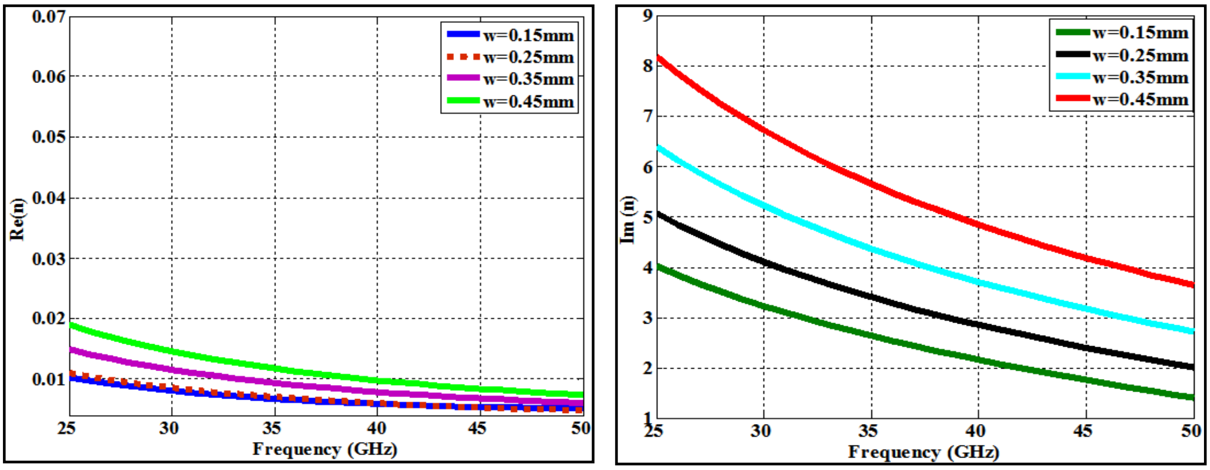

(e)(f)

Figure 3-32 Real and imaginary parts of the metamaterial effective parameters when the width *w* is varied (with a = 0.711 mm, d = 1.27 mm, ε_r = 2.2).

We observe a linear variation of the plasma frequency f_p with respect to the conducting strip width ***w***, as shown in figure 3-33.

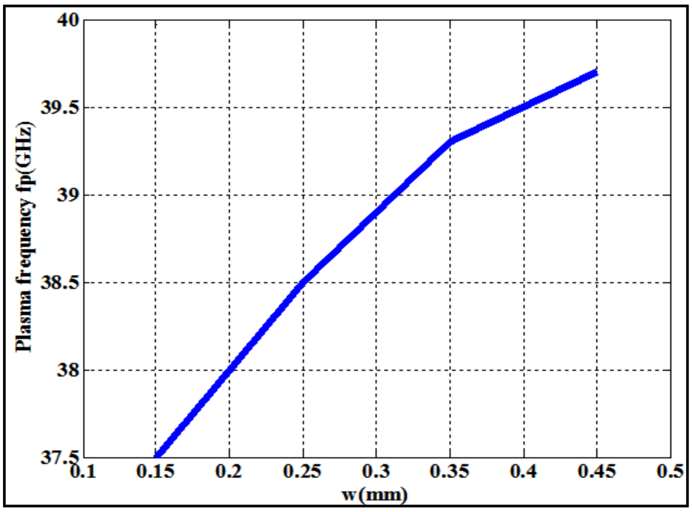

Figure 3-33 Plasma frequency f_p varying with respect to the width ***w***.

3.5.4 Effect of the substrate permittivity "ε_r"

The effect of the substrate permittivity ε_r on the effective constitutive parameters is presented in figure 3-34.

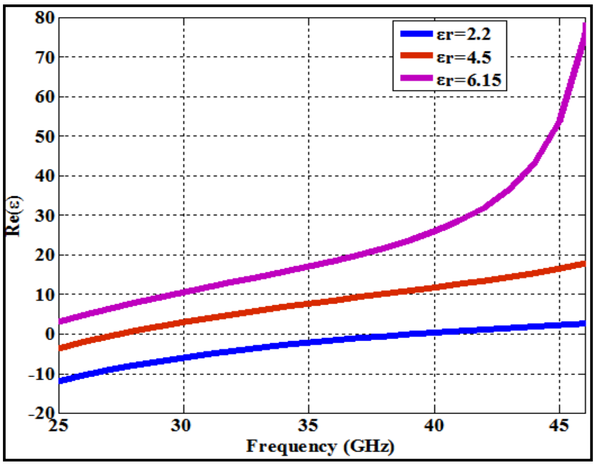

(a)

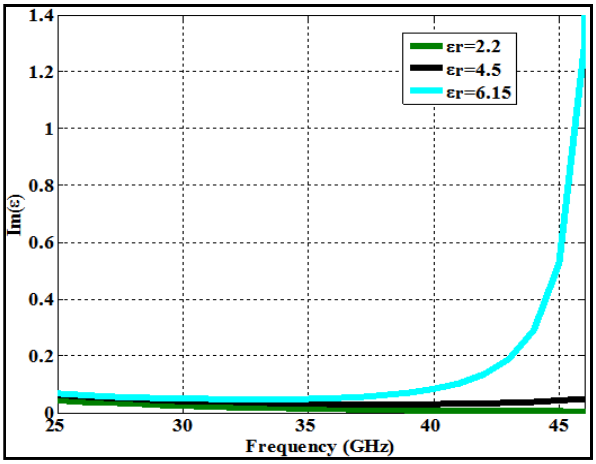

(b)

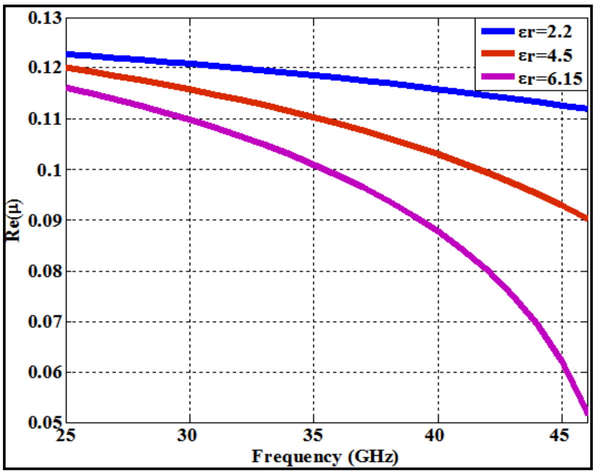

(c)

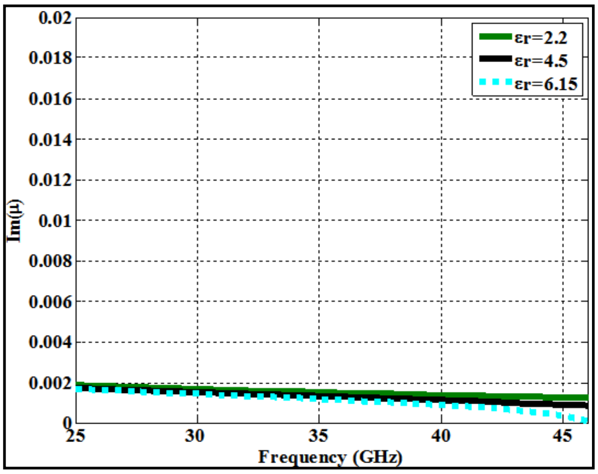

(d)

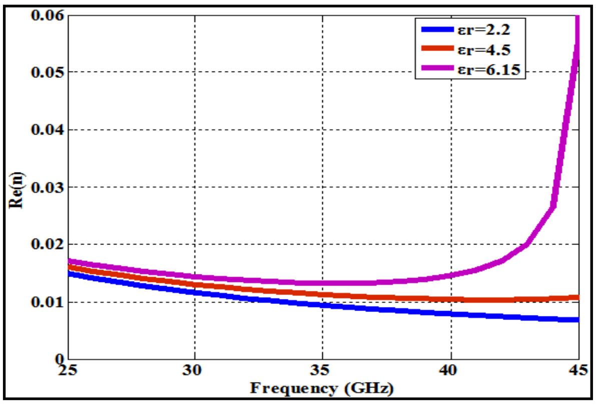

(e)

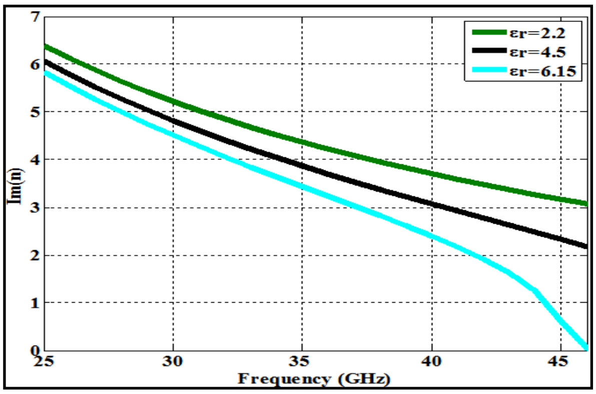

(f)

Figure 3-34 Real and imaginary parts of the metamaterial effective parameters when substrate permittivity ε_r is varied (with a = 0.711 mm, d = 1.27 mm, w = 0.35 mm).

From the figure 3-34, when ε_r is increased then, the f_p and the refraction index imaginary part are decreased. We have also $Im(\varepsilon_{eff})$ and $Im(\mu_{eff})$ close to zero.

As a conclusion, the fundamental characteristics of the connected cross type metamaterial are recapitulated in the following table.

Fundamental characteristics / Parameters effect ↗	Plasma frequency f_p (GHz)	Losses $Re(n)$	$\lvert Re(\xi_0)\rvert$	Resonance frequency f_r (GHz)
Period ***a*** (mm)	↘	↘	↘	↘
Substrate thickness ***d***(mm)	↘	↘	↘	↘
Width ***w*** (mm)	↗	↗	↗	↗
Substrate permittivity ε_r	↘	↘	↗	↘

Table 1. Connected cross type metamaterial characteristics variation with respect to the variation of ***a***, ***d***, ***w***, and ε_r, where ↗and ↘ denote the increasing and decreasing values.

3.5.5 Effect of the gap "g"

The effect of the gap ***g*** on the effective constitutive parameters is shown in figure 3-35.

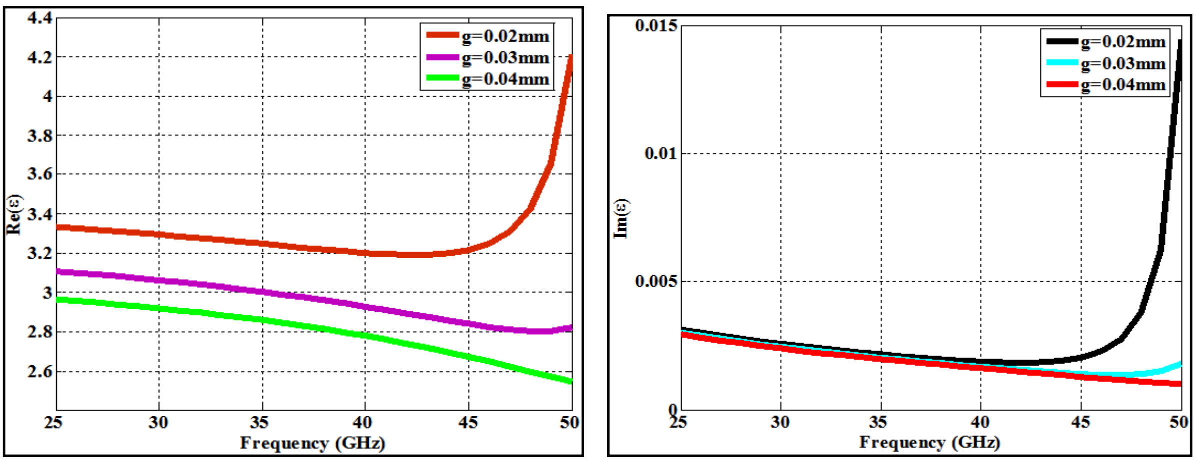

(a) (b)

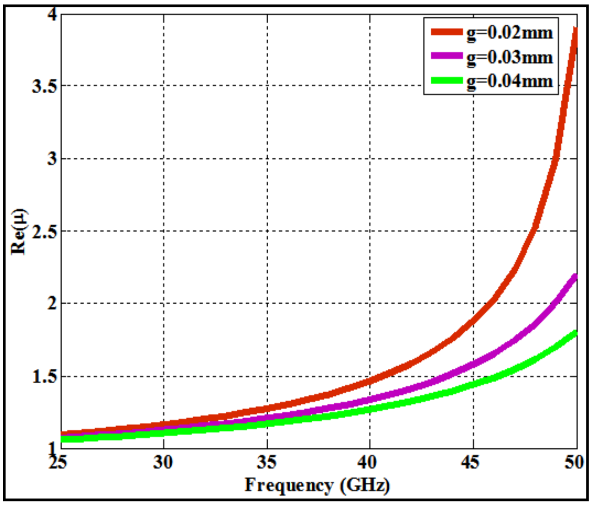

(c)

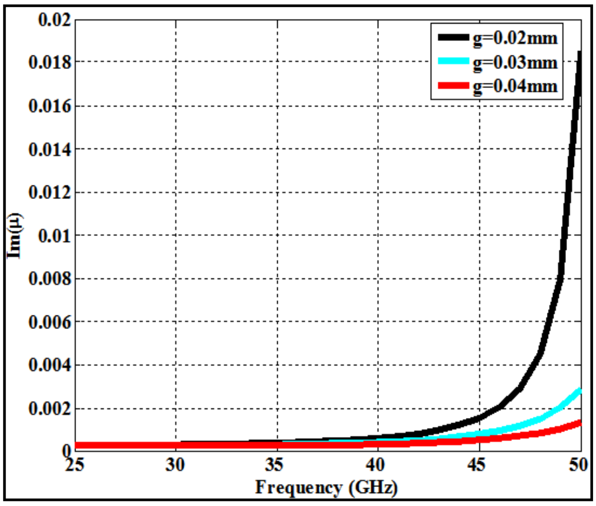

(d)

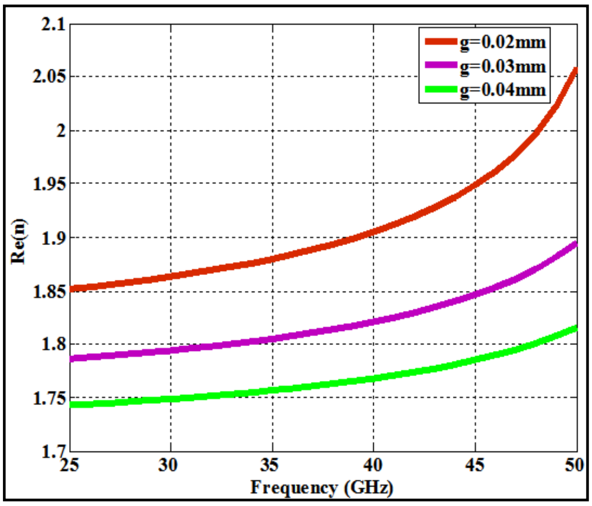

(e)

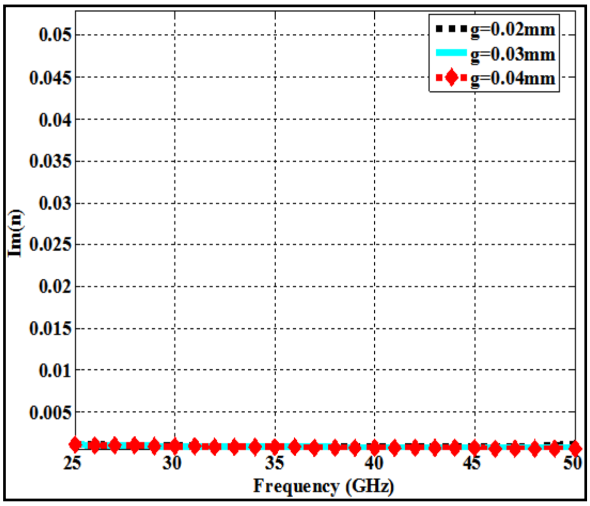

(f)

Figure 3-35 Real and imaginary parts of the meamaterial effective parameters when the gap *g* is varied (with *a* = 0.711 mm, *d* = 1.27 mm, *w* = 0.35 mm, ε_r = 2.2).

Figure 3-35 (a - b) demonstrate that $Im(\varepsilon_{eff})$ is less sensitive to the gap variation for the frequencies below a threshold value which increases with the gap and remains positive close to zero. Inversely to the connected unit cell, the disconnected one has $Re(\varepsilon_{eff}) > 2$ and it increases when ***g*** decreases. Specially, if ***g*** = 0.02 mm, $Re(\varepsilon_{eff})$ transits from 3.2 at 45 GHz to 4.2 at 50 GHz. In figure 3-35 (d), we have $Im(\mu_{eff}) \approx 0$ for frequencies below 40 GHz, for all values of the gap ***g***. In figure 3-35 (c) we observe that $Re(\mu_{eff}) > 1$ and it has non linear variation with the gap for frequencies greater than 35 GHz but this behavior decreases with ***g***. In figure 3-35 (e-f), one can see that the refractive index decreases with ***g*** ($n' > 1.85$ for $f = 40$ GHz and ***g*** = 0.02 mm) and has a very close to zero imaginary part.

The enhancement of our meatamaterial applications depends strongly on the two metamaterial unit cells (connected and disconnected type metamaterials) characteristics. They have to respect some constraints: more homogenized as possible, less losses as possible, having as flat responses as possible to be non dispersive in the operating frequency range and with a great refractive index contrast between the two configurations behavior. From the parametric study done above, we can choose the metamaterial unit cell dimensions which give the desired behaviors of our agile metamaterial that are: $\boldsymbol{a}$ = 0.711 mm, $\boldsymbol{d}$ = 1.27 mm, $\boldsymbol{w}$ = 0.35 mm, $\boldsymbol{g}$ = 0.02 mm and $\boldsymbol{\varepsilon_r}$ = 2.2.

3.6 Conclusion

Agility technical solutions such as agility devices like PIN diodes, varactor diodes or MEMS and agile materials like ferromagnetics, ferroelectrics, or liquid crystals (LC) make electronic systems such as (antennas, filters, phase shifters …) more flexible through the tuning in one or more frequency bands. Our agile metamaterial, based on the agile connected/ disconnected cross type unit cell, is an agile medium which can be controlled via MEMS switches. It can flip between two behaviors; the first one corresponds to the disconnected cross type metamaterial which has a refractive index greater than unity and the second one corresponds to the connected cross type metamaterial which has a refractive index close to zero. The refractive index contrast is a fundamental parameter in our agile microwave devices design. Our agile cross type unit cell has the physical dimensions: $\boldsymbol{a}$ = 0.711 mm, $\boldsymbol{d}$ = 1.27 mm, $\boldsymbol{w}$ = 0.35 mm, $\boldsymbol{g}$ = 0.02 mm and a substrate permittivity $\boldsymbol{\varepsilon_r}$ = 2.2.

4.Applications of agile metamaterials

4.1.Introduction

The agile metamaterial unit cell, studied in the previous chapter, which has two different switchable behaviors: a metamaterial with refractive index close to zero and other one with refractive index greater than unity is firstly arranged to obtain a planar agile and programmable metamaterial. Then, by stacking multiple agile metamaterial layers, we obtain an agile and programmable metamaterial bulk. This agile metamaterial bulk is used to 'emulate' microwave components or devices. In the literature the verb 'emulate' is the synonym of imitate or mimic. In this work, 'emulate' a microwave function means programming the metamaterial bulk to behaves like a desired conventional microwave device or component such as waveguides, horn antennas...

This chapter introduces the concept of emulation of microwave devices from the metamaterial bulk. As examples of microwaves devices emulation such as waveguides (circular and rectangular) and antennas (pyramidal and conical horn) will be presented.

4.2The agile metamaterial bulk

The concept of the agile unit cells is expanded to construct an agile metamaterial layer when they are elongated in the x and y directions as shown in figure 4-1 (a). Changing the switch states (ON/ OFF) in the metamaterial layer allows us to program it. Consequently, in the surface plane, distinct zones (sections) can be formed. These zones behave according to the switch states: if the switches are ON, the unit cells are connected and the metamaterial behaves as a medium with $Re(n) \approx 0$, and if they are switched OFF, the metamaterial behaves like a medium with $Re(n) > 1$ as shown in figure 4-1 (a).

To simplify the agile planar metamaterial layer concept, we compare it to the "black & white" picture. It is a matrix of N×M pixels as depicted in figure 4-1 (b). Each unit cell is represented by a pixel which can take two values; 0 if the switch is OFF and 1 if the switch is ON. Here, the agile metamaterial layer is compared to the pixilated picture.

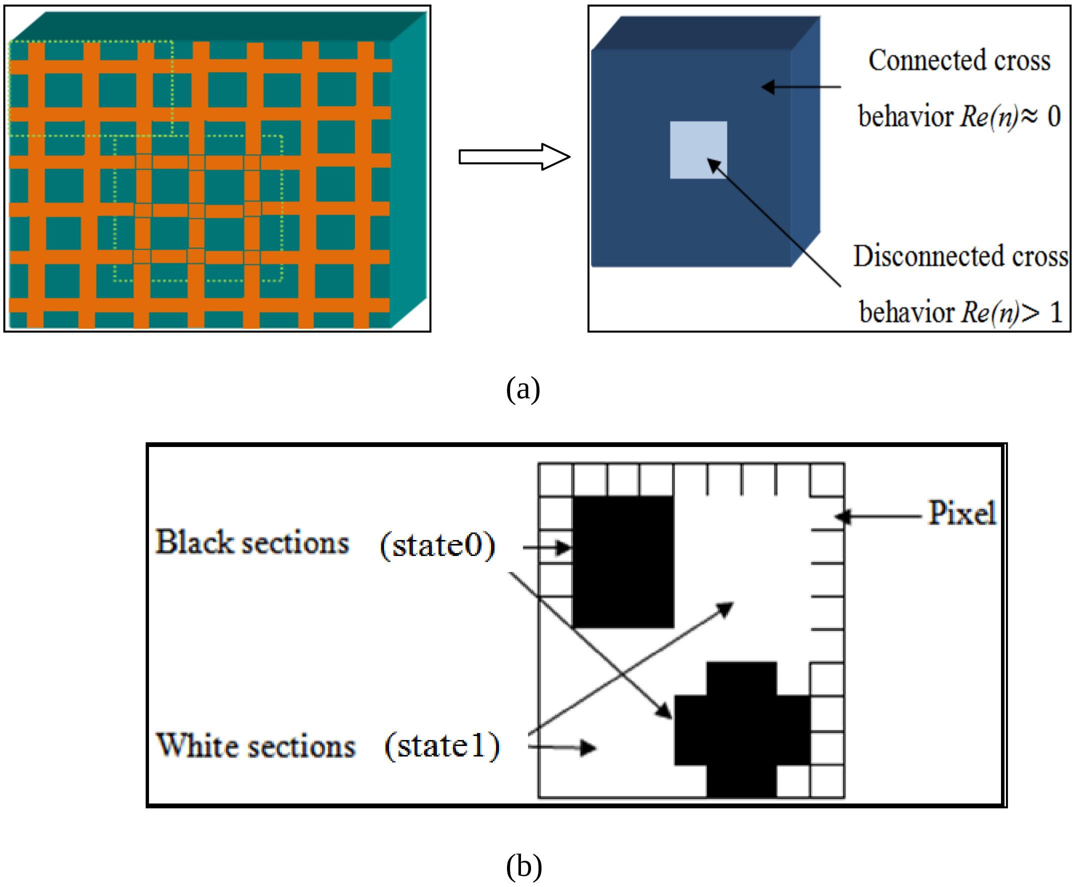

Figure 4-1 a) Effective connected and disconnected sections in planar metamaterial layer, b) Pixilated “black & white” image.

If multiple (say K) programmable metamaterial layers (but not necessarily identically programmed) are stacked in the wave propagation direction *z*, we get an agile metamterial bulk. It is like a 3D “black & white” image of N×M×K pixels. By actuating each switch (pixel), we can program a 3D object having a refraction index say n_1 in a 3D medium of refraction index n_2. The form of the 3D object is based on how the successive planar metamaterial layers are programmed. Finally, the 3D object is a key concept for the agile microwave devices. Hence, we are introducing a new concept of “functional” agile microwave devices. In other words, the agile metamaterial bulk can be programmed to have the same function (to behave) as, for example, a circular waveguide, a rectangular wave guide, a horn antenna, a pyramidal antenna, etc and this for different operating frequencies. So, we brew from computer science the terminology “emulate” to express the idea of “ to behave as”. The definition of “functional agility” becomes: The agile metamaterial device can “emulate” different components such as waveguides, antennas, and so on. Different microwave devices can be emulated with one programmable metamterial bulk.

4.2.1 Emulation of a rectangular waveguide

To emulate a rectangular waveguide using controllable (programmable) metamaterial bulk, we program every metamaterial layer from which the programmable metamaterial bulk is formed (figure 4-2-(a)). This metamaterial programming is performed through the control of the behavior of each agile unit cell, which constitutes the metamaterial layer. This unit cell control is achieved by acting on the switches situated on the unit cells to connect or disconnect the cross branches, see figure 4-2-(b).

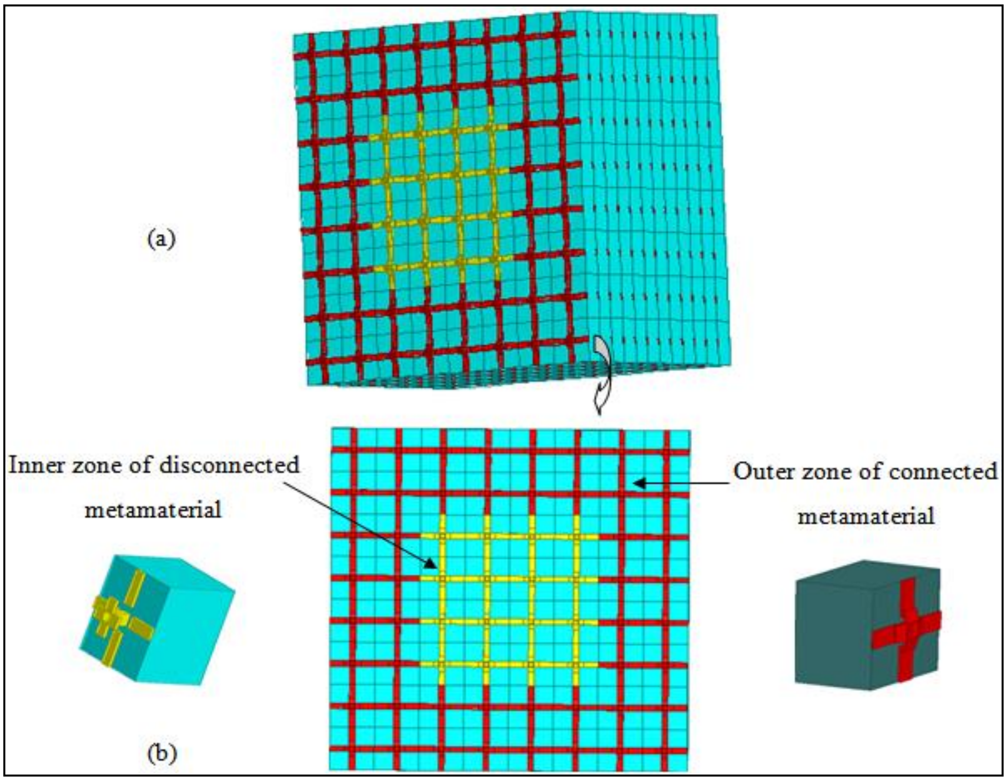

Figure 4-2 a) Metamaterial bulk, b) Switchable control in a metamaterial layer.

In programming a rectangular waveguide, every metamaterial layer is divided into two different zones, the first one constitutes the waveguide inner section and the second one constitutes the waveguide outer region as shown in figure 4-2-(b). For the waveguide inner section, which has a rectangular form and positioned in the center of the metamaterial layer (a grid of 8×4 unit cells), we use a disconnected cross type metamaterial with $Re(n) \approx 1.95$ and for the waveguide outer region, formed by the remaining area, we use a connected cross type metamaterial with $Re(n) \approx 0$. All the layers forming the metamaterial bulk are identical to the first one. The different steps of the emulation of such rectangular waveguide are illustrated in figure 4-3. To emulate the metamaterial rectangular waveguide using the commercial software code, we have simulated two effective continuous media. The first one is a continuous medium which behaves as disconnected cross type metamaterial with $Re(n) \approx 1.95$. The second one is a continuous medium which behaves as connected cross type metamaterial with $Re(n) \approx 0$.

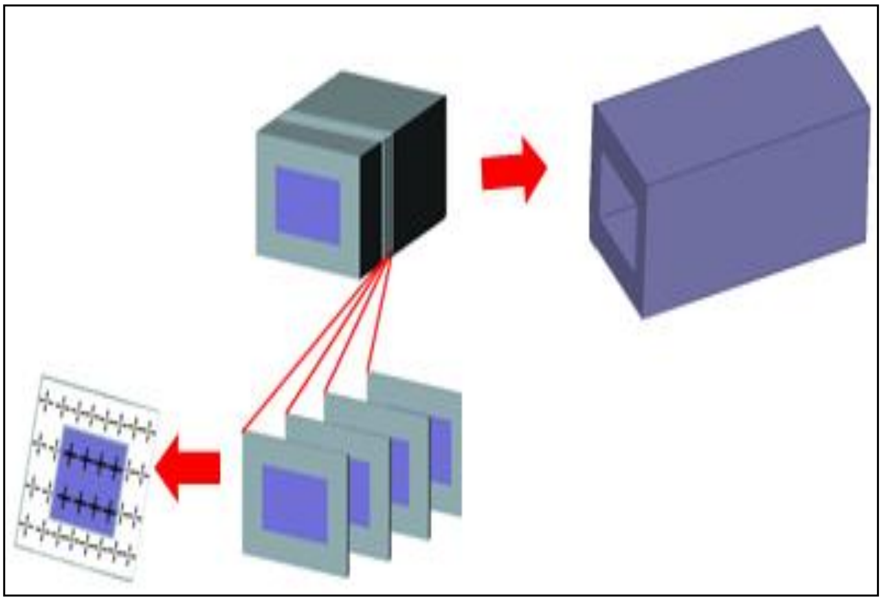

Figure 4-3 Rectangular waveguide emulation steps from agile metamaterial bulk.

In the figure 4-4 are presented the fundamental mode TE_{10} dispersion curve of the metallic rectangular waveguide (R400: 5.69 mm × 2.845 mm) [54] and the first seven propagation modes of simulated metamaterial rectangular waveguide.

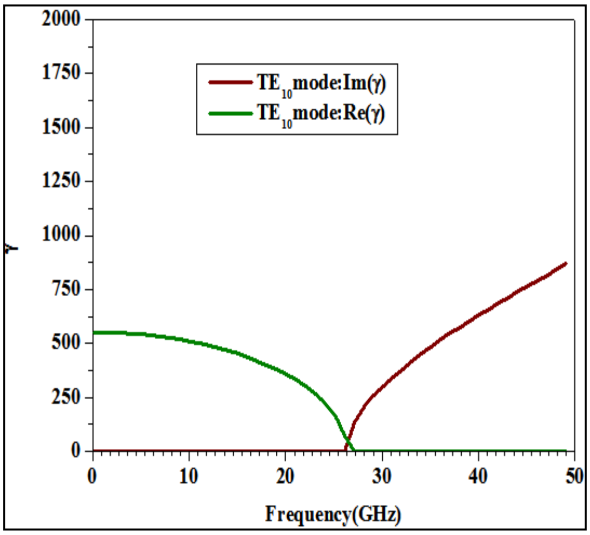

(a)

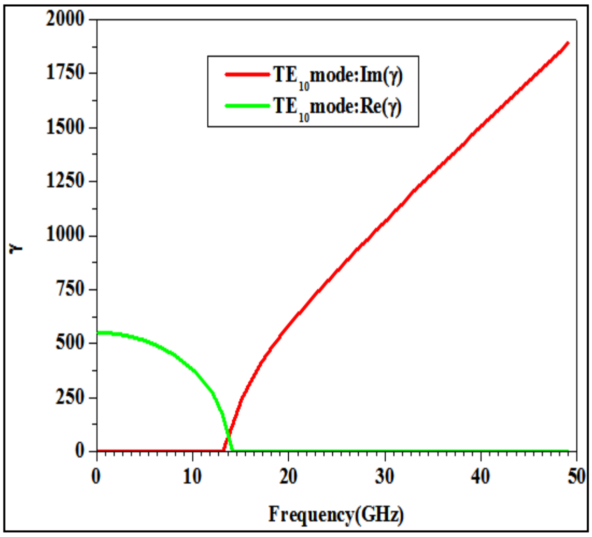

(b)

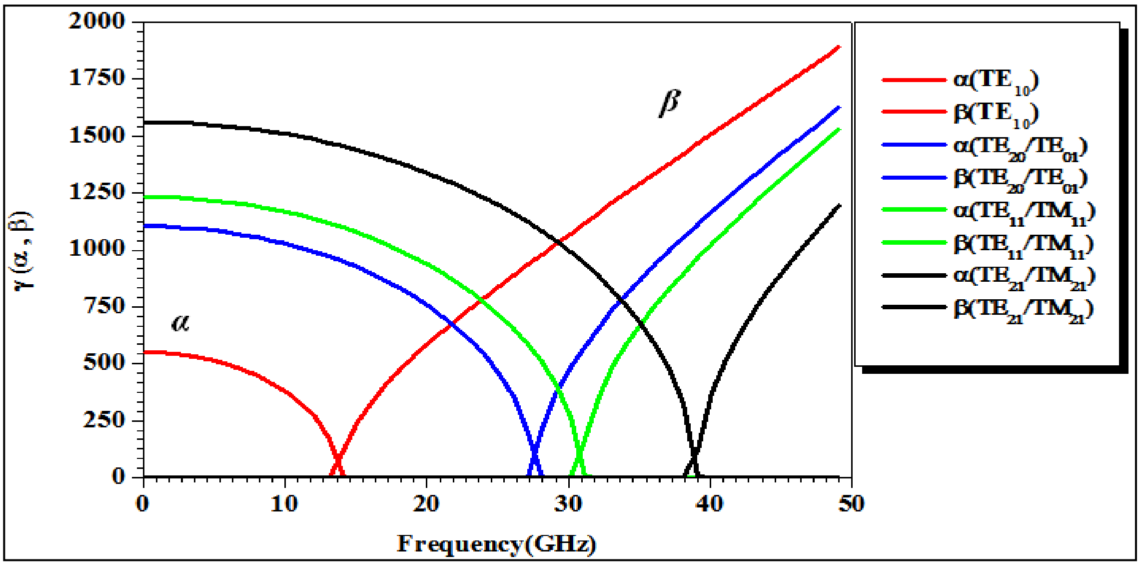

(c)

Figure 4-4 Complex propagation constant $\gamma(f)$ of: a) Metallic rectangular waveguide R400, b) Emulated rectangular waveguide from a metamaterial bulk, and c) The first seven modes of the emulated rectangular waveguide.

From the figure 4-4 (b) which represents the TE_{10} dispersion curve ($\gamma(f)$) of the programmed metamaterial bulk, we conclude that the metamaterial bulk really emulates a rectangular waveguide. It shows the same behavior as TE_{10} mode of a metallic rectangular waveguide as shown in figure 4-4 (a), even if the cutoff frequencies are not the same. The metallic and metamaterial waveguides are not filled by the same material. The propagation constant (β) in the emulated waveguide is greater than that of the conventional metallic waveguide. This is due to the greater refractive index ($\mathrm{Re}(n) > 1$) of the metamaterial filling the emulated waveguide inner section. We observe that there is only one mode (the fundamental one) for the standard metallic waveguide in the [0-50 GHz] frequency band, where the emulated rectangular waveguide, with the same section, presents seven modes in that band as shown in figure 4-4 (c). These modes are identified as: TE Modes (TE_{10}, TE_{20}, TE_{01}, TE_{11} and TE_{21}) and TM modes (TM_{11} and TM_{21}).

The cutoff frequency of the metamaterial rectangular waveguide modes can be written as [55-56]:

$$f_{c_{MTM}} = \frac{f_{c_0}}{\sqrt{n_1^2 - n_2^2}} \qquad (4\text{-}1)$$

Where:

n_1 is the refractive index of the inner rectangular metamaterial of $a \times b$ section,

n_2 is the refractive index of the outer metamaterial section,

$f_{c_{MTM}}$ is the cutoff frequency of the emulated rectangular waveguide,

f_{c_0} is the cutoff frequency of the standard metallic rectangular waveguide of section $a \times b$. It is written as:

$$f_{c_0} = \frac{c}{2}\sqrt{\left(\frac{m}{a}\right)^2 + \left(\frac{n}{b}\right)^2} \tag{4-2}$$

c is the speed of light, a and b are the length and the width of the standard waveguide.

The standard metallic waveguide R400 is 5.69 mm × 2.845 mm, the theoretical cutoff frequency value is f_{c_0} =26.36 GHz. Then, we know that $Re(n_1) \approx 1.95$ and $Re(n_2) \approx 0$. From equation (4-1) we obtain $f_{c_{MTM}} = 13.52 GHz$. The cutoff frequency of the emulated rectangular waveguide $f_{c_{MTM}}$ is in best agreement with that obtained in the simulated $\gamma(f)$ presented in figure 4-4 (b) where $f_{c_{MTM}}$ =13.1GHz. In the following table (table.1), we summarize a comparison between theoretical and simulated cutoff frequencies obtained for each mode of the imitated rectangular waveguide of the figure 4-4 (c).

Mode	f_{c_0}**(GHz)**	$f_{c_{MTM}}$ **(theoretical)(GHz)**	$f_{c_{MTM}}$ **(simulated)(GHz)**
TE_{10}	26.36	13.52	13.1
TE_{20}	52.72	27.03	27.1
TE_{01}	52.72	27.03	27.1
TE_{11}	58.98	30.25	30.1
TM_{11}	58.98	30.25	30.1
TE_{21}	74.63	38.27	38.1
TM_{21}	74.63	38.27	38.1

Table 1 Theoretical and simulated cutoff frequencies of the emulated rectangular waveguide.

From the equation (4-1). If we substitute the equation (4-2) into the equation (4-1) then we have:

$$f_{c_{MM}} = \frac{c}{2}\sqrt{\left(\frac{m}{A}\right)^2 + \left(\frac{n}{B}\right)^2} \tag{4-3}$$

Or

$$f_{c_{MM}} = \frac{c}{2}\sqrt{\left(\frac{m}{a\sqrt{\left(n_1^2 - n_2^2\right)}}\right)^2 + \left(\frac{n}{b\sqrt{\left(n_1^2 - n_2^2\right)}}\right)^2} \tag{4-4}$$

Where:

$$A = a\sqrt{n_1^2 - n_2^2} \tag{4-5}$$

$$B = b\sqrt{n_1^2 - n_2^2} \tag{4-6}$$

The equation (4-4) demonstrates that if we want to obtain the standard metallic waveguide from the metamaterial bulk, we must divide the section $A \times B$ by $\sqrt{n_1^2 - n_2^2}$. If n_1 = 1.95 and n_2 = 0, the inner section will be approximately a grid of (4×2) of disconnected unit cells (2.844 mm × 1.422 mm). Then, the R400 metallic rectangular waveguide can be emulated and it is shown in figure 4-5.

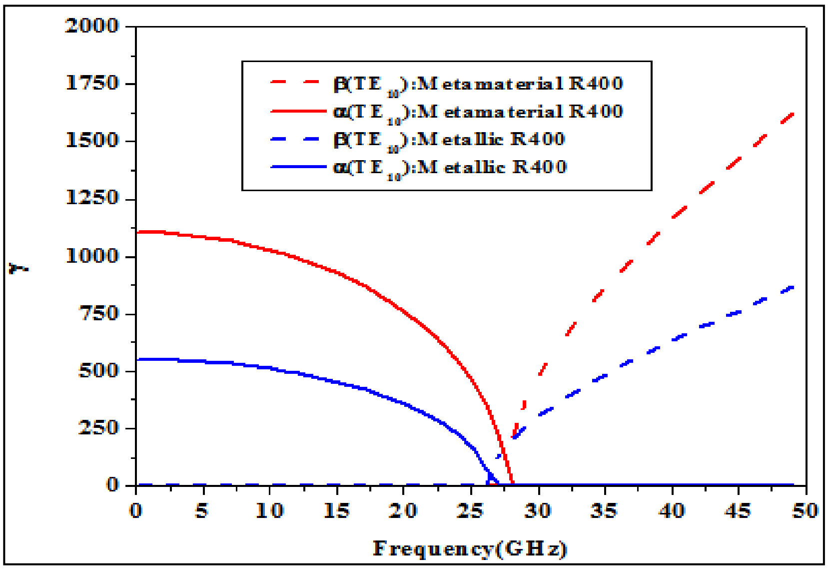

Figure 4-5 Comparison between the R400 metallic rectangular waveguide and the emulated one from the metamaterial bulk.

The TE_{10} mode of the emulated R400 waveguide represented in figure 4-5 is very comparable to that of the metallic R400 waveguide (figure 4-4 (a)). It presents a cutoff frequency of 27.1 GHz compared to 26.1 GHz of the conventional metallic R400. The emulated R400 waveguide propagation constant β is greater than that of the conventional metallic R400, in same time; it has high attenuation constant as shown in figure 4-5.

Figure 4-6 presents the electromagnetic field configuration of the TE_{10} mode in the emulated rectangular waveguide. The magnitudes of *E* and *H* fields are scaled in colors where the blue and red represent the low and high intensity respectively. Their energy is confined inside the disconnected inner metamaterial bulk (the parallelepepiped).

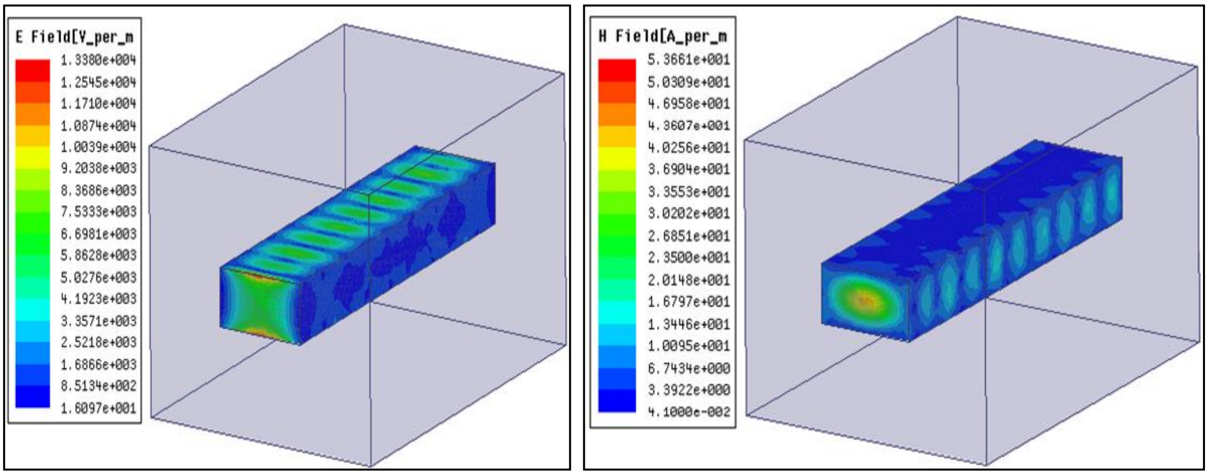

(a) (b)

Figure 4-6 TE_{10} distribution fields in emulated rectangular waveguide: a) *E* field, b) *H* field.

In the figure 4-7, the field lines, in the emulated rectangular waveguide (electric field *E*) of some modes are represented and compared with the same theoretical ones (of the standard metallic rectangular waveguide) cited in [55]. In the theoretical model, we note that *E* and *H* are presented in solid and dashed lines respectively.

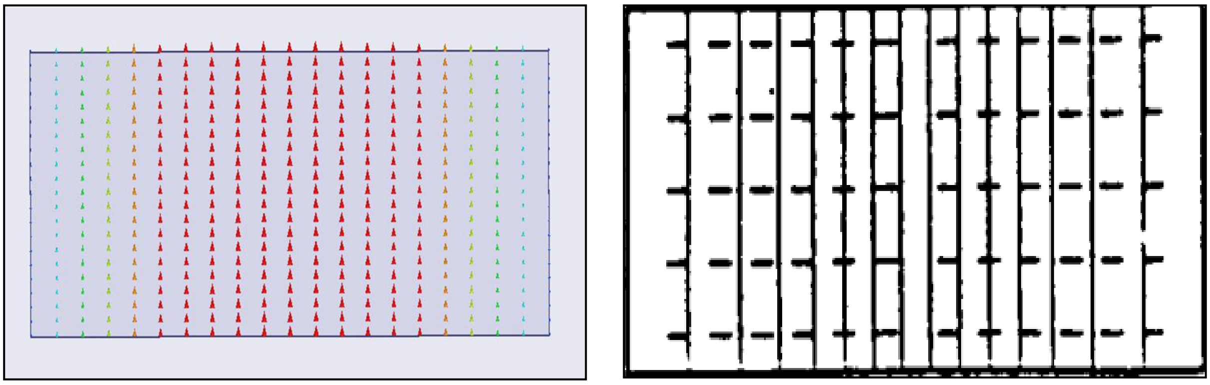

(a) TE_{10} (Simulated). (a′) TE_{10} (Theoretical).

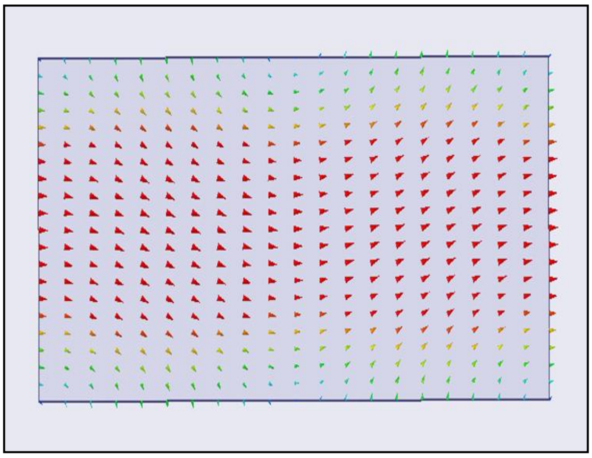

(b) TE_{01} (Simulated)

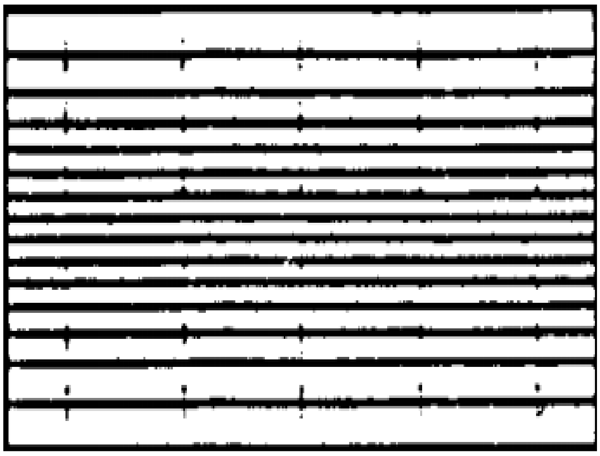

(b′) TE_{01} (Theoretical).

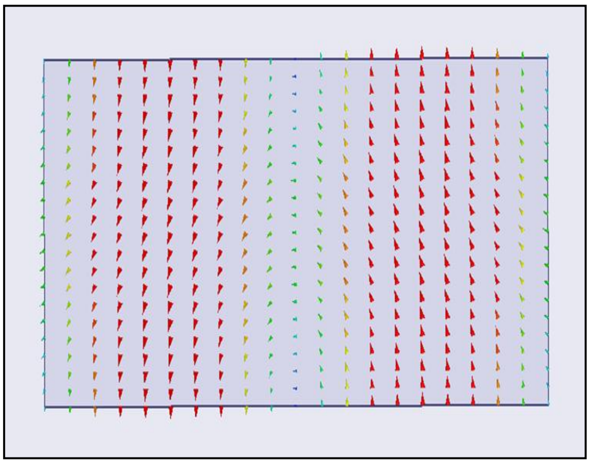

(c) TE_{20} (Simulated).

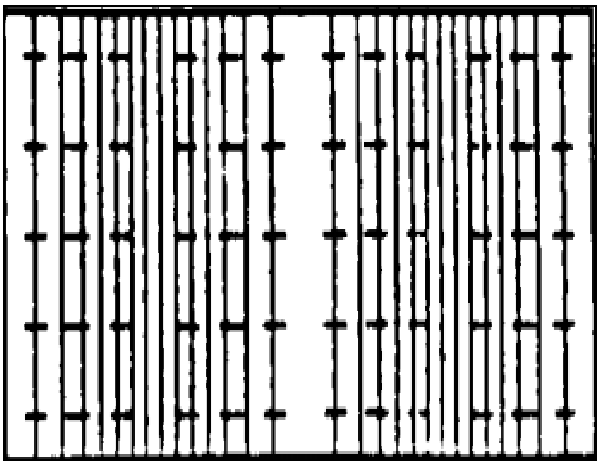

(c′) TE_{20} (Theoretical).

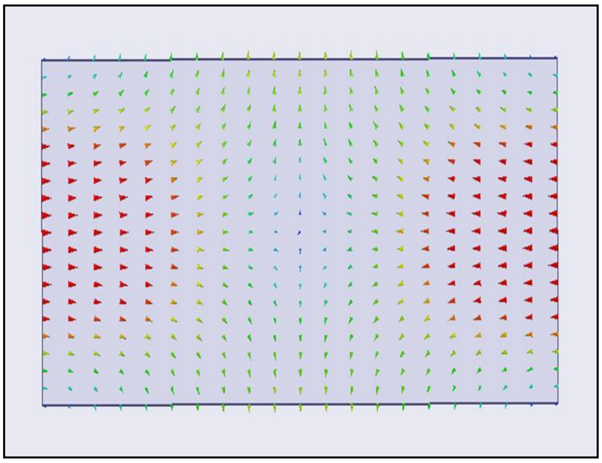

(d) TM_{11}(Simulated).

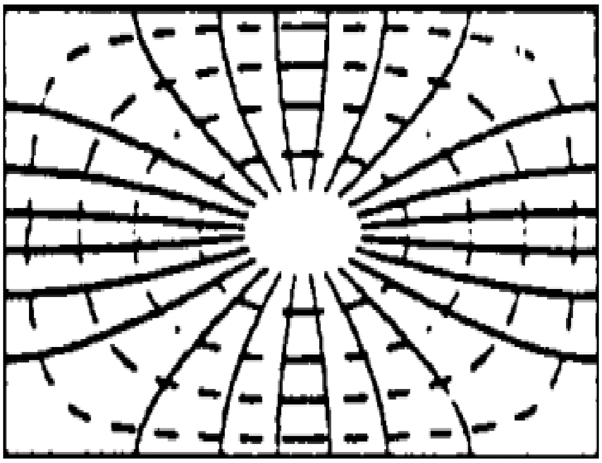

(d′) TM_{11}(Theoretical).

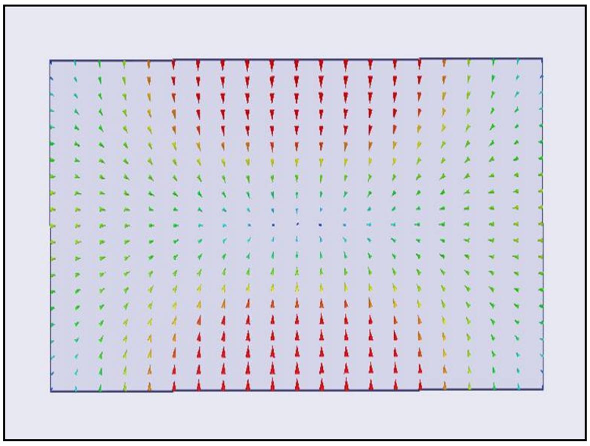

(e) TE_{11} (Simulated).

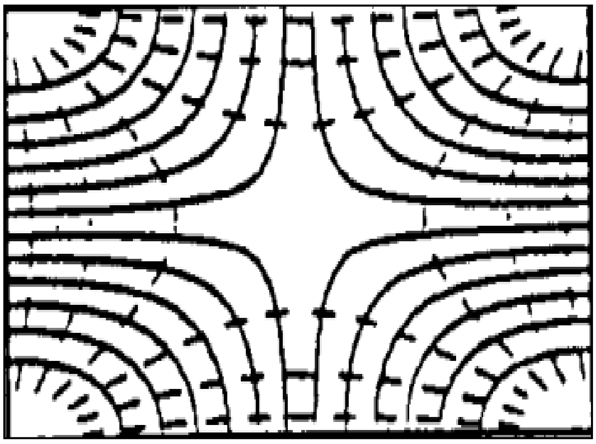

(e′) TE_{11} (Theoretical).

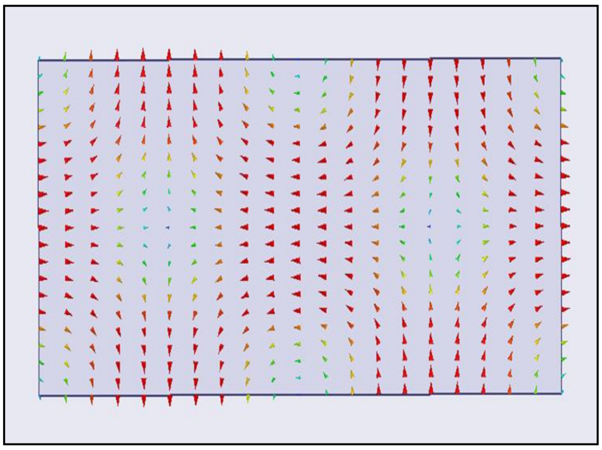

(f) TE_{21}(Simulated).

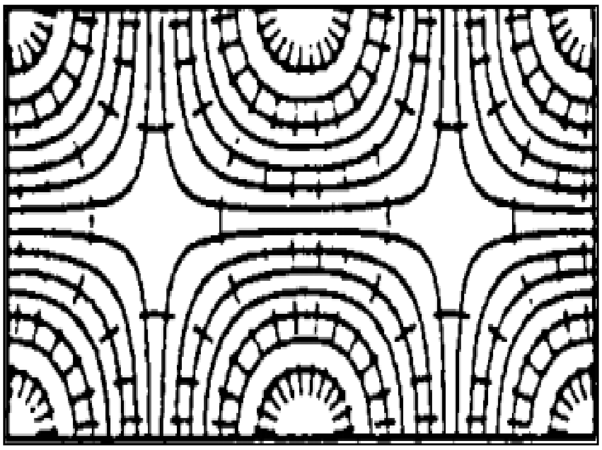

(f′) TE_{21} (Theoretical).

Figure 4-7 Field lines of some modes of the emulated and standard metallic rectangular waveguides of $a \times b$ inner section (E ——— H - - - - - -).

4.2.2 Emulation of a circular waveguide

Like for the rectangular waveguide emulation, to program such circular waveguide function, it is sufficient to control identically every metamaterial layer (pixilated 2 D image) that constitutes the metamaterial bulk. In this case the inner section has a circular form as shown in figure 4-8-(b), then, the identical metamaterial layers will be placed successively to build the desired bulk length. The inner programmed circular zone has a diameter of 12 disconnected cross type metamaterial with $Re(n) \approx 1.95$ and positioned in the center of the metamaterial layer. For the waveguide outer region, formed by the remaining area, we use a connected cross type metamaterial with $Re(n) \approx 0$ (figure 4-8-(b)).

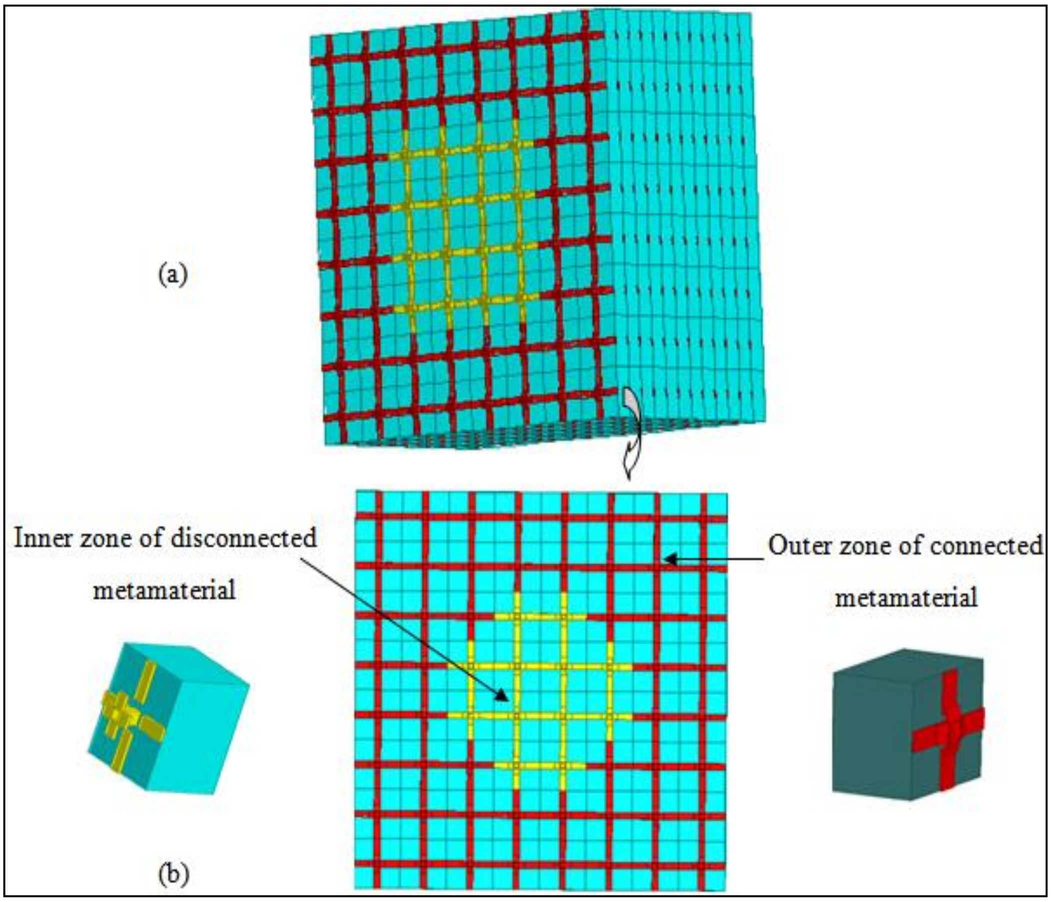

Figure 4-8 a) Metamaterial bulk, b) Switchable control in a metamaterial layer.

The steps of the circular waveguide emulation are presented in the figure 4-9.

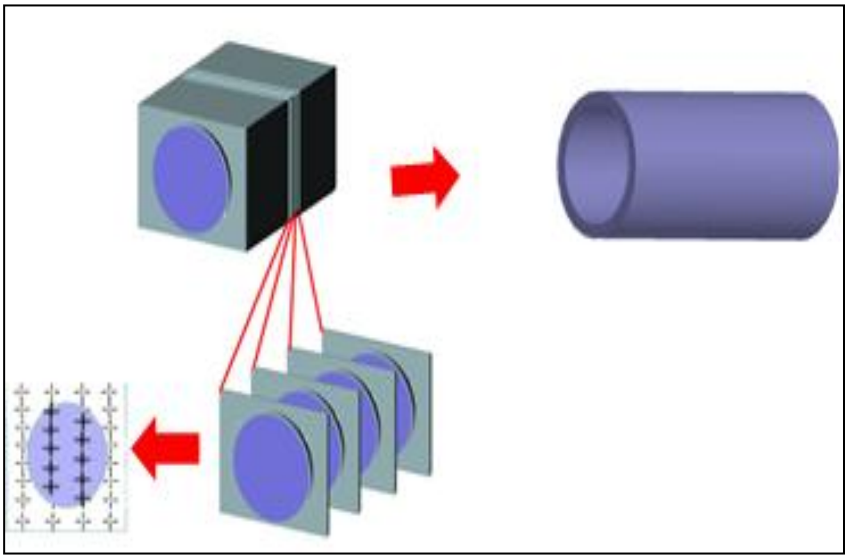

Figure 4-9 Circular waveguide emulation steps from agile metamaterial bulk

The complex propagation constant $\gamma = \alpha + j\beta$ of the dominant mode TE_{11} of both the standard metallic circular waveguide C255 (R = 4.165 mm) [54] and the emulated one are shown in the figure 4-10 where the first five modes are also presented.

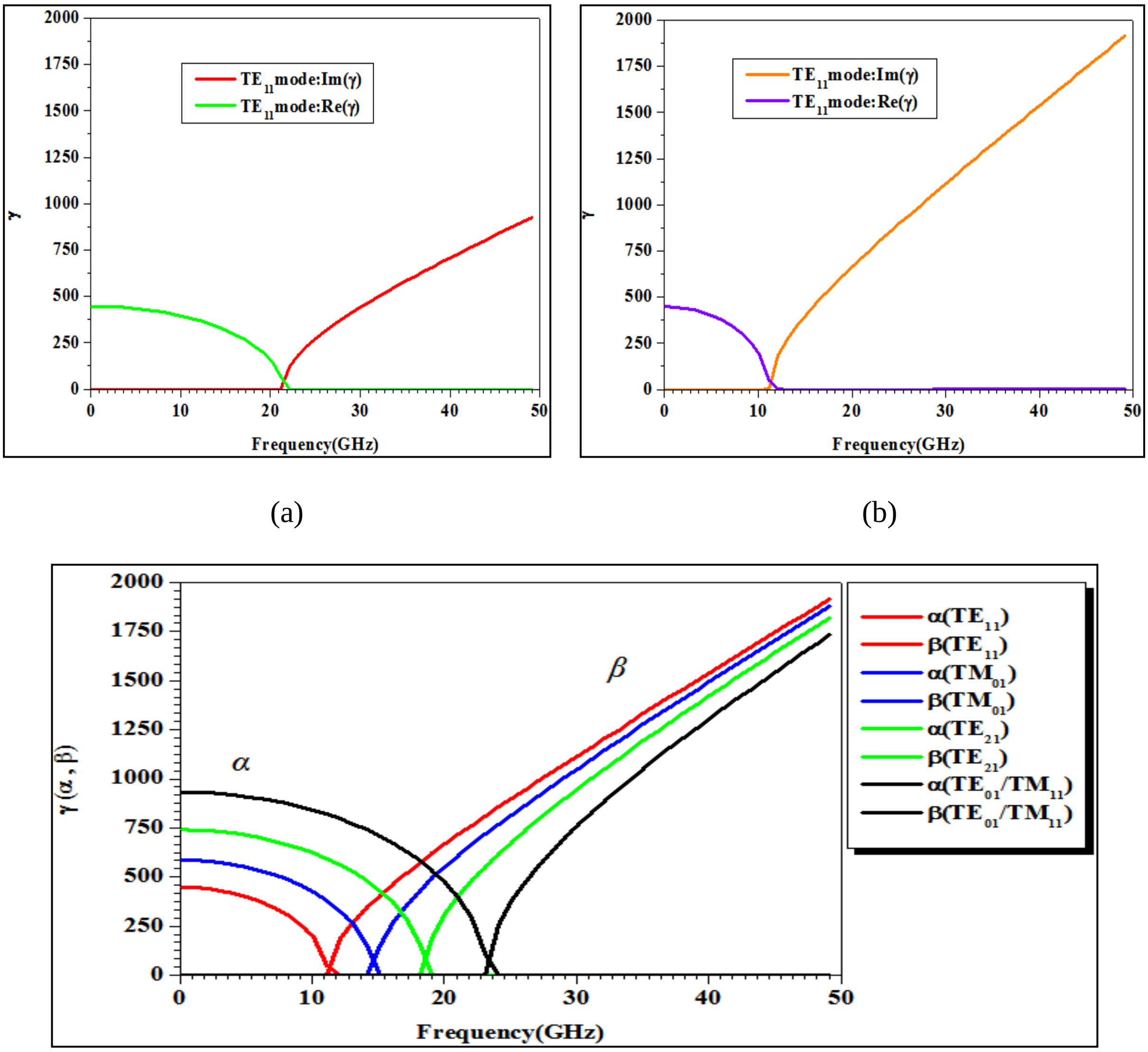

(a) (b)

(c)

Figure 4-10 Complex propagation constant $\gamma(f)$ of: a) Standard metallic circular waveguide C255, b) Emulated circular waveguide from bulk metamaterial, and c) The first five modes of the emulated circular waveguide.

From the figure 4-10 (b), we observe that the programmable metamaterial bulk behaves like a circular waveguide, if its dominant mode is compared to the metallic C255 waveguide (figure 4-10 (a)). The propagation constant (β) in the emulated circular waveguide is greater than in the conventional metallic C255 waveguide due to the greater refractive index (Re(n) $\approx$ 1.95) of the programmable inner section. There is more than one mode in the emulated circular waveguide from the figure 4-10-(c). These modes are TE (TE_{11}, TE_{21}, and TE_{01}) and TM (TM_{01} and TM_{11}).

The cutoff frequency of the metamaterial bulk depends on the radius of the circular zone and the refractive values of the inner and outer zones (n_1 and n_2) (equation (4-1)). The only difference is the cutoff frequency of the standard circular waveguide which is written as:

i) For the TE_{mn} mode:

$$f_{c_0,mn} = \frac{c}{2\pi\sqrt{\varepsilon_r \mu_r}} \frac{X'_{mn}}{R} \tag{4-7}$$

ii) For the TM_{pq} mode:

$$f_{c_0,pq} = \frac{c}{2\pi\sqrt{\varepsilon_r \mu_r}} \frac{X_{pq}}{R} \tag{4-8}$$

Where X'_{mn} and X_{pq} are the zeroes of the derivatives $J'(X'_{mn}) = 0$ and $J(X) = 0$ of Bessel function and R is the circle radius.

If the standard metallic waveguide C255 of $R = 4.165$ mm has f_{c_0} = 21.1 GHz, then $f_{c_{MTM}} = 10.82 GHz$ which is confirmed in the simulated $\gamma(f)$ where ($f_{c_{MTM}}$ = 11.1 GHz), as shown in the figure 4-10 (b). In the following table, are compared theoretical and simulated cutoff frequencies obtained for each mode of the emulated circular waveguide plotted in figure 4-10 (c).

Mode	f_{c_0} **(GHz)**	$f_{c_{MTM}}$ **(theoretical)(GHz)**	$f_{c_{MTM}}$ **(simulated)(GHz)**
TE_{11}	21.1	10.82	11.1
TM_{01}	27.58	14.14	14.1
TE_{21}	35.03	17.96	18.1
TE_{01}	43.95	22.54	23.1
TM_{11}	43.95	22.54	23.1

Table 2 Theoretical and simulated cutoff frequencies of the emulated circular waveguide.

The cutoff frequency of the emulated circular waveguide can also be written as:

i) For the TE$_{mn}$ mode:

$$f_{c_{MTM}} = \frac{c}{2\pi}\frac{X'_{mn}}{R'} = \frac{c}{2\pi}\frac{X'_{mn}}{R\sqrt{n_1^2 - n_2^2}} \quad (4\text{-}9)$$

ii) For the TM$_{pq}$ mode:

$$f_{c_{MTM}} = \frac{c}{2\pi}\frac{X_{pq}}{R'} = \frac{c}{2\pi}\frac{X_{pq}}{R\sqrt{n_1^2 - n_2^2}} \quad (4\text{-}10)$$

Equations (4-9) and (4-10) show that if we want to emulate the conventional metallic C255 from a metamaterial bulk, the circular section radius must be divided by. $\sqrt{n_1^2 - n_2^2} \approx 1.95$. The new radius will be about 3 disconnected unit cells of length (2.133 mm). The propagation constant of the emulated C255 is presented in figure 4-11.

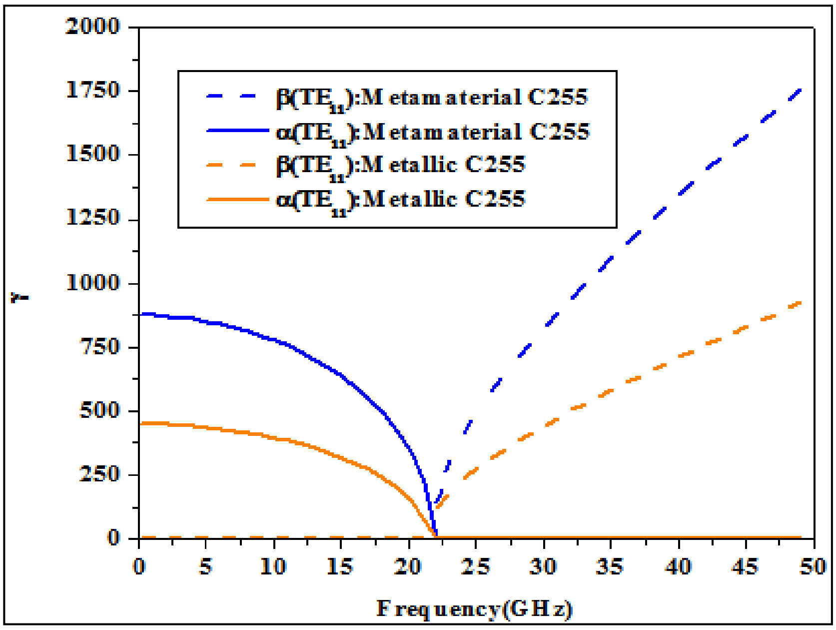

Figure 4-11 Comparison between the C255 metallic circular waveguide and the emulated one from a metamaterial bulk.

The TE$_{11}$ mode of the emulated C255 circular waveguide represented in figure 4-11 is very comparable to that of the metallic C255 waveguide (figure 4-10-(a)): the cutoff frequencies of their dominant mode match very well. It is found to be 21.1 GHz. The emulated C255 waveguide propagation constant β is greater than that of the conventional metallic C255, and has a high attenuation constant α, as shown in figure 4-11.

Figure 4-12 presents the field configuration of the TE_{11} mode in the emulated circular waveguide.

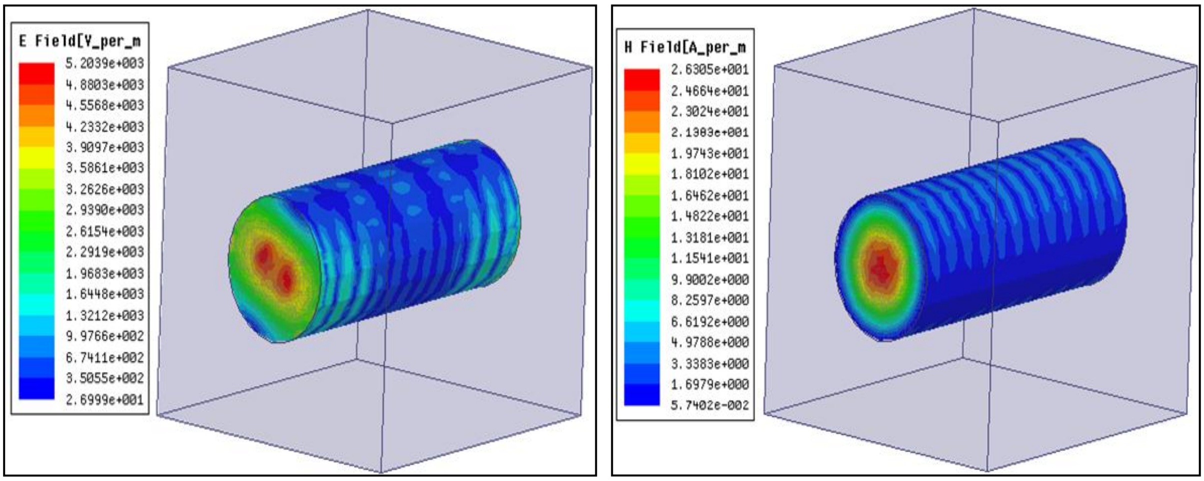

(a) (b)

Figure 4-12. TE_{11} distribution fields in circular waveguide bulk. (a) *E* field. (b) *H* field.

The magnitudes of *E* and *H* field are scaled in colors where the blue and red represent the low and high intensity respectively. They indicate that the maximum of energy is confined inside the disconnected inner metamaterial bulk (the cylinder)

In the figure 4-13, the field lines of some modes, in the emulated circular waveguide, are presented and compared with the same theoretical ones cited in [55].

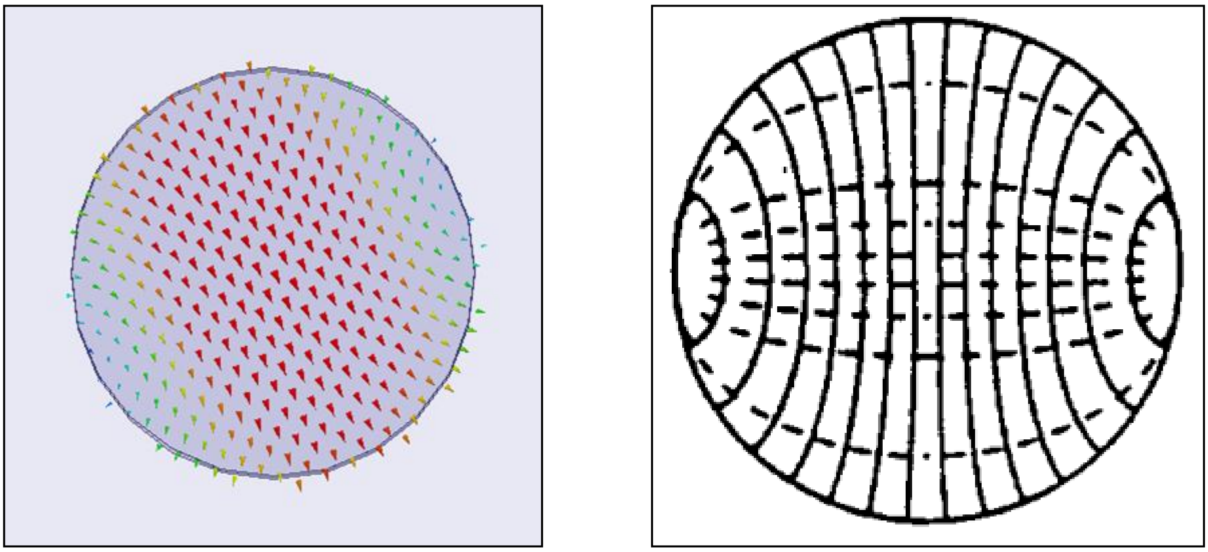

(a) TE_{11} (Simulated). (b) TE_{11} (Theoretical).

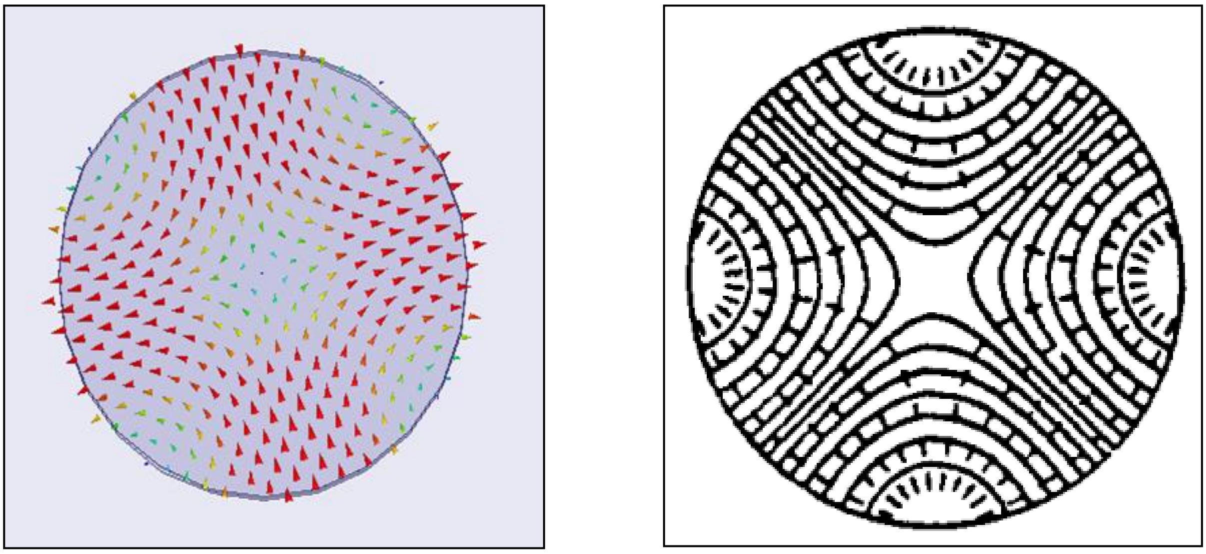

(c) TE_{21} (Simulated). (d) TE_{21} (Theoretical).

Figure 4-13 Field lines of some modes of the emulated and standard circular waveguides of R inner section radius (E ——— H -------).

4.2.3 Emulation of a pyramidal antenna

From a metamaterial bulk constituted of programmable layers, we can emulate an antenna functioning. This is done by suitably programming each metamaterial layer of the bulk. For example the emulation of pyramidal antenna is performed by the emulation of a rectangular waveguide as explained in the section 4.2.1 and then, the emulation of the pyramidal horn. The latter is programmed by gradually increasing the inner waveguide rectangular section, filled with the disconnected cross type metamateril having a refraction index $Re(n) \approx 1.95$, through the passage from a layer to another as shown in figure 4-14.

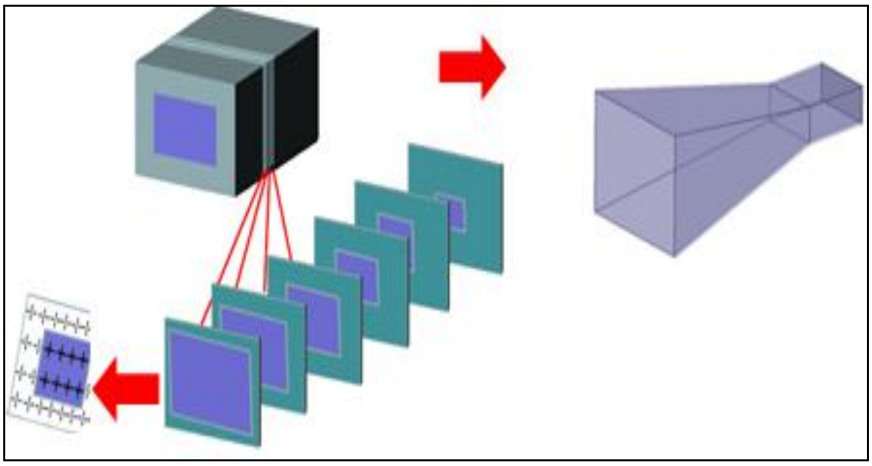

Figure 4-14 Pyramidal antenna emulation steps from agile metamaterial bulk.

For example, if the rectangular waveguide section is 8×4 cells (disconnected cells), the successive layers of the pyramidal horn will be 10×6, 12×8 unit cells, and so on. We complete the building by stacking successive layers until we obtain the desired pyramidal horn flare length. The emulated pyramidal antenna outer section is always constituted of connected cross type metamaterial having a refraction index real part ($Re(n) \approx 0$).

Figure 4-15 shows a comparison between the standard metallic pyramidal horn antenna and the metamaterial emulated one.

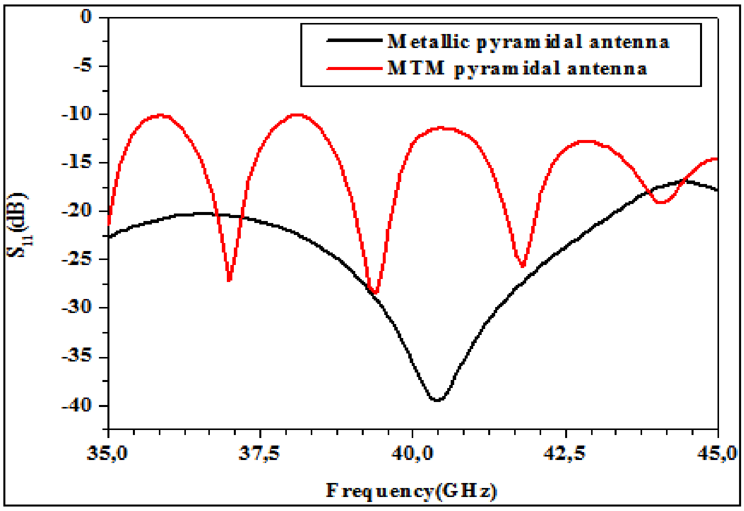

(a)

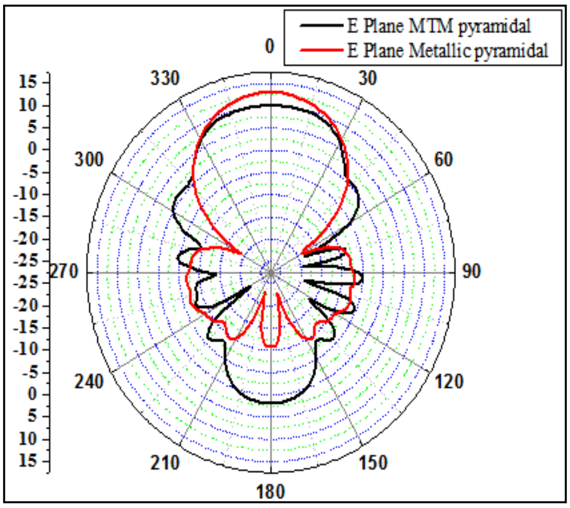

(b)

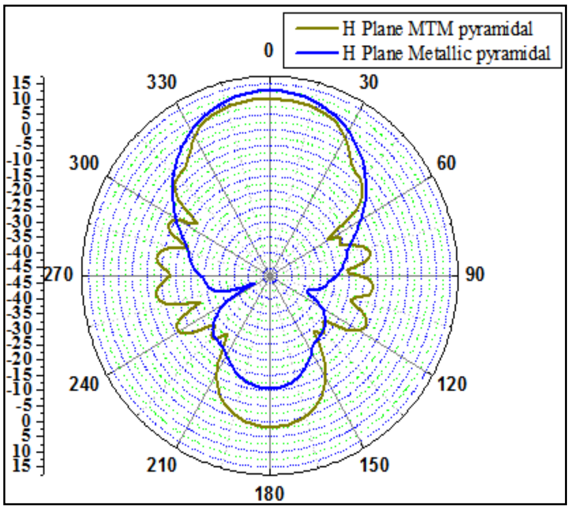

(c)

Figure 4-15 Comparison between the metallic and the emulated from metamaterial bulk pyramidal horn antennas: a) S_{11}(dB), b) *E* Plane gain radiation pattern, and c) *H* Plane gain radiation pattern.

The 3D radiation pattern of the metallic and metamaterial emulated pyramidal horn antennas are illustrated in the figure 4-16.

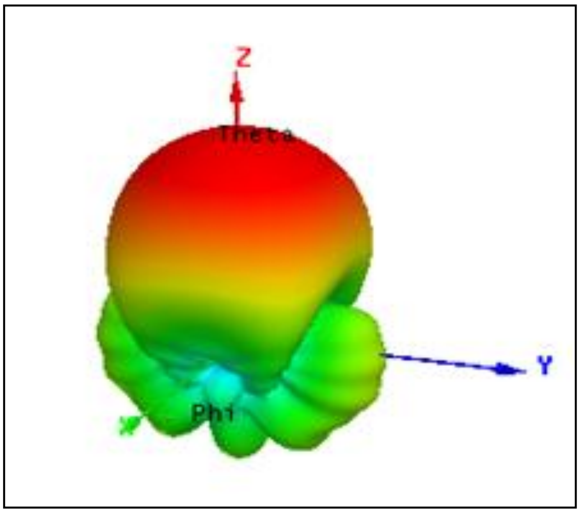

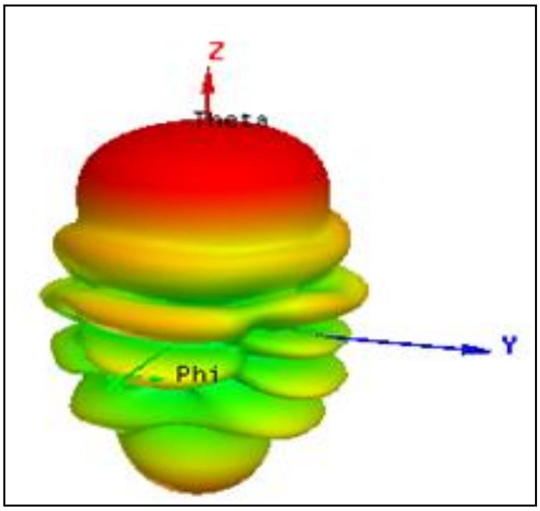

(a) (b)

Figure 4-16 3D gain model of: a) Metallic pyramidal horn antenna, b) Emulated from agile metamaterial bulk pyramidal horn antenna.

From the figures 4-13- 4-14, we conclude that the pyramidal horn antenna can be emulated from the agile metamaterial bulk. The aim of this comparison is not the gain or directivity enhancement but only to demonstrate that it is possible to emulate the behavior of the pyramidal antenna using the programmable metamaterial bulk.

In table 3 are summarized the main characteristics of the metallic and metamaterial emulated rectangular horn antennas.

Pyramidal antenna type	**$\|S_{11}\|$(dB) Over the band**	**Gain$_{max}$ (dB)**		**Beamwidth**		**Side lobe (dB)**	
		***E* Plane**	***H* Plane**	***E* Plane**	***H* Plane**	***E* Plane**	***H* Plane**
Metallic	<-16	12.96	12.96	44	44	-10.63	-6.82
Emulated	<-10	8.22	8.22	68	68	-2.04	-1.96

Table 3 Characteristics comparison between the metallic and the metamaterial emulated pyramidal horn antennas at 41 GHz.

From table 3, we observe that the presence of a metamaterial in the emulated pyramidal antenna does not affect the matching properties of the antenna where S_{11} amplitude stays below the reference value of -10 dB over the frequency operating band. The maximum gain on both E and H planes of the emulated pyramidal horn is lower than that of the metallic one. The beamwidths in the E and H planes are the same for the two antennas. But, they are wider for the emulated pyramidal antenna compared to that of the metallic one. We note also that the side lobes in the metamaterial emulated antenna are higher than those in the metallic one.

4.2.4 Emulation of a conical antenna

The same steps as detailed above in the section 4.2.3 are followed to create a conical metamaterial antenna as shown in figure 4-17. The inner disconnected section diameter of the circular waveguide is 8 unit cells of length.

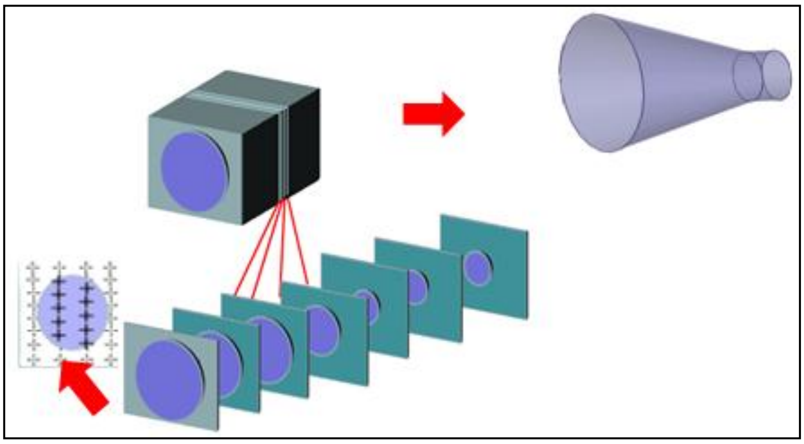

Figure 4-17 Conical antenna emulation steps from agile metamaterial bulk.

The figure 4-18, shows a comparison between the standard metallic conical horn antenna and the metamaterial emulated one.

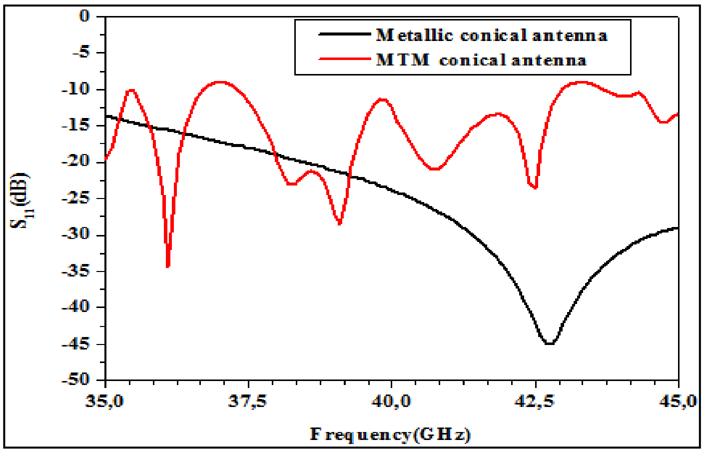

(a)

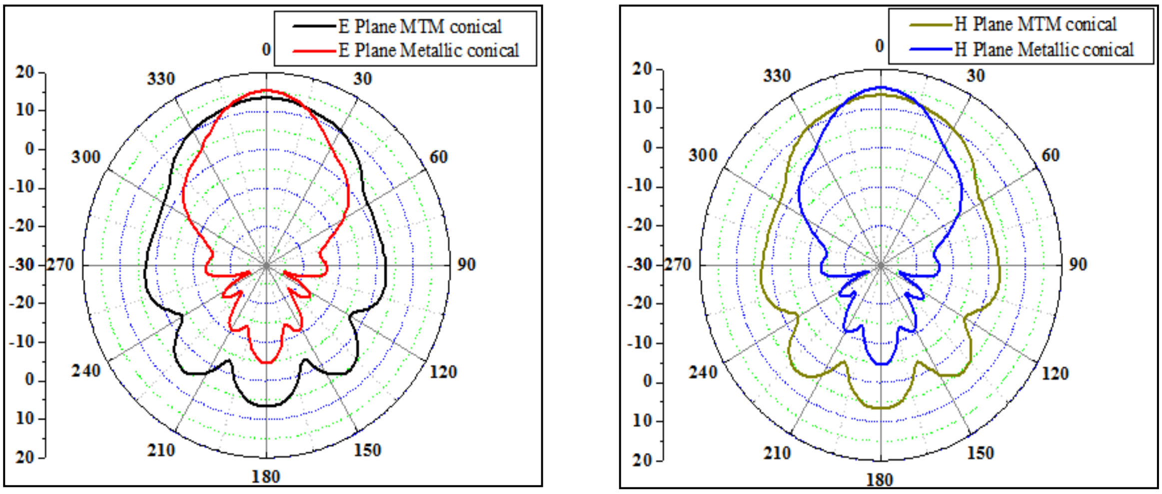

(b) (c)

Figure 4-18 Comparison between the metallic and the emulated from metamaterial bulk conical horn antennas: a) S_{11}(dB), b) *E* Plane gain radiation pattern,

and c) *H* Plane gain radiation pattern.

The 3D radiation pattern of the metallic and metamaterial emulated pyramidal horn antennas are illustrated in figure 4-19.

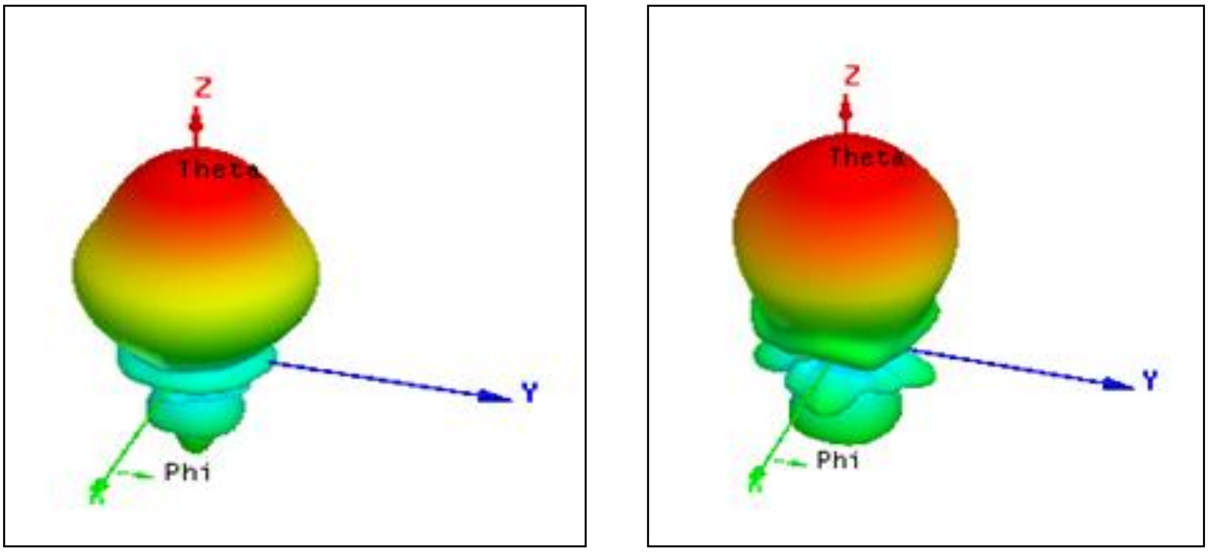

(a) (b)

Figure 4-19 3D gain model of: a) Metallic conical horn antenna, b) Emulated from agile metamaterial bulk conical horn antenna.

In the Figure 4-18- 4-19, the metamterial and the metallic conical antennas radiation pattern gain are very similar which allow us to conclude that the conical antenna's function is accomplished.

In table 4 are summarized the main characteristics of the metallic and metamaterial emulated conical horn antennas.

Conical antenna type	**$\|S_{11}\|$(dB) Over the band**	**Gain$_{max}$ (dB)**		**Beamwidth (°)**		**Side lobe (dB)**	
		***E* Plane**	***H* Plane**	***E* Plane**	***H* Plane**	***E* Plane**	***H* Plane**
Metallic	<-12.5	15.1	15.1	30	30	-13.45	-13.45
Emulated	< -9	13.85	13.85	60	60	1.92	1.92

Table 4 Characteristics comparison between the metallic and the metamaterial emulated conical horn antennas at 42 GHZ.

We observe that the presence of a metamaterial in the emulated conical antenna does not affect the matching properties of the antenna where S_{11} amplitude stays below the reference value of -10 dB over the [37.3 – 43] GHz band. The maximum gain on both *E* and *H* planes of the emulated conical horn is lower than in the metallic one. The radiation pattern beamwidth in the two planes are the same. But they are wider in the emulated conical antenna than in the metallic one (twice). We observe also that the side lobes in the metamaterial emulated antenna are higher than in metallic one.

4.3Conclusion

The agility concept is extended to construct agile planar and bulk meatamaterials by programming different zones that are made of connected and disconnected cross unit cells inside the planar metamaterial. Different microwave devices like rectangular and circular waveguides, pyramidal and conical horn antennas can be emulated from an agile metamaterial bulk. In this work we have extend the agility concept. In literature the adjective “agility” concerns one of the device properties such as the frequency (frequency agile antenna), the radiation pattern (radiation pattern agile antenna), the polarization (polarization agile antenna), etc. In our work, the concept is extended to the “device functioning”: device functioning agility. In other words, the same material bloc can be programmed to “emulate” or to “behave as” a specific desired component such as, for example, waveguide (rectangular, circular), antennas (pyramidal horn antenna, conical horn antenna), etc.

Conclusion

The main goal of this work is to design agile metamaterial microwave devices. For this purpose we designed an agile metamaterial layer made of connected / disconnected cross unit cells. The agile metamaterial effective parameters are extracted and validated by two different methods detailed in chapter 2: The S parameters method that depends on the reflection and transmission coefficients, and the field summation method.

The agile unit cell, we designed, is the core of the agile metamaterial layer. It has two different behaviors between we can flip by an external switching control systems. The agile unit cell is optimized, to obtain the desired metamaterial behaviors, by varying the period $\boldsymbol{a}$, the dielectric thickness $\boldsymbol{d}$, the width $\boldsymbol{w}$, the dielectric permittivity $\boldsymbol{\varepsilon_r}$ and the gap $\boldsymbol{g}$. If $\boldsymbol{g} = 0$, the cross is connected and the connected cross type metamaterial has a refractive index close to zero. If $\boldsymbol{g} > 0$, the cross is disconnected and the disconnected cross type metamaterial has a refractive index greater than the unity. The optimized unit cell has the following dimensions $\boldsymbol{a} = 0.711$ mm, $\boldsymbol{d} = 1.27$ mm, $\boldsymbol{w} = 0.35$ mm, $\boldsymbol{\varepsilon_r} = 2.2$ and $\boldsymbol{g} = 0.02$ mm (case of the disconnected cross). The average refractive index contrast between the connected and disconnected behaviors is about 1.95.

The agile metamaterial is constituted of several programmable metamterial layers, stacked to form the metamaterial bulk In each metamaterial layer different regions of different shapes and sizes can be programmed to behave as a connected or disconnected cross type metamaterial. The metamaterial programming is performed by aging on the switches, connecting the unit cell cross type conductor.

The emulation of waveguides from the metamaterial bulk is performed by programming the refraction index of the metamaterial bulk outer region to $Re(n) \approx 0$ and that of the inner region to $Re(n) \approx 1.95$. When we give to the metamaterial bulk inner region a rectangular / circular shape the metamaterial bulk emulates a rectangular / circular waveguide, respectively. In this work we have emulated the metallic R400 (5.69×2.845) mm rectangular and C255 (R = 4.165 mm) circular waveguides. In a similar way, the metamaterial bulk was programmed to emulate the functioning of pyramidal and conical horn antennas. The obtained results are very conclusive.

References

[1] W. Cai, V. Shalaev, “Optical metamaterials fundamentals and applications,” Springer, 2010.

[2] T. J. Cui, D. R. Smith, R. Liu, “Metamaterials theory, design and applications,” Springer, 2010.

[3] W. Kock, ‘‘Metallic delay lenses,’’ Bell. Syst. Tech. J, vol. 27, pp. 58-82, 1948.

[4] J. B. Pendry, A. J. Holden, W. J. Stewart, and I. Youngs, “Extremely low frequency plasmons in metallic mesostructures,” Physical Review Letters, vol. 76, no. 25, pp. 4773–4776, 1996.

[5] J. B. Pendry, A. J. Holden, D. J. Robbins, and W. J. Stewart, “Magnetism from conductors and enhanced nonlinear phenomena,” IEEE Transactions on microwave theory and techniques, vol. 47, no. 11, pp. 2075–2084, 1999.

[6] H. S. Chen, L. X. Ran, and J. T. Huangfu, “Left handed materials composed of only S shaped resonators,” Physical review E, vol. 70, no. 5, 2004.

[7] C. Caloz, T. Itoh, “Electromagnetic metamaterials: transmission line theory and microwave applications The Engineering approach,” A John Wiley & Sons, INC, 2006.

[8] N. Engheta, R. W. Ziolkowski, “Metamaterials physics and engineering explorations,” IEEE, 2006.

[9] J. Pendry, A. Holden, D. Robbins, and W. Stewart, “Low frequency plasmons in thin wire structures,” Journal of physics: Condensed matter, vol. 10, p. 4785, 1998.

[10] S. Schelkunoff, H. Friis, “Antennas: Theory and practice,” John Wiley & Sons, 1952.

[11] H. J. Schneider, P. Dullenkopf, “Slotted tube resonator: a new NMR probe head at high observing frequencies,” Rev. Sci. Instrum, vol. 48, no. 1, pp. 68-73, 1977.

[12] W. H. Hardy, L. A. Whitehead, “Split ring resonator for use in magnetic resonance from 200-2000 MHz,” Rev. Sci. Instrum., vol. 52, no. 2, pp. 213-216, 1981.

[13] M. V. Kostin, V. V. Shevchenko, “Artificial magnetics based on double circular elements,” Proc. of bianisotropics ’94, Perigueux, France, pp. 49-56, 1994.

[14] M. E. Chaib, « Modélisation et caractérisation de fonctions électroniques générées par des dispositifs à métamatériaux », Memoir of magistriate, Abou Bakr Belkaid University of Tlemcen, 2012.

[15] K. Ganguar, Dr. Paras, and Dr. R. P. S. Ganguar, “Metamaterials: characteristics, process and applications,” Advance in Electronic and Electric engineering, vol 4, no 1, pp. 97-106, 2014.

[16] S. E. Mendhe, Y. P. Kosta, “Metamaterial properties and applications,” International Journal of Information Technology and Knowledge Management, vol 4, no. 1, pp. 85-89, January-June, 2011.

[17] S. Raghavan, V. Rajeshkumar, “An overview of metamaterials in biomedical applications,” Piers Proceedings, Taipei, March 25-28, 2013.

[18] S. M. Anlage, “The physics and applications of superconducting metamaterials,” IOP science, Journal of Optics, 2011.

[19] Y. P. Lee, P. V. Tuong, and H. Y. Zheng, “An application of metamaterials: perfect absorbers,” Journal of the korean physical society, vol. 60, no. 8, pp. 1203-1206, 2012.

[20] L. Vogt, “Metamaterials and their applications,” www.oxforddictionaries.com/definition/english/metamaterial.

[21] L. Y. Wu, T. Y. Chiang, C. N. Tsai, M. Wu, and L. W. Chen, “Design of an acoustic bending waveguide with acoustic metamaterials via transformation acoustics.” Appl Phys A, Springer, 2012.

[22] P. Kiddle, “Information on frequency selective surfaces,” RRAC, www.ofcom.org.uk, 2001.
[23] B. Hooberman, “Everything you ever wanted to know about frequency selective surface filters but were afraid to ask,” Columbia Astrophysics Laboratory, Columbia University, 2005.
[24] S. N. Burokur, « Mise en œuvre de métamatériaux en vue d’application aux circuits microonde et antennes », Doctoral thesis, Department of Electronics, Electronic high school of Angers, 2005.
[25] Z. Sahraoui, « Les antennes agiles à base de metamateriaux », Memoir of Masters, Department of Electronics, Amar Telidji University of Laghouat, 2013.
[26] T. J. Cui, D. R. Smith, and R. Liu, “Metamaterials theory, design, and applications,” Springer, 2010.
[27] C. Caloz, and T. Itoh, “Electromagnetic metamaterials: transmission line theory and microwave applications,” A John Wiley and Sons, INC, 2006.
[28] Alireza, V. Amirkhizi, and S. Nemat-Nasser, “Microstructurally based homogenization of electromagnetic properties of periodic media,” Science Direct. C. R. Mecanique, no. 336, pp. 24–33, 2008.
[29] L. Solymar, and E. Shamonina, “Waves in metamaterials,” Oxford, 2009.
[30] W. Cai, and V. Shalaev, “Optical metamaterials fundamentals and applications” Springer, 2010.
[31] S. Arslanagić, T. V. Hansen, N. A. Mortensen, A. H. Gregersen, O. Sigmund, R. W. Ziolkowski, and O. Breinbjerg, “A review of the scattering parameter extraction method with clarification of ambiguity issues in relation to metamaterial homogenization,” The Danish Research Council For Technology And Production Sciences, 2012.
[32] U. C. Hasar, and J J. Barroso, “Retrieval approach for determination of forward and backward wave impedances of bianisotropic metamaterials,” Progress In Electromagnetics Research, vol. 112, pp. 109-124, 2011.
[33] H. Wallén, H. Kettunen, and A. Sihvola, “Mixing formulas and plasmonic composites. in metamaterials and plasmonics: fundamentals, modelling, applications,” Springer, pp. 91-102, 2009.
[34] O. F. Mosotti, “Discussione analitica sull’influenza che l’azione di un mezzo dielettrico ha sulla distribuzione dell’elettricità alla superficie di più corpi elettrici disseminato in esso, “Memorie di matematica e di fisica della società italiana delle scienze (Modena), XXIV(Parte Seconda): 49-74, 1850.
[35] L. Rayleigh, “the influence of obstacles arranged in rectangular order upon the properties of a medium,” Philosophical magazine, no. 31, pp. 481-502, 1892.
[36] Z. Lei, R. Yang, X. Shi, and J. Zhang, “Determining the effective electromagnetic parameters of bianisotropic metamaterials with periodic structures,” Progress In Electromagnetics Research, vol. 29, pp. 79-93, 2013.
[37] J. W. Shehan, J. M. C. Covington III, V. S. Kshatri, T. P. Weldon, and R. S. Adams, “Permeability and permittivity extraction issues for non-foster and active metamaterials,” IEEE, Antennas and Propagation, 2013.
[38] U. C. Hasar, J. J. Barroso, M. Ertugrul, C. Sabahand, and B. Cavusoglu, “Application of a useful uncertainty analysis as a metric tool for assessing the performance of electromagnetic properties,” Progress In Electromagnetics Research, vol. 128, pp. 365-380, 2012.
[39] D. R. Smith, “Electromagnetic parameter retrieval from inhomogeneous metamaterials,” Physical Review E, vol. 71, 2005.

[40] Alireza, V Amirkhizi, and S Nemat-Nasser, “Numerical calculation of electromagnetic properties including chirality parameters for uniaxial bianisotropic media,” IOP Publishing. Smart Matter. Struct, vol. 17, 2008.
[41] C. Croenne, J. M. Lerat, N. Malléjac, O. Acher, and D. Lippens, «Extraction ab-initio des paramètres effectifs des métamatériaux», Journées Nationales Microondes (JNM), 23-25 May 2007, Toulouse-France.
[42] S. M. Chaker, « Optimisation des dimenssions du motif élementaire d’une grille métamatériau utilisée pour améliorer la directivité d’une antenne imprimé travaillant à 43 GHz », engineering memoir, Department of Electronics, Amat Telidji University of Laghouat, 2010.
[43] S. M. Chaker and M. Bouzouad, “Metamaterial patch antenna radiation pattern agility,” App Phys A, vol. 115, pp. 459-465. 2014.
[44] F. Bararat, « Dispositifs micro onde agiles à base de métamateriaux », Mémoire de Master, Université de Laghouat, Juin 2013.
[45] V. Laur, « Contribution à la réalisation de circuits hyperfréquence reconfigurable à partir de couches minces féroelectriques: de matériaux aux dispositifs », Doctoral thesis, Bretagne Occidentale University, 2007.
[46] N. Tentillier, « Contribution à la caractérisation diélectrique micro-onde de cristaux liquides. Application aux circuits agiles en fréquences », Doctoral thesis, sciences and technologie University of Lille, 2003.
[47] S. D. Robinson, “MEMS technology micromachines enabling the all optical network,” IEEE, 2001.
[48] L. Mercier, « Synthèse de propriétés d’agilité électromagnétique par des matériaux artificiels périodiques intégrants des microcomposants. Application à la conception d’antennes à résonateur BIE configurable », Doctoral thesis, University of Limoges, 2005.
[49] A. Giere1, Y. Zheng, H. Maune, M. Sazegar, F. Paul, X. Zhou, J. R. Binder, S. Müller and R. Jakoby, “Tunable dielectrics for microwave applications, ”
[50] J. B Mills, C. J. Stevens, and D. J. Edwards, “Composite materials for planar frequency agile microwave devices, “, IEEE, 2001.
[51] S. Gevorgian, “Ferroelectrics in agile microwave components,” Armenian Journal of Physics, vol. 2, issue 1, pp. 64-70, 2009.
[52] R. Jakohy, P. Scheele, S. Muller, and C. Weil, “Nonlinear dielectrics for tunable microwave components, ”
[53] Éric Lheurette, “Metamaterials and wave control,” John Wiley and Sons, Inc, 2013.
[54] F. Gardiol, « Traité de l’Electricité, » volume III, Georgi, 1981.
[55] C. A. Balanis, “Advanced engineering electromagnetics,” John Wiley and Sons, 1938.
[56] Z. S. A. Mebark, « Support de transmission et composant micro-ondes, » OPU, 1995.